FABRICATION AND CHARACTERIZATION OF BIO-EPOXY EGGSHELL COMPOSITES

A Thesis Submitted to the College of

Graduate and Postdoctoral Studies

In Partial Fulfillment of the Requirements

For the Degree of Master of Science

In the Department of Mechanical Engineering

University of Saskatchewan

Saskatoon

By

Stephen Ifeanyichukwu Owuamanam

PERMISSION TO USE

In presenting this thesis in partial fulfillment of the requirements for a Postgraduate degree from the University of Saskatchewan, I agree that the Libraries of this University may make it freely available for inspection. I further agree that permission for copying of this thesis in any manner, in whole or in part, for scholarly purposes may be granted by Prof. Duncan Cree, the professor who supervised my thesis work or in their absence, by the Head of the Department or the Dean of the College in which my thesis work was done. It is understood that any copying or publication or use of this thesis or parts thereof for financial gain shall not be allowed without my written permission. It is also understood that due recognition shall be given to me and to the University of Saskatchewan in any scholarly use which may be made of any material in my thesis.

Requests for permission to copy or to make other uses of materials in this thesis in whole or part should be addressed to:

Head of the Department of Mechanical Engineering
57 Campus Drive
University of Saskatchewan
Saskatoon, Saskatchewan S7N 5A9
Canada

OR

Dean
College of Graduate and Postdoctoral Studies
University of Saskatchewan
116 Thorvaldson Building, 110 Science Place
Saskatoon, Saskatchewan S7N 5C9
Canada

ABSTRACT

Low cost fillers such as mineral limestone (LS) are added to polymers in an effort to improve their properties. Waste eggshells (ES), a by-product of the egg breaking plant industry, contain high content of calcium carbonate ($CaCO_3$) but are generally discarded to landfills at a cost to the company. The use of waste ES as an alternative to mineral LS filler added to bio-epoxy resin was investigated in this study.

Untreated and stearic acid (SA) treated ES and LS fillers (5, 10 and 20 wt. %) were used in fabricating bio-epoxy composite materials via a solution mixing method. Chemical analysis of the filler materials, microstructural examination, physical and mechanical properties of the fabricated composites were evaluated.

The particle density of ES was found to be smaller than that of LS particles. The average particle size was 21.2 ± 2.0 µm, 11.5 ± 1.0 µm, 25.1 ± 2.2 µm and 12.8 ± 2.2 µm for ES, SA treated ES, LS and SA treated LS, respectively. SEM images showed untreated ES and LS particles varied in shape possibly due to grinding during processing. Both untreated and SA treated fillers had rhombohedral-like morphology. Pores were observed in ES due to its characteristic structure compared to the LS particles, which had no visible pores. Fractured surfaces of the composites showed flat and cleavage features for unfilled bio-epoxy composites compared to filled composites which showed jagged surfaces. The density of the composites increased with increase in filler loading for all filler types. Similarly, the void content and water absorption increased with increase in filler loading with 20 wt. % ES composites having the highest values. XRD analysis indicated the presence of calcite, while ICP-MS showed 88 wt. % ± 0.7 $CaCO_3$ in ES, slightly less than the mineral LS as a result of the residual organic membranes still attached. The tensile strength, flexural strength and Charpy impact toughness of the composites reduced with increase in filler loading. However, the flexural modulus improved with increasing filler loading and was maximum at a filler content of 20 wt. % for all filler types. The Charpy impact energy of unfilled bio-epoxy at – 40 °C dropped appreciably to about 58 % of its room temperature value. Economic analysis showed that ~ 18,117,000 kg of $CaCO_3$ can be recovered from waste ES annually in Canada for various applications and can serve as potential replacement of about 1.00 % of mined mineral LS.

This research presents promising results for the use of ES as an alternative to LS in bio-epoxy composites for selected applications such as laminating surfboards and skateboards.

ACKNOWLEDGEMENTS

My sincere appreciation and gratitude go to the Almighty God for making the completion of my M.Sc. program possible. His favor and grace brought me to Canada from a far continent and has kept me thus far in life.

I would like to express my profound appreciation to my supervisor, Prof. Duncan Cree for his love, support, encouragement, guidance and immense contribution towards the course of this program. I also thank him for accepting to supervise my M.Sc. program in the first instance. My deepest and profound appreciation goes to my advisory committee members, Prof. Akindele Odeshi and Prof. Ike Oguocha for their guidance and scientific contributions to the success of this program. I will also like to extend my sincere appreciation to Dr. Majid Soleimani for his time and contributions to my research. My sincere appreciation also goes to Mr. Rob Peace and Mr. Nanfang Zhao for providing me with technical assistance in the laboratory and guiding my experiments.

I give my appreciation to my parents, Prof. and Prof. (Mrs.) Donatus Owuamanam and siblings Dr. Stanley, Lilian and Dr. Marcellius for their prayers, words of encouragement, financial and moral support.

Special thanks to Dr. Rev. Sr. Agatha Ogunkorede and my friends, Jude Okolie, Ejalonibu Adewale, Peter Bankole, Akinola Ogbeyemi and Mary Bajomo for their love, prayers and advice. I cannot omit mentioning past and current students, Opeoluwa Fadele, Anthony Loeffen, Tiamiyu Ahmed, Dayo Oke, Joseph Omale, Ericmoore Jossou, Linu Mahakal, George Enyinnaya and Gaurang Golakiya for guiding me on some test procedures.

God bless you all.

DEDICATION

This thesis is dedicated to almighty God for his favor, grace and protection and to my parents, for their love and assistance.

TABLE OF CONTENTS

PERMISSION TO USE ….....……...…….....…. i

ABSTRACT ……...…….…….……...….. ii

ACKNOWLEDGEMENTS …….…….…….…… iv

DEDICATION …….……...…….……..…….... v

TABLE OF CONTENTS ……...…….……...…..... vi

LIST OF TABLES ……...……...…….……..... x

LIST OF FIGURES ……..…….……...…….... xi

LIST OF ABBREVIATIONS AND SYMBOLS …….……...…..... xiv

CHAPTER 1: INTRODUCTION ……...…….……..…...…….. 1

1.1 Overview …….……...…….. 1

1.2 Objectives …….……...…… 2

1.3 Thesis organization …….……..……. 3

CHAPTER 2: LITERATURE REVIEW…….……..…… 4

2.1 An overview of composite ……..……..…… 4

2.2 Particulate reinforcements ……...……..…….…… 5

2.3 Mineral (limestone) calcium carbonate …….……...….... 5

2.4 Bio calcium carbonate fillers (eggshells) …….…….……. 5

2.4.1 Sources of eggshell waste .……...….. 6

2.4.2 Current uses of eggshell waste …….…….…..... 7

2.4.3 Porosity of eggshells …….……..… 9

2.5 Seashell ……..... 10

2.6 Mechanism of stearic acid surface treatment of $CaCO_3$ fillers …….…….……..... 10

2.7 Thermosetting polymers..…..……..... 13

2.7.1 Synthetic epoxy ……..... 13

2.7.2 Bio-based epoxy ……..... 13

2.8 Mechanical properties of calcium carbonate based/epoxy composites ……..... 14

2.8.1 Epoxy/untreated limestone composites 14
2.8.2 Epoxy/untreated eggshell composites 15
2.8.3 Epoxy/untreated seashell composites..... 17
2.9 Effect of stearic acid treatment on the mechanical properties of calcium carbonate/epoxy composites 17
2.10 Effect of filler content on the density of epoxy composites 18
2.11 Effect of $CaCO_3$ fillers on the glass transition temperature of epoxy composites (thermal property) 18
2.11.1 Mineral limestone 19
2.11.2 Bio-limestone 19
2.12 Microstructural examination of fractured epoxy composites 20
2.12.1 Calcium carbonate filler materials..... 20
2.12.2 Epoxy composite fractured surfaces 20
2.13 Summary 21

CHAPTER 3: MATERIALS AND EXPERIMENTAL METHODS 23

3.1 Materials 23
3.1.1 Eggshell powder preparation 23
3.2 Characterization of eggshell powder 24
3.2.1 X-ray diffraction analysis (XRD) 24
3.2.2 Chemical composition of ES 25
3.2.3 Microstructural analysis 25
3.2.4 Density measurements 26
3.2.5 Particle size analysis 27
3.2.6 Surface modification of $CaCO_3$ powders (ES and LS) using stearic acid 28
3.3 Preparation of composites 29
3.3.1 Preparation of silicone rubber molds 29
3.3.2 Manufacture of bio-epoxy/ES and bio-epoxy/LS composites 30
3.4 Characterization of bio-epoxy/ES and bio-epoxy/LS composites 32
3.4.1 Tensile tests of composites 32
3.4.2 Flexural tests of composites 34

3.4.3 Charpy impact tests of composites 35
3.4.4 Density measurement..... 36
3.4.5 Void content of the composites 38
3.4.6 Water absorption test 38
3.4.7 Thermal analysis 39
3.4.8 Statistical analysis 39

CHAPTER 4: RESULTS AND DISCUSSION 41

4.1 Characterization of ES powder 41
4.1.1 Chemical composition of ES 41
4.1.2 X-ray diffraction analysis 41
4.1.3 Microstructural examination 43
4.1.4 Particle density measurement 44
4.1.5 Particle size analysis 46
4.2 Mechanical characterization of the composites 47
4.2.1 Tensile properties of the composites 47
4.2.2 Fractography of fractured tensile specimens..... 50
4.2.3 Flexural properties of the composites 51
4.2.4 Fractography of fractured flexural specimens..... 54
4.2.5 Charpy impact toughness of the composites 56
4.2.6 Fractography of fractured Charpy impact specimens 58
4.3 Effect of filler addition on the bulk density of bio-epoxy resin 61
4.4 Void content of the composites 62
4.5 Water absorption tests 63
4.6 Thermal analysis 67
4.7 Economic analysis 68
4.7 Statistical analysis 69

CHAPTER 5: CONCLUSIONS AND RECOMMENDATIONS 74

5.1 Conclusions 74
5.2 Recommendations for future work 76

REFERENCES ……..……..…….....……. 77

LIST OF TABLES

Table 2.1	$CaCO_3$ composition of eggshell.	6
Table 2.2	Annual egg production by the top thirty one countries.	8
Table 3.1	Properties of Super Sap CPM epoxy and CPL hardener.	23
Table 3.2	Formulation of filler in the bio-epoxy composites.	32
Table 4.1	Particle density of ES, LS and stearic acid treated ES and LS fillers.	45
Table 4.2	Density and void content of bio-epoxy composites with different filler loadings.	62
Table 4.3	Onset, midpoint and end temperature of bio-epoxy composites.	68
Table 4.4	Results of two-way analysis of variance of the effect of SA treatment and filler loading (ES and LS) on the tensile strength of bio-epoxy resin.	70
Table 4.5	Results of two-way analysis of variance of the effect of SA treatment and ES loading on the flexural strength and flexural modulus of bio-epoxy resin.	71
Table 4.6	Results of two-way analysis of variance of the effect of SA treatment and LS loading on the flexural strength and flexural modulus of bio-epoxy resin.	72
Table 4.7	Results of three-way analysis of variance of the effect of SA treatment, filler loading (ES and LS) and temperature on the Charpy impact toughness of bio-epoxy resin.	73

LIST OF FIGURES

Figure 2.1	A flow chart for the classification of polymer matrix composites.	4
Figure 2.2	Global pie chart of eggs produced annually (2017).	7
Figure 2.3	Structure of an eggshell.	10
Figure 2.4	Schematic representation of SA treatment of $CaCO_3$ particles.	12
Figure 3.1	A photograph of the procedure of converting as-received eggshells to eggshell fillers. (a) as-received eggshells (b) coarse grinding and (c) fine ball milling.	24
Figure 3.2	A photograph of (a) Rigaku Ultima IV powder X-ray diffractometer and (b) specimen in in the equipment sample holder.	25
Figure 3.3	A photograph of (a) Ohaus Precision Model TS400D weighing scale and (b) helium gas Micromeritics Accupyc 1340 pycnometer.	26
Figure 3.4	A photograph of Malvern Mastersizer S (long bench) laser particle size analyzer dry powder feeder.	27
Figure 3.5	A photograph of (a) stearic acid filler solution being filtered (b) dried agglomerated stearic acid coated filler on the filter paper.	29
Figure 3.6	A photograph of (a) plastic mold with aluminum tensile samples and (b) prepared silicone mold for tensile samples.	30
Figure 3.7	A photograph of the ultrasonic homogenizer sonicator with liquid composite.	31
Figure 3.8	A photograph of (a) CPM epoxy and CPL hardener (b) ES or LS filler and (c) cured bio-epoxy/ES or LS composites.	31
Figure 3.9	An AutoCAD image of dog-bone shaped specimens for tensile test (dimensions in mm).	33
Figure 3.10	A digital image of (a) cured tensile composite sample (b) composite sample fractured by Instron tensile machine.	34
Figure 3.11	A photograph of the Charpy impact test machine.	35
Figure 3.12	A photograph of the Tenney TJR temperature chamber used to condition specimens prior to Charpy impact toughness test.	36
Figure 3.13	A photograph of the apparatus used for determining composite bulk density.	37
Figure 3.14	A digital image of DSC Model 2910 V4.4E used in determining the Tg of the composites.	39

Figure 4.1	XRD diffraction pattern of (a) ES (b) SA treated ES (c) LS (d) SA treated LS and (e) stearic acid (SA) particulates.	42
Figure 4.2	SEM micrographs showing morphologies of: (a) ES, (b) LS, (c) SA treated ES and (d) SA treated LS particles.	43
Figure 4.3	SEM micrographs of (a) ES showing the presence of pores (b) SA treated ES with the absence of pores and (c) LS with the absence of pores (d) SA treated LS with the absence of pores.	44
Figure 4.4	Particle density of ES, LS and stearic acid treated ES and LS.	45
Figure 4.5	The particle size distribution curves for ES and SA treated ES.	46
Figure 4.6	The particle size distribution curves for LS and SA treated LS.	47
Figure 4.7	Effect of ES, LS and stearic acid treated ES and LS loadings on the tensile strength of bio-epoxy composite.	49
Figure 4.8	SEM micrographs of tensile fractured surfaces of (a) unfilled bio-epoxy resin, (b) 5 wt. % ES loading, (c) 20 wt. % ES loading, (d) 5 wt. % LS loading and (e) 20 wt. % LS loading.	50
Figure 4.9	SEM micrographs of tensile fractured surfaces of (a) 5 wt. % SA treated ES loading, (b) 20 wt. % SA treated ES loading, (c) 5 wt. % SA treated LS loading and (d) 20 wt. % SA treated LS loading.	51
Figure 4.10	Effect of ES, LS and stearic acid treated ES and LS loadings on the flexural strength of bio-epoxy composites.	53
Figure 4.11	Effect of ES, LS and stearic acid treated ES and LS loadings on the flexural modulus of bio-epoxy composites.	54
Figure 4.12	SEM micrographs of flexural fractured surfaces of (a) unfilled bio-epoxy resin, (b) 5 wt. % ES loading, (c) 20 wt. % ES loading, (d) 5 wt. % LS loading and (e) 20 wt. % LS loading.	55
Figure 4.13	SEM micrographs of flexural fractured surfaces of (a) 5 wt. % SA treated ES loading, (b) 20 wt. % SA treated ES loading, (c) 5 wt. % SA treated LS loading and (d) 20 wt. % SA treated LS loading.	55
Figure 4.14	Effect of filler loading on the impact energy absorbed for bio-epoxy composites at 23 °C.	56

Figure 4.15	Effect of filler loadings on the impact energy absorbed for bio-epoxy composites at -40 °C.	58
Figure 4.16	SEM micrographs of Charpy impact fractured surfaces at room temperature for (a) unfilled bio-epoxy resin, (b) 5 wt. % ES loading, (c) 20 wt. % ES loading, (d) 5 wt. % LS loading and (e) 20 wt. % LS loading.	59
Figure 4.17	SEM micrographs of Charpy impact fractured surfaces at room temperature for (a) 5 wt. % SA treated ES loading, (b) 20 wt. % SA treated ES loading, (c) 5 wt. % SA treated LS loading and (d) 20 wt. % SA treated LS loading.	60
Figure 4.18	SEM micrographs of Charpy impact fractured surfaces at – 40 °C for (a) unfilled bio-epoxy resin, (b) 5 wt. % ES loading, (c) 20 wt. % ES loading, (d) 5 wt. % LS loading, and (e) 20 wt. % LS loading.	60
Figure 4.19	SEM micrographs of Charpy impact fractured surfaces at – 40 °C for (a) 5 wt. % SA treated ES loading, (b) 20 wt. % SA treated ES loading, (c) 5 wt. % SA treated LS loading and (d) 20 wt. % SA treated LS loading.	61
Figure 4.20	Effect of untreated ES and LS filler content on the water absorption of bio-epoxy composites.	64
Figure 4.21	Effect of SA treated ES and LS filler content on the water absorption of bio-epoxy composites.	65
Figure 4.22	Effect of 5 wt. % ES and LS filler content (untreated and SA treated) on the water absorption of bio-epoxy composites.	65
Figure 4.23	Effect of 10 wt. % ES and LS filler content (untreated and SA treated) on the water absorption of bio-epoxy composites.	66
Figure 4.24	Effect of 20 wt. % ES and LS filler content (untreated and SA treated) on the water absorption of bio-epoxy composites.	66
Figure 4.25	A DSC thermograph showing the effect of 5 wt. % ES, LS and SA treated ES and LS fillers on the T_g of bio-epoxy composites.	67

LIST OF ABBREVIATIONS AND SYMBOLS

ABBREVIATIONS

b	Flexural sample width (mm)
d	Flexural sample thickness (mm)
Df	Degree of freedom
DSC	Differential scanning calorimeter
E_f	Flexural modulus (GPa)
E_a	Impact energy (J)
BE	Bio-epoxy
BE/ES	Bio-epoxy/eggshell
BE/LS	Bio-epoxy/limestone
SA	Stearic acid
L	Length of support span (mm)
L_o	Gauge length (mm)
m	Slope of the load-deflection curve
MS	Mean square
P	Flexural load (N)
RH	Relative humidity
RT	Room temperature (23 °C)
SEM	Scanning electron microscope
SS	Sum of squares
T_g	Glass transition temperature (°C)
XRD	X-ray diffraction
v_p	Volume fraction of filler
v_m	Volume fraction of matrix
W_p	Weight fraction of filler
W_m	Weight fraction of matrix
M_a	Weight in air
M_w	Weight in liquid

SYMBOLS

ρ_c	Density of composite (gcm^{-3})
ρ_m	Density of matrix (gcm^{-3})
ρ_p	Density of filler (gcm^{-3})
ρ_d	Density of liquid (gcm^{-3})
σ_f	Flexural strength (MPa)

CHAPTER 1

INTRODUCTION

1.1 Overview

Composites are materials formed from a combination of two or more materials in which the material formed is of better properties than the individual materials used alone [1]. They are produced by reinforcing a matrix material either polymeric, metallic or ceramic with particles, fibers or whiskers [1,2]. They are widely used in aerospace, automobile and other industrial applications [3].

In recent years, there has been an increased use of polymer reinforced composites in structural applications due to their light weight, high specific stiffness and high strength. This presents polymer composites as alternatives to metals in several structural applications. The polymer market is dominated by commodity plastics, in which 80 % of the raw materials used in their production is based on non-renewable petroleum resources [4]. In contrast, bio-based resins are synthesized from renewable sources such as modified plant oils, sugars, polyphenols, and terpenes [5], with some resins having about 31-55 % bio-content [6–9]. Consequently, this has led to bio-based polymers serving as alternatives to synthetic polymers. A common bio-based thermoplastic polymer studied is bio-polyethylene [10], while a bio-based thermosetting polymer is bio-epoxy [7,8,11]. Generally, epoxy is more widely used than other thermosets in various applications due to its characteristic simple processing techniques, better performance at elevated temperature, and superior strength. For example, despite epoxy being more expensive than other polymer matrices, more than two-thirds of the polymers used in aerospace applications are epoxy based [12].

As a result of increased use of polymers, low cost fillers can be added to reduce cost and improve their properties. Limestone (LS) derived from sedimentary rock is the most widely used inorganic filler for polymers due to their low cost, abundance, high calcium carbonate ($CaCO_3$) content, and chemical stability up to 800 ℃. Waste chicken eggshells (ES) consist of several layers namely cuticle (outer layer), testa (calcium carbonate layer) and mammillary layer (inner layer) [13]. The major component of ES is $CaCO_3$. Chemical analysis of ES showed it contains 94-96 wt. % $CaCO_3$, 3-4 wt. % organic matter and minor traces of magnesium and phosphorus [10,14,15].

Other wastes such as seashells (e.g. marine mollusks, mussels, shellfish, oysters, scallops, and cockles) were reported to contain high $CaCO_3$ content in the range of 92-99 wt. % [11,19–26]. Large quantities of ES waste from egg breaking plants are dumped in landfills. It is worthwhile to acknowledge the biodegradability of ES and its decomposing effect, but their disposal emits toxic and harmful gases such as ammonia (NH_3) and hydrogen sulfide (H_2S) which can be harmful to the environment and cause diseases to human [16,17]. Large costs are equally associated with their disposal. Companies in the United States of America spend approximately US $100,000 annually to dispose ES at landfills [18]. Diverting this waste to novel applications would reduce the large disposal cost, the negative effect of their disposal on the environment, and partially reduce quarry and underground exploration of sedimentary rocks. Several studies have been conducted on the use of waste materials with high $CaCO_3$ contents as fillers for polymer composites to improve their properties. Fombuena et al. [11] reported a 47 % increase in flexural modulus with 30 wt. % loading while the Charpy impact toughness decreased by 84 % with 5 wt. % loading in GreenPoxy/ground seashell composites. Similarly, Tiimob et al. [8] reported approximately an 8 % increase in flexural strength and 11 % increase in flexural modulus when 5 wt. % filler (nano ES) was added to a Super Sap bio-epoxy.

The use of a solution mixing method to produce sustainable bio-epoxy/$CaCO_3$ composite materials was investigated in this study. The aim of this work is to fabricate and evaluate the physical, mechanical and thermal properties of bio-epoxy resins reinforced with varying amounts of ES and LS fillers.

1.2 Objectives

The goal of this study is to produce and characterize bio-epoxy matrix composites filled with calcium carbonate based fillers (ES and LS) for structural applications. To achieve this goal, the following objectives were pursued:

1. Determine the effect of varying filler content (5, 10, and 20 wt. %) of untreated ES and LS on the physical (density, water absorption), mechanical (tensile, flexure, Charpy) and thermal properties (glass transition temperature) of bio-epoxy matrix composites.

2. Determine the effect of stearic acid treatment of ES and LS fillers on the physical, mechanical and thermal properties of the composites mentioned in objective 1.
3. Determine the amount of $CaCO_3$ filler that can be recovered from waste ES in Canada.

The major research contribution of this study is the information provided on the effect of high loading of untreated and SA treated ES fillers on the properties of bio-based epoxy resin.

1.3 Thesis organization

This thesis contains five chapters. Chapter 1 contains an overview of the study, objectives and research contributions. A review of previous works on epoxy calcium carbonate based composites is presented in Chapter 2. In Chapter 3, the experimental materials and procedures adopted in this research are outlined. The research results obtained from tests conducted in Chapter 3 are presented and discussed in Chapter 4. The conclusions from the analysis of test results and recommendations for future work are presented in Chapter 5.

CHAPTER 2
LITERATURE REVIEW

A review of previous and related studies on various forms of $CaCO_3$-based filler materials ((e.g. eggshell (ES), limestone (LS), and seashell)) and their uses in thermoset epoxy polymer composites are presented in this Chapter.

2.1 An overview of composite materials

The goal of combining different materials to form a composite material is to attain properties superior to the properties of the individual materials that make up the composite. In general, composite materials are utilized in several applications such as aerospace, automobile, and construction due to their low weight and improved properties. The combination of different materials to produce a composite is often responsible for their improved properties such as strength, stiffness, and thermal stability. A composite material consists of two major components: the matrix and the reinforcement [1]. Basically, matrix materials are classified into three categories: polymer, metal, and ceramic. The matrix holds the reinforcement together, while reinforcements carries the majority of the load. The reinforcing materials can be particles, fibers or whiskers as shown in Figure 2.1.

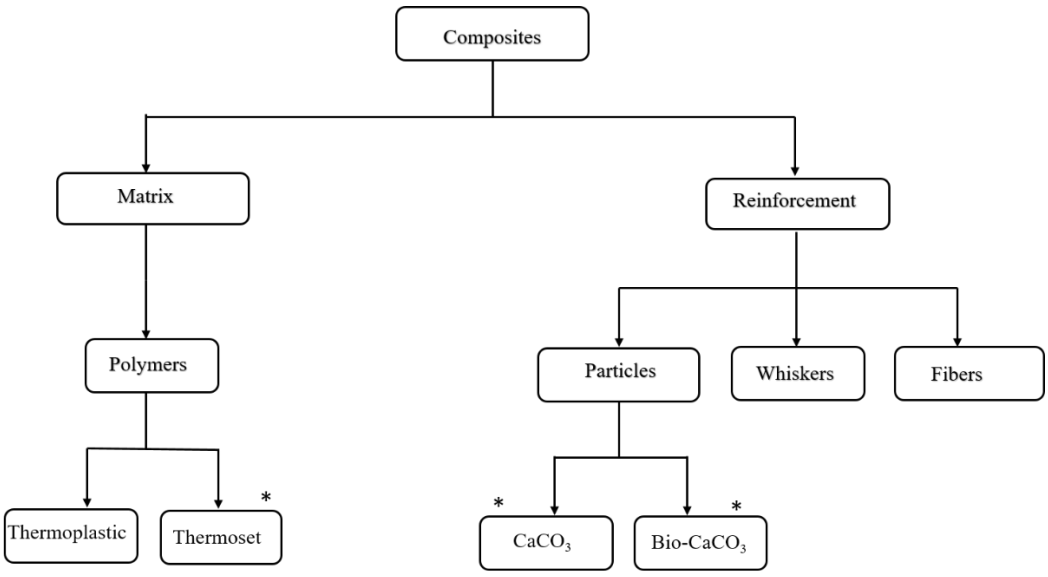

Figure 2.1. A flow chart for the classification of polymer matrix composites (* indicates the materials used in this study).

2.2 Particulate reinforcements

The most commonly used filler (particle) for reinforcing polymer is $CaCO_3$ derived from LS. They serve as reinforcements and fillers to polymer matrices by improving their properties. Strengthening with this form of reinforcement is dependent on particle size and uniform distribution across the matrix since this powdered substance ranges from nano- to macro-sized [2,27,28]. Particles bear a fraction of the load being transferred by the matrix provided a good bonding is formed between the particles and matrix [27]. Evenly distributed particles within the matrix form a strong bond with the matrix as opposed to agglomerated particles [27]. Beside mined LS, waste materials containing high $CaCO_3$ contents are found in chicken eggshells and various seashells. Finding new uses for these discarded materials have led to studies for their utilization as fillers in polymer composites.

2.3 Mineral (limestone) calcium carbonate

LS is a sedimentary rock mainly composed of $CaCO_3$. It exists in various forms such as marble and chalk and are often extracted via quarry or underground mining. The density of natural limestone ranges from 2.5-2.71 g/cm^3 [29,30]. Its major application in engineering materials have been for fillers in polymer composites [31], as well as raw materials for cement and mortars [29].

2.4 Bio calcium carbonate fillers (eggshells)

A chicken ES is the hard outer layer of an egg, which can be brown or white coloured [32]. By weight, a chicken egg comprises of 60 % albumen (white colored substance), 30 % yolk (the yellow colored substance) and 10-11 % shell (eggshell and membrane) [33]. The total weight of an egg was reported to be between 60.0-60.2 g [34,35], while the empty shell weight ranges between 6.6-7.3 g [33,34]. Small percentage of organic matter is contained in the shell which has been reported to be about 3-4.5 wt. % [14,34–37]. The density of the ES with membrane was reported by various studies to range from 2.50 to 2.62 g/cm^3 [14,15,37,38]. The density of the membrane was reported to be approximately 1.36 g/cm^3 [37].

The chemical composition of ES consist mainly of $CaCO_3$ in the form of calcite ranging from 94 to 98 wt. % with minor traces of other elements such as magnesium and phosphorus, and 3-4 wt. % organic matter [14,15,37,38]. Some of the reported $CaCO_3$ contents are summarized in Table

2.1. The composition of ES may vary according to the feed of the chicken consumed and contamination from the inner membrane [10]. Studies reported that brown ES contain 96-97 wt. % $CaCO_3$ and 3-4 wt. % organic matter [15,39] while white ES were found to have 94 wt. % $CaCO_3$ content with 6 wt. % organic matter [35,40]. On the basis of reported findings, the $CaCO_3$ content in both brown and white ES were considered equivalent [14].

Table 2.1. $CaCO_3$ composition of eggshell.

$CaCO_3$ content (wt. %)	Eggshell density (g/cm^3)	References
94.00	2.53	[37]
96.41	2.59	[15]
97.30	2.62	[38]
97.80	2.50	[14]

2.4.1 Sources of eggshell waste

Households and restaurants are not viable sources of waste eggshells; they are obtained from the egg breaking plant industry referred to as 'breaker plants' [13]. The first known egg breaking plant was set up in 1928 in the United States of America (USA) before World War II [41]. In this process, the liquid egg is mechanically separated from the shells, which leads to ES being obtained in larger quantities. Eggs are classified into sizes and standards where below standard eggs (e.g. deformed, too small) not suitable for the general market are sent to breaker plants while quality medium, large and extra-large eggs are sent market. A modern breaker plant can process 188,000 eggs per hour [13]. The top ten egg producing countries are shown in Figure 2.2 and Table 2.2. It is estimated that roughly 30 % of eggs produced in the developed countries are sent to breaker plants for processing into liquids [42]. The possible total amounts of $CaCO_3$ from eggshell waste that could be recovered for uses in a variety of applications are summarized in Table 2.2. The amount of $CaCO_3$ recovered in kilograms (kg) are based on one empty eggshell weight of approximately 6.6 g, which is approximately 10 % of the whole egg. For example, China's annual production of eggs in 2017 was 536,818,007,000. Of this amount 30 % amount to 161,045,402,000 eggs. Based on the empty shell weighing 6.6 g, about 1,062,899,654,000 g or 1,062,899,654 kg of

$CaCO_3$ could be recovered. To put this into perspective, this can be ~ 35,429,988 bags of $CaCO_3$ each weighing 30 kg can be recovered from ES waste annually for use in various applications.

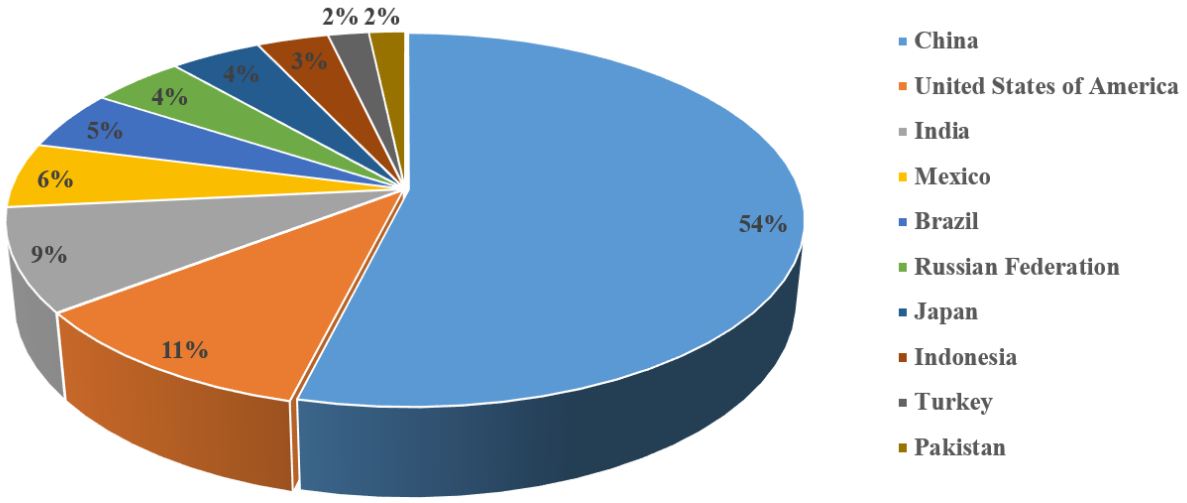

Figure 2.2. Global pie chart of eggs produced annually (2017). The data for this plot were extracted from [43].

2.4.2 Current uses of eggshell waste

Researchers have worked towards making ES waste suitable for various applications. For example, ES have been suggested for use as effective adsorbents for the removal of organic and inorganic hazardous chemicals from wastewater [37]. Waste ES have been used in the removal of divalent metal ions such as lead, cadmium, and copper from aqueous solutions and as alternative to LS for immobilization of heavy metals in soils [44–46]. Due to their high calcium and nitrogen contents, they are often used as agricultural fertilizers [47,48] to correct the pH of acidic soils [49]. They have also been used as animal feed for poultry by heating at approximately 80 °C to minimize microbiological contamination and subsequently crushed and milled to obtain fine particles [47]. In addition, powdered ES have been used as pharmaceutical excipients, food additives, and calcium supplements [48]. ES have also found uses as fillers in cement mortar [10] and polymer composites [14] as they have been reported to be an alternative source of $CaCO_3$.

Table 2.2. Annual egg production by the top thirty-one countries.

Country	Number of eggs produced annually in 2017* [43]	30 % of eggs are sent to breaker plants*	Amount of $CaCO_3$ recuperated (kg)
China	536,818,007	161,045,402	1,062,899,654
USA	106,688,700	32,006,610	211,243,626
India	88,137,000	26,441,100	174,511,260
Mexico	55,418,430	16,625,529	109,728,491
Brazil	43,352,883	15,283,022	100,867,948
Russia	44,351,037	13,305,311	87,815,053
Japan	43,352,883	13,005,865	85,838,708
Indonesia	33,940,000	10,182,000	67,201,200
Turkey	19,281,196	57,84,359	38,176,768
Pakistan	17,083,000	5,124,900	33,824,340
France	15,916,667	4,775,000	31,515,001
Ukraine	15,350,700	4,605,210	30,394,386
Malaysia	14,293,061	4,287,918	28,300,261
Spain	13,503,425	4,051,028	26,736,782
Colombia	13,316,667	3,995,000	26,367,001
Italy	13,220,000	3,966,000	26,175,600
Korea	13,000,000	3,900,000	25,740,000
Argentina	12,987,100	3,896,130	25,714,458
United Kingdom	12,885,000	3,865,500	25,512,300
Germany	12,086,893	3,626,068	23,932,048
Iran	12,040,000	3,612,000	23,839,200
Myanmar	11,700,000	3,510,000	23,166,000
Nigeria	11,300,000	3,390,000	22,374,000
Thailand	11,000,000	3,300,000	21,780,000
Netherlands	10,902,000	3,270,600	21,585,960
Poland	10,693,517	3,208,055	21,173,164
Vietnam	10,637,100	3,191,130	21,061,458
Bangladesh	10,453,170	3,135,951	20,697,277
Philippines	10,049,000	3,014,700	19,897,020
South Africa	10,000,000	3,000,000	19,800,000
Canada	9,150,000	2,745,000	18,117,000

(* values multiplied by 1000)

If eggshells are heated above 750-800 °C, the $CaCO_3$ is transformed into calcium oxide (CaO) for the production of lime by chemical industries [49,50]. ES has been used as a substitute to mineral $CaCO_3$ for the treatment of white paper to improve opacity, strength, appearance, brightness and texture [49,51]. Also, calcination of ES to obtain less expensive solid catalyst utilized in the production of bio-diesels by the transesterification of vegetable oils with methanol [52]. Hydroxyapatite have been derived from ES, which offers a potential application as components for bone implants, fillers in teeth, repair of hard tissues, bones augmentation and catalysts for bone repair [53–55]. The organic membrane of eggshells is composed of glycoprotein (type I, V and X collagen) [49] and has found uses in the production of cosmetics.

2.4.3 Porosity of eggshells

The ES is composed of three layers, namely: a thin film (10 µm) layer of cuticle (outer layer), testa (calcium carbonate layer), and mammillary layer (inner layer) [13,37] as shown in Figure 2.3. The outer layer consists of the thickest layer of the eggshell called the palisade layer (spongy layer) [13]. The shell membrane is the layer between the albumen and inner shell surface and it has a thickness of 100 µm [37,56]. The cuticle (dried mucus) protects the embryo from bacterial infection and moisture loss, while the mammillary layer serves as a foundation to the testa which provides calcium and aids in coloration to the growing egg [37,57]. Cuticle and mammillary layers form a matrix composed of protein fibers that are bonded to the calcium carbonate (calcite) crystal [37,58]. Testa layer is composed of 95 wt. % inorganic substance, mainly $CaCO_3$, 3.3 wt. % protein, and 1.6 wt. % moisture [59].

One chicken ES contains about 7,000 to 17,000 unevenly distributed circular pore openings naturally present to allow exchange of oxygen and carbon dioxide (CO_2) from the baby chicken and transpiration of water throughout the shell [56,60]. These pores are covered by the cuticle [13]. Betancourt and Cree [61] compared SEM images of ES powders with LS powders and observed a more porous structure for ES compared to LS. This study also investigated water absorption behavior of ES powder fillers in a polymer matrix and observed that the porous structure of ES led to the composite absorbing more water than LS composites [61]. The authors suggested the increase in water absorption may be attributed to the porous surface of the ES.

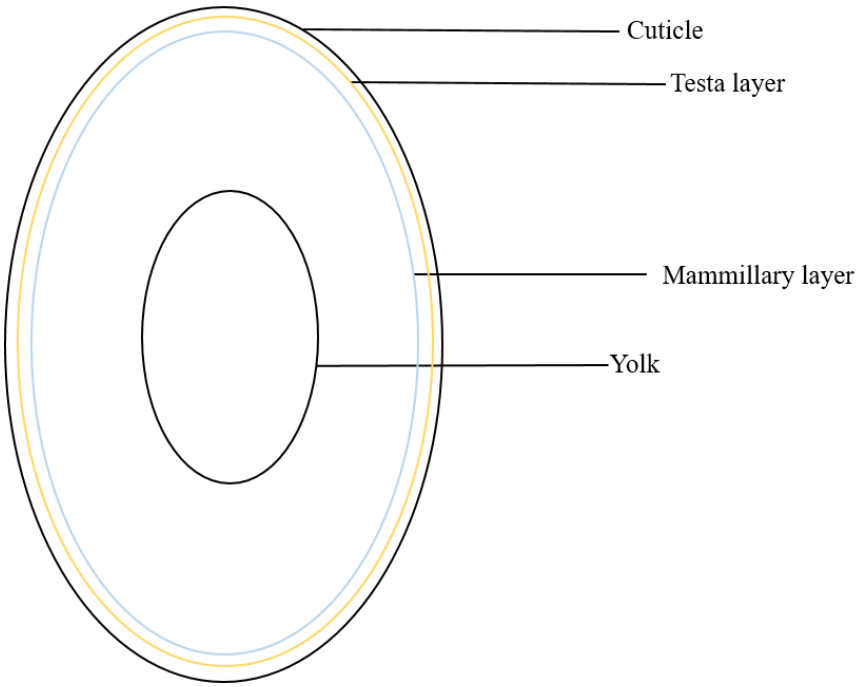

Figure 2.3. Structure of an eggshell.

2.5 Seashell

A seashell can be defined as the hard outer layer from the body of an animal that lives in the sea, lakes and rivers such as marine mollusks, mussels, shellfish, oysters, scallops, cuttlebone, and cockles. These aquatic animals are food proteins extensively consumed by humans and their shells are widely disposed to landfills [23]. The chemical composition of seashells were found to consist mainly of bio-$CaCO_3$ in the range of 92-99 wt. % [11,19–26] with about 5 wt. % organic matter [62]. Many studies on the use of seashell waste have reported the CaO contents rather than the $CaCO_3$ contents [24,63–69]. The removal of organic material from seashells may be more difficult than removal from eggshells or perhaps, this is performed to remove organic materials to obtain a purified form prior to using in an application. The densities of dried seashells (may contain dried organic material) were reported to be 1.33 g/cm^3 (mussel shell) [19] and 1.15-2.62 g/cm^3 (oyster shell) [21,25,67].

2.6 Mechanism of stearic acid surface treatment of $CaCO_3$ fillers

The problem of agglomeration of fine filler particulate reinforcements such as $CaCO_3$ powders added to polymers has been identified in many studies [31,70–72]. Different approaches have been used to reduce agglomeration of particles such as ultrasonication [73], treatment using fatty acids

(e.g. stearic acid (SA)) [31], anionic dispersant (surfactant) [74,75] and the use of silane coupling agents to promote the bonding between the matrix and fillers [76]. Despite $CaCO_3$ being the most widely used inorganic filler for polymers, its hydrophilic characteristics is a problematic issue limiting their wide use in the industry [77]. Polymers are hydrophobic while $CaCO_3$ fillers are hydrophilic. In addition, due to high surface energy, van der Waals and electrostatic forces are induced between $CaCO_3$ particles, which tend to agglomerate in powder form [78]. The agglomeration of particle fillers in polymer composites cause micro-cracks which lead to brittle fractures [38,71]. Hence, good dispersion of fillers minimizes or may prevent agglomeration to attain improved mechanical properties. In an effort to enhance dispersion of fillers and improve bonding at the interface between matrix and filler, SA has been used to modify the $CaCO_3$ powder surface before dispersion in the matrix. This treatment process has been suggested to minimize agglomeration of $CaCO_3$ particles, thus leading to improved properties [72,79,80].

Stearic acid is a universal and inexpensive fatty acid often used to improve hydrophobic properties of $CaCO_3$ [81,82]. It is made up of two parts, namely: a hydrophobic tail and a hydrophilic head [31]. There are two major treating techniques used to coat $CaCO_3$ powders with SA, which are the dry and wet treatment methods. The dry treatment process involves the addition of SA to $CaCO_3$ with the use of high shear mixing at a higher or same melting temperature of SA [83]. The wet method involves adding a concentrated aqueous (ethanol) suspension of dissolved SA to a hot aqueous slurry (water or ethanol) of $CaCO_3$ [31,79]. These chemical treatments create a hydrophobic layer on the surface of the $CaCO_3$ particles from the chemical reaction of the SA and calcium cation [31,84,85], thus making $CaCO_3$ powder hydrophobic as shown in Figure 2.4. A novel treatment process, referred to as the complex treatment method, was introduced by Cao et al. [31]. This method is similar to the wet treatment method but permits higher percentages of SA and calcium cation reactions to take place. The authors compared the effects of the three methods (e.g. dry, wet, and complex) on the properties of $CaCO_3$ added to high density polyethylene (HDPE) and reported better mechanical properties for wet and complex treatment methods.

The quantity of SA required to coat $CaCO_3$ powders to attain desirable properties for polymer composite was investigated by Mihajlović et al. [85]. They studied the effect of different weight percentages of SA (0.5-4 wt. %) on the surface properties of calcite fillers. The authors reported

an optimal amount required to cover the calcite surface with a monolayer of organic molecules ranged between 1.5 and 2 wt. %.

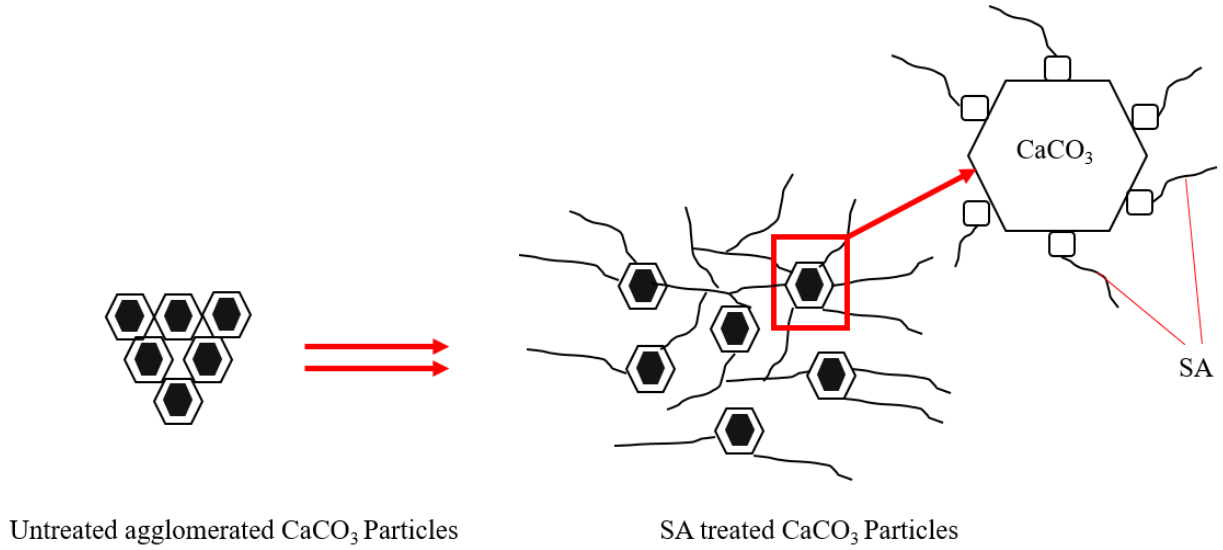

Figure 2.4. Schematic representation of SA treatment of $CaCO_3$ particles.

The effect of the surface modification was evaluated using the active ratio method which compared the active ratio value with different wt. % of SA treatment. The higher the active ratio, the better the effect of surface modification [86]. They reported an increase in the active ratio from 65.50 % at 0.5 wt. % SA concentration to 99.90 % at 1.5-2 wt. %. The authors suggested any addition in excess of 2 wt. % SA concentration may deteriorate the properties due to lower active ratios. In a similar study, Shah et al. [70] optimized the condition for effectively modifying ES powder with SA and the best concentration, treatment time and temperature for improved mechanical properties was determined to be 2.5 wt. % SA, 50 min and 85 °C, respectively for synthetic epoxy composite. Furthermore, Osman et al. [87] determined the effect of coating concentrations of SA (1- 3 wt. %) onto $CaCO_3$ fillers (1.8 µm) and adding them to low density polyethylene (LDPE). The composites were made via compression molding. Composites containing 10-20 vol. % fillers treated with 1-2 wt. % SA had their Young's modulus increased by 11-13 %. However, excess coating above 2 wt. % resulted in a decrease in the Young modulus. The authors suggested the decrease may be due to SA bilayer formation. The amount of SA for this type of composite was recommended to be 2 wt. %.

2.7 Thermosetting polymers

Thermosetting polymers consist of a resin and a compatible hardener (or curing agent) which are cured via chemical reactions [1,88]. Common examples of thermoset polymers are epoxies, polyesters, polyurethanes and phenolics. Curing occurs at room temperature and can further be heated to increase the cross-linking density until it is fully cured [1]. Highly cross-linked resins are relatively rigid and brittle [88]. Thermosets are amorphous polymers that do not present a melting temperature but have a glass transition temperature (T_g). These polymers can be grouped as synthetic (petroleum based) and bio-based depending on the type of raw materials/ingredients used in their production. Generally, epoxy resins are used over other thermosetting polymers due to their ability to produce high performance composites since they can be used in various processing techniques, have excellent strength and good performance at elevated temperature [1].

2.7.1 Synthetic epoxy

Synthetic epoxy resins are synthesized from diglycidyl ether of bisphenol-A (DGEBA), trifunctional epoxy resins, cycloaliphatic epoxies, or diglycidyl ethers of novolac resins [88,89]. They are primarily made from petrochemicals [90]. In formulating epoxy networks, DGEBA represents approximately 90 % of the epoxy precursors in the world production [91]. More than 67 % of the molar mass of DGEBA is strongly dependent on fossil resources [92]. Epoxy resins have been used in several applications such as aerospace, electronics (circuit board) in electronic packaging, high performance adhesives (for aircrafts, boats) and decorative flooring (terrazzo) [88]. Globally, 41 % of epoxy resins are produced for coating application, 31 % for adhesives and the remaining 28 % are for other various applications [93].

2.7.2 Bio-based epoxy

Although synthetic epoxy cannot be easily recycled as thermoplastics, producing it using a lower petroleum content is an alternative. Bio-based epoxy resins and their curing agents differ from synthetic epoxies due to the bio-renewable raw materials used in their production. They are obtained/synthesized from renewable natural plant sources such as linseed oil, lactic acid, corn, soy-bean oil, pine and vegetable oils [94]. In an effort to promote environmental sustainability, a percentage of the bio-based contents have been utilized in their production. Common bio-based epoxy resins on the market are Super Sap (Entropy resins) [7,8], Climate change bio-epoxy resin

(Change Climate Pty Ltd.) [95] and GreenPoxy® (Sicomin resins) [11]. Super Sap epoxy, Climate change resin and GreenPoxy® resin contain 31-37 % bio-based content [6–8], 77 % bio-content [95], and 55 % plant sourced content [9], respectively. Subsequently, this has led to bio-based thermoset polymers serving as alternatives to synthetic polymers. This effort is to reduce global dependence on petroleum and further promote sustainable polymer materials [5].

2.8 Mechanical properties of calcium carbonate based/epoxy composites

Several studies have carried out on the mechanical properties of epoxy/$CaCO_3$ based composites. A review on the effect of $CaCO_3$ fillers (mineral LS, ES, and seashells) on the mechanical properties (tensile, flexure, and Charpy) of epoxy polymer-based composites is presented in this section.

2.8.1 Epoxy/untreated limestone composites

Jain et al. [96] investigated the effect of nano-$CaCO_3$ particles (44 nm) filler loading of 2, 4, 6, 8 and 10 wt. % on the mechanical properties of synthetic epoxy. The composites were fabricated via a solution mixing method utilizing an ultrasonic sonicator (30 min) to disperse the filler materials and cured by heating in air at 80 °C (1 h); 100 °C (1 h); 120 °C (1.5 h), and 180 °C (4 h). The flexural strength increased by approximately 1 %, 33 %, 23 %, 17 % and 10 %, respectively. In a similar way, the Charpy impact toughness increased by 21 %, 85 %, 68 %, and 29 %, respectively. However, the Charpy impact toughness decreased by 39 % when 10 wt. % filler was added. The results suggested inclusion of nano-$CaCO_3$ particles decreased the Charpy impact toughness at high filler loading (> 8 wt. %). The authors suggested the decrease in toughness may be due to agglomeration of particles at high filler loadings. In another study, Mishra et al. [97] investigated the effect of nano-$CaCO_3$ (39 nm) fillers on the mechanical properties of synthetic epoxy resin. The composites were made utilizing a magnetic stirrer to disperse the fillers at loadings of 2, 4, 6, 8 and 10 wt. %. The tensile strength, Young's modulus and Charpy impact toughness increased by 9-40 %, 33-197 %, and 137-158 %, respectively. Furthermore, the authors compared the effect of the nano-sized particles with micro-sized particles. Both particle sizes exhibited similar trends in tensile strength, Young's modulus and Charpy impact tests. However, the nano-sized composites showed better improvements in mechanical properties than micro-sized fillers. Li et al. [98] determined the effect of nano-$CaCO_3$ (40 nm) on the mechanical properties of synthetic

epoxy resins containing 2, 4, 6, 8 and 10 wt. % filler loading. The composites were made using a magnetic stirrer to disperse the fillers and cured at room temperature for 4 days. Filler loading of 6 wt. % presented a decrease by 2 % in tensile strength and an increase in Young's modulus, flexural strength, flexural modulus, Charpy impact toughness of approximately 6 %, 3 %, 31 %, and 8 %, respectively. These results suggested that the inclusion of 6 wt. % nano-$CaCO_3$ loadings did not significantly decrease the tensile strength and did not substantially increase the flexural strength. In a similar study, an improvement in the flexural strength and flexural modulus of synthetic epoxy composites containing 0.5, 1.0, 1.5 and 2.0 wt. % $CaCO_3$ fillers was reported by Yang et al. [99]. The composites were produced via a solution mixing method. To aid with dispersion, acetone was added to the epoxy/$CaCO_3$ fillers and sonicated for 30 min. The composites were cured at room temperature and post-cured at 110 °C (1 h), 140 °C (2 h), and at 170 °C (1 h). The composites had approximately 30-89 % and 19-38 % higher flexural strengths and flexural modulus, respectively. In a related study, Shimpi et al. [100] determined the mechanical properties of synthetic epoxy/nano-$CaCO_3$ (10 nm) composites containing 2, 4, 6, 8, and 10 wt. % filler contents manufactured via a solution mixing technique utilizing a magnetic stirrer to disperse the fillers for 1 h and further sonicated for 5 min. The composites were initially cured at 110 °C for 1 h (primary curing), 150 °C for 2 h (secondary curing) and 180 °C for 1 h (post curing). They reported an increase in both tensile strength and Young's modulus with an increase in filler content. The tensile strengths increased by 100 %, 107 %, 133 %, 170 %, and 200 % at 2, 4, 6, 8, and 10 wt. % filler loading, respectively, while the Young modulus improved by 82 %, 86 %, 86 %, 93 %, and 107 %, respectively. The authors suggested the improvement in tensile strength may be due to better interaction between the resin and the filler.

2.8.2 Epoxy/untreated eggshell composites

Ji et al. [101] improved the Charpy impact toughness of synthetic epoxy resins using ES fillers (1-9 µm) by 2, 5, 8 and 10 wt. %. The inner membranes were initially manually removed from the fresh eggshells. Then the eggshells were washed, vacuum dried and ground into powder using a planetary ball mill. The powders were then immersed in 4 wt. % NaOH and dried. The composites were produced via a solution mixing method utilizing a mechanical stirrer and ultrasonic mixing to disperse the fillers in a mixture of acetone and liquid epoxy. After heating to remove the solvent, the mixture was poured into a steel mold coated with a release agent. The composites were cured

at 90 °C for 2 h and at 150 °C for 5 h. The Charpy impact toughness increased by approximately 60 %, 72 %, 45 %, and 27 %, respectively compared to unfilled epoxy. In a related investigation, Mohan and Kanny [38] studied the effect of nano-ES (50 nm) bio-filler in amounts of 1, 2, 3, 4, and 5 wt. % on mechanical properties of a synthetic epoxy resin (LR-20). The ES were washed with water and disinfected with sodium hypochlorite followed by vacuum drying. They were then made into a coarse powder using a blender and 5 wt. % of sodium lauryl surfactant was added to the ES powders in order to enhance the dispersion and adhesion with the epoxy. The ES were then dry ball milled to the final powder size. The composites were made using a resin casting method, in which the resin and fillers were mixed in an electric shear mixer and cast onto a glass mold containing a wax release agent. The composites were cured at room temperature for 24 h. The tensile strength, tensile modulus and impact energy improved by 9-95 %, 23-108 %, and 5-15 %, respectively. The authors suggested the increase in tensile strength was due to the nano-sized particles having better adhesion to the matrix material. Also, the increase in tensile modulus was due to the inclusion of stiffer nanoparticles to the matrix.

Tiimob et al. [8] studied the effect of nano-ES particle (< 100 nm) filler loadings of 1, 2, 3, 4, 5 and 10 wt. % on the flexural properties of a bio-epoxy resin (Super Sap 100/1000). The ES were initially boiled at 100 °C for 6 h, reduced in size using a laboratory blender, washed with water, ethanol and dried. They were further ball milled, washed with ethanol and centrifuged. Ethanol was again added to the eggshell particles, magnetically stirred and irradiated with ultrasound followed by centrifuging and vacuum drying. The composites were fabricated via the solution mixing method utilizing a magnetic stirrer to disperse the filler materials. The mixture was poured into silicone molds, cured at room temperature for 2 h and post-cured at 48.8 °C for 2 h. The test results showed an improvement in both flexural strength and flexural modulus for all composites in comparison to unfilled bio-resin. The flexural strength and flexural modulus improved by 6-31 % and 11-37 %, respectively. The composites exhibited similar trend in both properties for a filler loading of 4 wt. % as the optimum. The authors attributed the improvement to enhanced interaction between the filler and matrix due to hydrogen bonding promoted by amine, carboxylic, and hydroxyl functional groups in eggshells

2.8.3 Epoxy/untreated seashell composites

Periasamy et al. [30] compared the effect of cuttlebone shells (15-25 μm) and commercial $CaCO_3$ (<10 μm) fillers in loadings of 3, 6, 9, 12 and 15 wt. % in a synthetic epoxy resin (Rotex EP 306). Cuttlebones were washed with water, scrubbed with a steel brush and dried, followed by crushing and grinding using a pulverizer. One batch of cuttlebone powders were used as prepared (CB) and another batch were heated to 400 °C for 3 h. The composite was made via a hand lay-up method in which the fillers were added to the epoxy and stirred using a homogenizer. The mixture was poured into a steel mold with an applied release agent and cured at room temperature for 24 h, demolded and post-cured at 80 °C for 4 h. The tensile strengths for epoxy/CB composites increased by 17 %, 38 %, 62 %, 44 % and 31 %, respectively compared to epoxy/heated CB and epoxy/$CaCO_3$ composites which increased by 25 %, 54 %, 72 %, 67 % and 46 % and 4 %, 8 %, 42 %, 13 % and 8 %, respectively. Similarly, the Young's modulus of epoxy/CB and epoxy/heated CB increased by 2 %, 7 %, 9 %, 18 % and 6 %, and 0.2 %, 7 %, 12 %, 27 % and 35 %, respectively. However, epoxy/$CaCO_3$ composites increased by 0.2 %, 6 %, 3 %, and 1 %, and decreased by 7 % at 15 wt. % loading. For all composites, 9 wt. % loading had the best tensile strength while 15 wt. % loading had the highest Young's modulus. In a similar study, Fombuena et al. [11] produced composites with mollusks shells with filler particle sizes of < 250 μm and added them to a bio-epoxy (GreenPoxy 55) in amounts of 5, 10, 20, 30 and 40 wt. %. The mollusks were washed with 4 % NaOH, dried and ground using an ultra-centrifugal mill. The powders were treated with a silane solution to improve the chemical interaction between the filler and the matrix. The composites were made via a solution mixing method where the seashell particles were added to the epoxy resin, homogenized and then poured into a mold and cured at 100 °C for 45 min. The flexural modulus increased by 3 %, 25 %, 53 %, 56 % and 44 % with increase in filler loading. In contrast, the Charpy impact toughness decreased with increase in filler loading by 86 %, 87 %, 90 %, 90 % and 92 %, respectively.

2.9 Effect of stearic acid treatment on the mechanical properties of calcium carbonate/epoxy composites

Shah et al. [70] determined the effect of nano-eggshell (< 500 nm) on the tensile strength properties of synthetic epoxy resin at 15 and 20 wt. % loadings. The inner membranes of the ES were removed

manually, then the shells were boiled in water for 30 min and dried for 24 h at 80 °C. The composites were produced via a solution mixing method utilizing a mechanical stirrer (30 min) at 300 rpm and a sonicator (30 min) to disperse the fillers in the resin. The liquid composites were cured at room temperature for 24 h and post-cured at 90 °C for 2 h. A SA treatment was conducted using the wet treatment method 2.5 wt. % SA concentration. The authors reported a decrease in tensile strength with an increase in filler loading. For example, the tensile strength decreased by approximately 9 % for both untreated and treated composite at 15 wt. % filler loading. Similarly, at 20 wt. % filler loadings, the tensile strength decreased by 11 % and 16 % for untreated and treated composite, respectively. From these results, 15 wt. % filler contents for untreated and treated, presented no significant decrease but 20 wt. % SA treated filler composites presented further reductions in tensile strength. It was further observed that irrespective of the treatment conducted, there was no significant increase in tensile strength.

1.10 Effect of filler content on the density of epoxy composites

Periasamy et al. [30] determined the effect of seashell (cuttlebone) of particle size (5- 25 μm) and mineral LS on the density of synthetic epoxy composites. The composites were made via a hand lay-up method in filler amounts of 3, 6, 9, 12, and 15 wt. %. The addition of seashells and LS were reported to have increased the density of epoxy resin up to a maximum of 15 wt. %. The authors suggested the increase to be due to the inclusion of particles with higher density than the matrix material. For example, at 15 wt. % seashells and LS contents, the experimental density increased by approximately 6 % and 7 %, respectively. Furthermore, the theoretical density of the seashell and LS composites were determined, which indicated an increase of 2-4 % and 3-5 %, respectively over their corresponding experimental densities for all filler loadings. They suggested the increase in theoretical density may have been due to the presence of voids in the as-prepared composites.

2.11 Effect of $CaCO_3$ fillers on the glass transition temperature of epoxy composites (thermal property)

Glass transition temperature (T_g) is the temperature below which plastics changes to glassy state and above which they change to rubbery state [27]. The inclusion of $CaCO_3$ fillers into epoxy polymers has been reported to influence the glass transition temperature of the polymer. To

determine thermal properties such as glass transition temperature, thermal analysis tests are conducted on polymer composites using a differential scanning calorimeter (DSC).

2.11.1 Mineral limestone

Jain et al. [96] determined the effect of nano-$CaCO_3$ (44 nm) (mineral LS) filler loadings on the T_g of synthetic epoxy resin (DGEBA). About 5 mg of the composites in powder form were heated from room temperature to 200 °C at a heating rate 10 °C/min. The T_g was reported to be 58.0 °C, 88.9 °C, 101.3 °C, 113.2 °C, 129.0 °C and 142.0 °C for unfilled epoxy resin containing filler loadings of 0, 2, 4, 6, 8, and 10 wt. %, respectively. This presented an increase in T_g with an increase in filler content. The authors suggested the increase in T_g was due to nano-$CaCO_3$ restricting polymer chain mobility. In a similar study Shi et al. [102] produced an epoxy/$CaCO_3$ composite via a solution mixing method using a mechanical stirrer to disperse the fillers. Only 15 wt. % fillers were tested. The particle size ranged from 100 – 500 nm. The T_g was determined by heating the powdered composites from 30–140 °C at a heating rate 20 °C/min. They reported the T_g of synthetic epoxy resins increased by 5 °C with the inclusion of 15 wt. % nano-$CaCO_3$ filler contents. Another study conducted by Jin et al. [103] determined the effect of 2, 4, 6 and 8 wt. % nano-$CaCO_3$ on the T_g of synthetic epoxy resin. These composites were prepared using both magnetic stirrer (1 h) and sonicator to disperse the fillers and were cured at 110 °C for 1 h (primary curing), at 150 °C for 2 h (secondary curing) and post-cure at 180 °C for 1 h. The T_g was determined by heating the samples from 30 to 300 °C at a heating rate of 10 °C/min. The T_g obtained were 240 °C, 238 °C, 240 °C, 239 °C and 232 °C for 0, 2, 4, 6, and 8 wt. %, respectively. In this study, the authors did not observe significant changes in the T_g of epoxy resins with additions of filler contents up to 6 wt. %. However, a 3 % decrease was reported for 8 wt. %.

2.11.2 Bio-limestone

The effect of seashells (obtained from conch shell of Rapana thomasiana) bio-$CaCO_3$ filler (57 µm) on the T_g of synthetic epoxy was determined by Mustata et al. [104]. The seashell fillers were firstly heated to 600 °C to remove organic material. The composites were fabricated using a magnetic stirrer and sonicator (twice for 5 min) to disperse the fillers and were cured at 140 °C for 1 h and post-cured at 240 °C for 4 h. In determining the T_g, the fine powder composites were heated up to 300 °C at a heating rate of 5 °C/min. The inclusion of this bio-filler resulted in an

increase in the T_g with increase in filler content. For example, the T_g of 0, 5, 10, and 15 wt. % filler loadings were reported to be 105 °C, 120 °C, 121 °C and 116 °C, respectively. The authors noted a decrease occurred when more than 10 wt. % filler loadings were added. This could be due to the high filler concentrations causing a restriction on chain mobility. From these results, the T_g improved by approximately 10 -15 % for 5, 10 and 15 wt. % filler loadings, respectively.

2.12 Microstructural examination of fractured epoxy composites

The morphology of the filler materials and the fractured surfaces of epoxy/$CaCO_3$ composites subjected to tensile, flexure and Charpy impact have been determined using secondary electron microscopy (SEM).

2.12.1 Calcium carbonate filler materials

Boronat et al. [10] examined and compared the morphology of ES and commercial mineral LS powders using SEM. The micrographs showed ES particles having irregular shapes and rough particle surfaces with high surface irregularities. However, the commercial LS micrographs exhibited a characteristic rhombohedral morphology with less rough surfaces. The authors suggested the differences in morphologies may be due to their different origins. For instance, the ES were obtained from a milling process, while LS was from a precipitation process. Furthermore, Bootklad and Kaewtatip [105] compared the morphology of ES and LS. ES was ground to powder form while LS was purchased. In this study, they reported similar morphologies with both fillers having a plate-like shape. In a similar study, Betancourt and Cree [61] compared the SEM images of ES powders with mineral LS powders and observed pores in eggshells compared to LS powders, which had no pores. Both ES and LS have similar structure with jagged edges and irregular shape.

In a related study, SEM images of untreated and SA treated mineral LS was compared by Azadi et al. [106]. They observed a polygonal shape for stearic acid modified LS particles and narrow, non-spherical, and non-uniform shapes for unmodified LS particles.

2.12.2 Epoxy composite fractured surfaces

Mohan and Kanny [38] examined the fractured specimens of synthetic epoxy/nano-eggshell composites. They reported smooth and cleavage type failures for 0, 1, 2, 3 4, and 5 wt. % tensile

fractured composite surfaces. The major difference was observed for the unfilled epoxy matrix which did not have small cracks branching out during propagation which suggested brittle failure. In contrast, the nanoparticles may have stopped the crack propagations in the composite materials. The fractured surface of 5 wt. % composite appeared rough and agglomeration of the ES were observed, which may have induced stress concentrations and subsequently resulted to crack propagation. Particle pull-out was also observed for composites with 5 wt. % filler loadings which suggested the presence of agglomeration. Another study conducted by Khalil et al. [107] examined the tensile fractured surface of unfilled synthetic epoxy resin. They observed smooth surfaces with river markings parallel to the direction of crack propagation, which indicated rapid crack propagation with little resistance leading to brittle failure. In a similar work, the unfilled bio-epoxy and its composites had similar fractured surfaces as synthetic epoxy composites [38,107]. For example, Tiimob et al. [8] compared the fractured SEM image of unfilled bio-epoxy and 4 wt. % ES nano-composite. They observed a smooth fractured surface for unfilled bio-epoxy resin, which suggested brittle fracture. However, the 4 wt. % ES nano-composite microstructure showed rough ridge-like patterns and river markings suggesting some plastic deformation due to the presence of nano-ES particles.

2.13 Summary

The literature review showed the potentials of ES for use as an alternative to mineral LS filler for epoxy polymer matrix. The quantity of eggs produced annually, the incorporation of ES and mineral LS fillers in epoxy resin and their effect on the physical, mechanical and thermal property were reviewed in this Chapter. In addition, a comprehensive review was conducted on the mechanism and the effect of stearic acid treated fillers on the properties of epoxy resin. Few researchers have investigated the effect of high ES loading (> 10 wt. %) and the utilization of SA treated ES filler on the physical, mechanical and thermal properties of synthetic epoxy resin. However, no studies have been conducted on the amount of $CaCO_3$ that can be recovered from waste eggshells, the disposal cost and the extent to which it can replace mineral LS in epoxy-based composites. Also, studies have not been carried out on the use of high ES filler content (> 10 wt. %), utilization of SA treatment on ES and their effect on physical, mechanical and thermal properties of bio-based epoxy polymers. The research gap is to determine the amount of $CaCO_3$ that could be recovered from waste ES for use in various applications, the disposal cost, extent of

mineral LS replacement and the effect of high loading of untreated and SA treated ES and LS filler on the properties of bio-based epoxy resin. These gaps motivated the study to produce a bio-epoxy eggshell composite.

CHAPTER 3
MATERIALS AND EXPERIMENTAL METHODS

The materials, methods and procedures adopted to achieve the objectives of this study are presented in this Chapter.

3.1 Materials

The eggshells (ES) and limestone (LS) fillers used in this study were obtained from Maple Lodge Farms Hatchery, Ontario, Canada and Imasco Minerals Inc., respectively. The matrix (Super Sap CPM epoxy and CPL hardener) (Figure 3.8a) used is a green bio-polymer purchased from entropy resins, San Antonio, CA and contains 31 % bio-based content. The main characteristics of the polymer matrix obtained from the manufacturers' data sheet are presented in Table 3.1. Silicone, Mold Max^{TM} 10T for making polymer composite molds for test specimens was purchased from Smooth-On Inc. and the stearic acid (SA) particulates used for filler modification was supplied by Fisher Scientific.

Table 3.1. Properties of Super Sap CPM epoxy and CPL hardener [6].

Properties	Bio-epoxy resin
Density (g/cm^3)	1.08
Tg (DSC, midpoint) (°C)	54
Mix ratio resin: hardener (by weight)	100:40
Tensile strength (MPa)	62
Young modulus (GPa)	3
Flexural strength (MPa)	92.7
Flexural modulus (GPa)	2.8

3.1.1 Eggshell powder preparation

The as-received ES was coarse ground into smaller particles as shown in Fig 3.1 (a) and (b), respectively. The coarse ground ES were further ball milled for 6 h into fine powders using a small scale milling apparatus to further reduce the particle size (Figure 3.1 (c)). Distilled water was

added to the ES powders to form a slurry. The combination was manually agitated and a precipitation process was used to remove the water and some inner organic membranes. The slurry mixture was dried at 105°C for 24 h to achieve the fine powdered ES [14]. The required particle size was obtained using sieve analysis with the aid of a vibrating sieve shaker machine (Ro-tap). The obtained ES powder and purchased LS powder were sieved with 20 μm (no. 635) sieving mesh.

Figure 3.1. A photograph of the procedure of converting as-received eggshells to eggshell fillers. (a) as-received eggshells, (b) coarse grinding and (c) fine ball milling.

3.2 Characterization of eggshell powder

To understand the behavior of ES as a filler for composites, microstructural crystalline phase (XRD), analysis of chemical composition (ICP-MS), microstructural analysis (SEM), particle density measurements and particle size analysis were conducted.

3.2.1 X-ray diffraction analysis

This analysis was conducted to identify the qualitative composition of both ES and LS powders. The crystalline phases of the ES and LS particles were analyzed by X-ray diffraction analysis using a Cu kα radiation (Rigaku Ultima IV Powder X-ray diffractometer, Japan) as shown in Figure 3.2 of wavelength, $\lambda = 0.15406$ nm (1.54056 Å) at room temperature. The kβ filter used was nickel. The measurements were performed at a diffraction angle (2θ) ranging between 20° and 50° at an operating voltage 40 kV and tube current of 44 mA with a step size of 0.02°. A scan rate of 4.0°/min was used. The phase identification was done using MDI Jade 2010 Software.

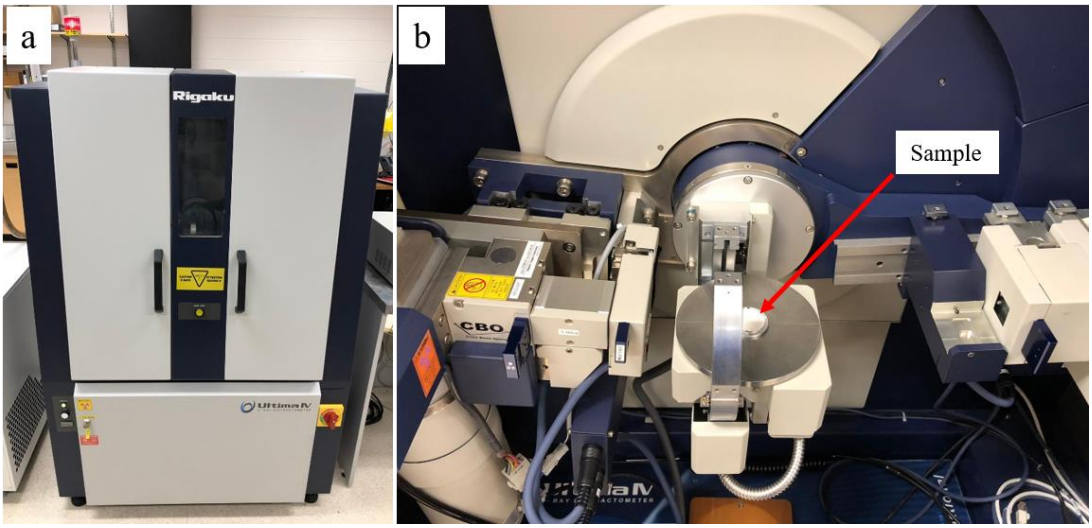

Figure 3.2. A photograph of (a) Rigaku Ultima IV powder X-ray diffractometer and (b) specimen in the equipment sample holder.

3.2.2 Chemical composition of ES

Analysis of chemical composition was done to determine the calcite ($CaCO_3$) content in the as-prepared ES. This was done by the application of a microwave digestion system and an inductively coupled plasma mass spectrometer (ICP-MS). Firstly, the powdered samples were digested in 65 wt. % concentrated nitric acid (HNO_3) at 200 °C in a closed vessel employing a microwave digestion system (Model CEM Corporation Mars 6, United States of America) using approximately 1800 watts microwave energy at a frequency of 2450 MHz. ICP-MS (Agilent 7700x ICP MS, Japan) was used for further measurement/analysis to determine elemental composition. The obtained elemental composition of ES was compared with the $CaCO_3$ content value reported for LS in the suppliers technical data sheet [108].

3.2.3 Microstructural analysis

Scanning electron microscope (JEOL JSM-6010 LV) was used for microscopic evaluation of the filler (ES and LS) powders, the morphology of the composites fractured surfaces of the specimens that fail during tensile, flexure and Charpy tests for all composite formulations. For better image quality, the samples were first sputter gold coated to make them conductive before being examined under the microscope.

3.2.4 Density measurements

The particle density of the fillers (ES, LS and SA treated ES and LS) was determined at room temperature. The mass of the fillers were measured with a high sensitivity weighing scale (Ohaus Precision Model TS400D) with a precision of 0.001g (Figure 3.3 a). In operating the weighing scale, the ground fillers were poured into a tethered steel cup and placed on the scale to obtain the mass value in grams (g). The volume (cm^3) of the samples were determined by a non-destructive technique using a helium gas micromeritics Accupyc 1340 pycnometer (Figure 3.3 b) at a pressure of 134,448 Pa (19.5 psi). After mass measurements, the steel cup containing the fillers was inserted into the gas pycnometer and gently locked into place. The volume and density was determined using the equipment software which employed Archimedes principle, Equation (3.1) and (3.2).

$$D_{sample} = \frac{M_{sample}}{V_{sample}} \tag{3.1}$$

$$V_{sample} = V_{cell} - V_{exp} \times \left(\frac{P_1}{P_2} - 1\right) \tag{3.2}$$

where, V_{cell} = sample chamber volume (cm^3), V_{exp} = expansion chamber volume (cm^3), V_{sample} = sample volume (cm^3), M_{sample} = sample mass (g), D_{sample} = sample density (g/cm^3), P_1 = gauge pressure after fill (Pa), P_2= gauge pressure after expansion (Pa).

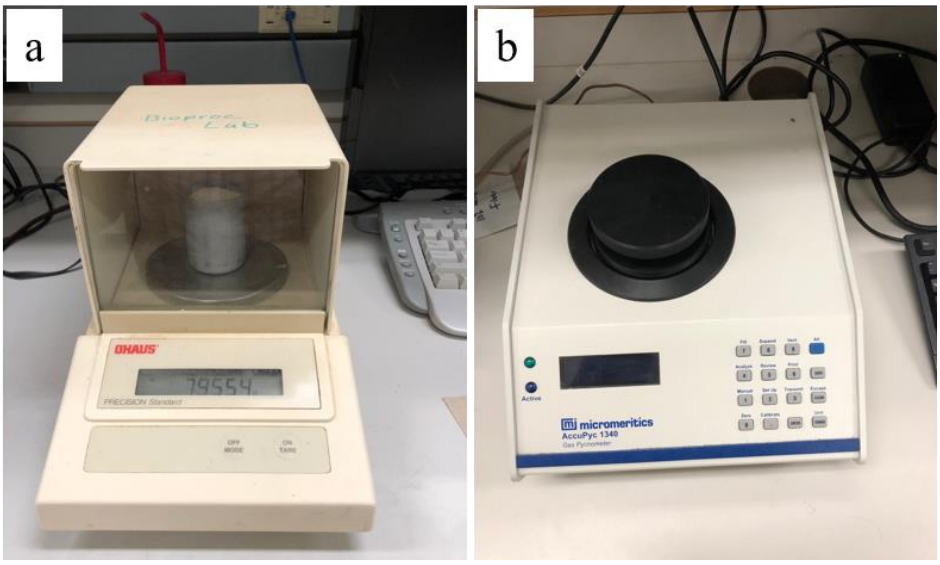

Figure 3.3. A photograph of (a) Ohaus Precision Model TS400D weighing scale and (b) helium gas Micromeritics Accupyc 1340 pycnometer.

3.2.5 Particle size analysis

In this study, the filler (ES, LS and stearic acid treated ES and LS) particle size distributions (PSD) were determined at room temperature using a Malvern Mastersizer 2000 S (long bench) laser diffraction particle size analyzer according to ISO 13320:2003 standard [109]. The instrument is capable of providing size in the range of 0.05 µm to 3500 µm. For obtaining the particle size distribution (PSD), the apparatus uses two laser light sources namely, a blue light (wavelength 466 nm) and a red light (wavelength 633 nm). The Mastersizer 2000 software provides calculated particle size results such as the average particle size of the sample. In operating this equipment, the sieved (dry) filler particles were fed into the dry powder feeder section of the equipment (Figure 3.4) and transferred via vacuum and passed through a focus laser beam. The particle samples scatter or obscure light at an angle inversely proportional to their size. Subsequently, photosensitive detectors measure the angular intensity of the scattered light and the results are displayed as volume fractions of the particle size distribution of the sample using the software. The process was repeated three times to ensure reproducibility and the average results were reported.

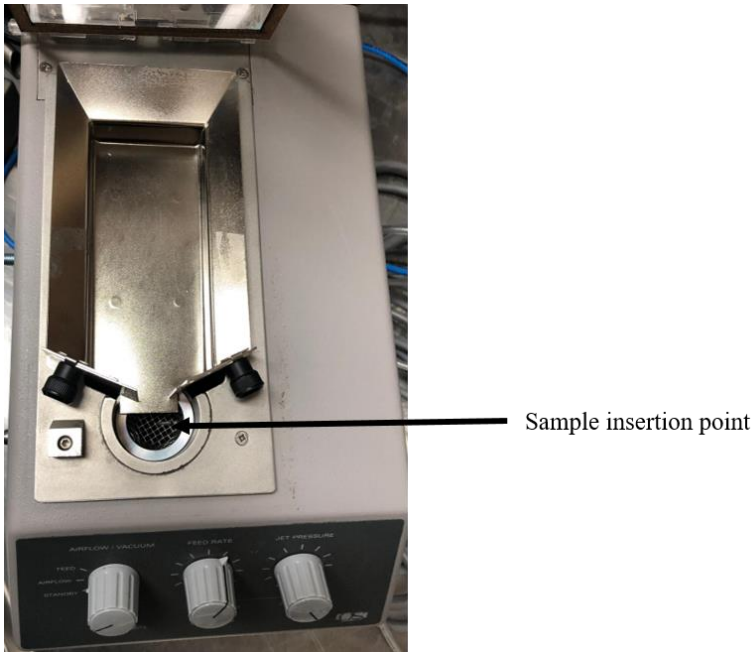

Figure 3.4. A photograph of Malvern Mastersizer S (long bench) laser particle size analyzer dry powder feeder.

3.2.6 Surface modification of $CaCO_3$ powders (ES and LS) using stearic acid (SA)

Due to high surface energy, particles in powder form induce van der Waals and electrostatic forces acting between the particles, thus resulting in particles tending to stick together [78]. This has been reported to have led to poor dispersion of filler particles in an epoxy matrix [110]. A stearic acid modification process was conducted to improve the adhesion of filler to the matrix. The stearic acid has been reported to enhance dispersion of fillers and promote effective stress transfer from the matrix to filler [31,72]. The filler particles were coated with stearic acid before being dispersed in the bio-epoxy matrix. This treatment was aimed at making hydrophilic ES and LS more hydrophobic, thus achieving improved adhesion with the hydrophobic epoxy resin. Reduction of agglomerates at high concentration of filler contents, along with improved adhesion, and better dispersion was expected to be achieved in composites prepared with stearic acid coated fillers when compared with untreated filler composites. The quantity of stearic acid used for the treatment was 2 wt. % of the ES or LS filler sample size based on previous studies [70,85,87]. The $CaCO_3$ powder (ES or LS) was added to a solution of ethanol and distilled water at a volume ratio (1:1:3) and stirred using a magnetic stirrer for 2 h at room temperature. This was done to completely wet the particles. After 2 h, the solution was heated to 80 °C while stirring. Stearic acid in the form of solid chips was dissolved in ethanol in a separate glass beaker. The dissolved stearic acid was added to the warm $CaCO_3$ powder/water/ethanol mixture. After complete addition, the mixture was stirred for an additional 2.5 h to homogenize. The mixture was filtered using filter paper of particle retention 5-10 µm as illustrated in Figure 3.5 (a). The stearic acid coated $CaCO_3$ powder with the filter paper was placed on a petri dish and subsequently dried in an oven at 105°C for 24 h. The dried particles are shown in Figure 3.5 (b). Finally, a mortar and pestle was used to separate the agglomerated particles.

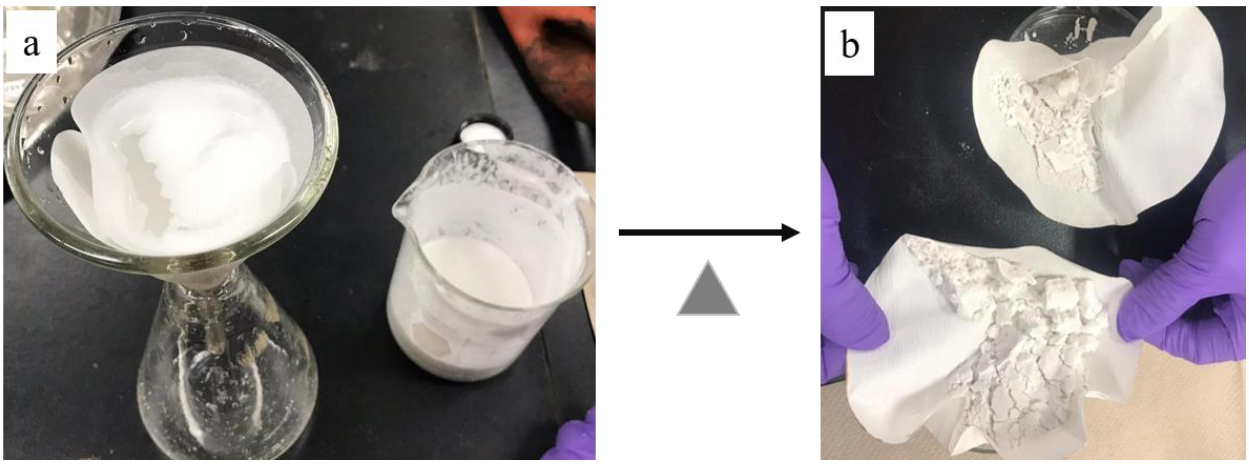

Figure 3.5. A photograph of (a) stearic acid filler solution being filtered (b) dried agglomerated stearic acid coated filler on the filter paper.

3.3 Preparation of composites

The procedure for manufacturing the composites as well as the preparation of the molds are presented in this section.

3.3.1 Preparation of silicone rubber molds

Mold Max 10T was received as a silicone rubber in liquid form. The choice of this silicone rubber mold was its excellent tear strength, maximum use up to a temperature of 204 °C and ease of cured sample removal without requirements of a release agent. This product is supplied in two parts namely: silicone rubber and hardener. Silicone rubber and hardener was mixed at a weight ratio of 100:10 as instructed on the supplier's data sheet using a stir stick for 3 min at room temperature. The mixture was degassed (shell lab Model SVAC1E) under vacuum of >28 in Hg for 3 min. The degassed liquid mixture was poured into a square plastic container containing five of the desired aluminum-shaped samples of either tensile, flexure or Charpy specimens. The aluminum samples were initially fixed to the plastic box using a two-sided adhesive tape (Figure 3.6 (a)). Afterwards, the silicone rubber was allowed to cure for 24 h at room temperature. Then, the cured silicone rubber was demolded, and subjected to a post-cure at 65°C for 4 h to eliminate any residual moisture that could affect the curing process of products as well as improve the tearing properties of the silicone mold. The mold was finally allowed to cool for 24 h. A silicone tensile specimen mold is shown in Figure 3.6 (b).

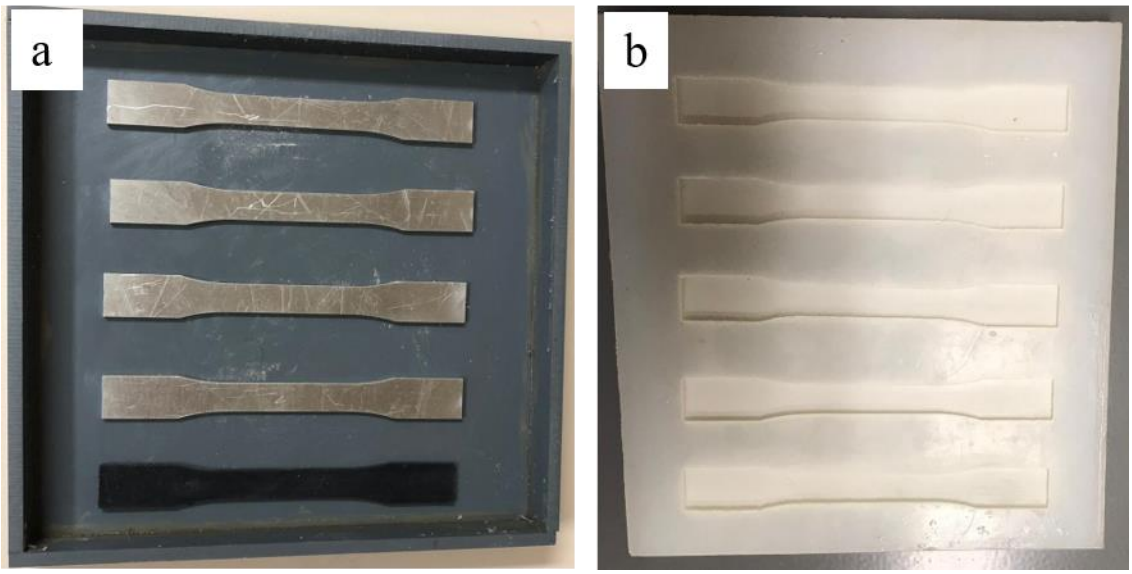

Figure 3.6. A photograph of (a) plastic mold with aluminum tensile samples and (b) prepared silicone mold for tensile samples.

3.3.2 Manufacture of bio-epoxy/ES and bio-epoxy/LS composites

The composites were prepared using a solution mixing method with bio-epoxy serving as the matrix. The two filler materials ES and LS as well as the stearic acid treated ES and LS were used in making composites at different formulations as listed in Table 3.2. The weight fractions of fillers in the composites are 5, 10, and 20 wt. %. Prior to dispersing into the polymer matrix, the ES powder was degassed under vacuum > 28 inHg for 30 min at room temperature to eliminate air in the pores of the eggshell.

The required quantity of bio-epoxy was placed in a plastic beaker and the $CaCO_3$ powder (ES or LS of required weight percent) was dispersed in the matrix. The mixtures were initially stirred at room temperature using a magnetic stirrer for 1 h rotating at 700 rpm. To help with dispersion of the particles within the bio-epoxy, an ultrasonic homogenizer sonicator (Model FS-900N) as shown in Figure 3.7 was used to further disperse the fillers for 5 min. According to Bittmann et al. [73], Xu et al. [90] and West and Malhotra [91], a duration of 5 min was suggested for dispersion of fillers using an ultrasonic homogenizer to avoid degradation of epoxy resin mechanical properties. Also, the temperature and viscosity increase caused by excessive sonication could

prevent effective dispersion of fillers due to start of resin curing without addition of the hardener [110]. The liquid composite mixtures were degassed under vacuum (>28 inHg) for 30 min to evacuate air bubbles generated as a result of mixing. Subsequently, the required hardener was poured into the liquid mixture and hand stirred manually for 3 min followed by degassing under vacuum (>28 inHg) for 15 min. Afterwards, the mixture was gently poured into the silicone rubber mold to prevent excessive air bubbles and allowed to cure for 24 h at room temperature. Finally, a post-cure treatment was done at a temperature of 82 °C for 40 min in an oven (shell lab Model SVAC1E) as suggested in the manufacturers' technical data sheet [6]. The post-cured samples (Figure 3.8 (c)) were demolded and subjected to various mechanical tests.

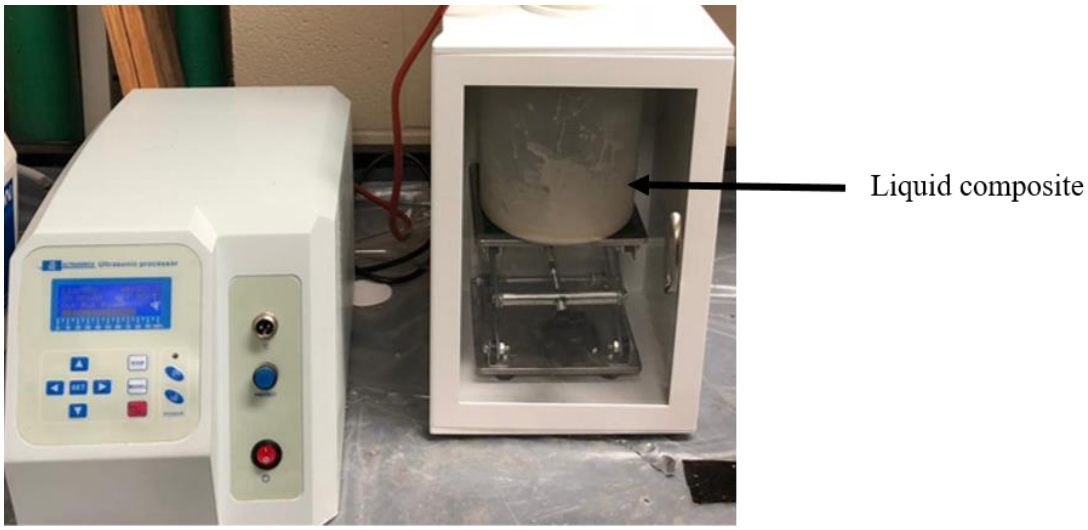

Figure 3.7. A photograph of the ultrasonic homogenizer sonicator with liquid composite.

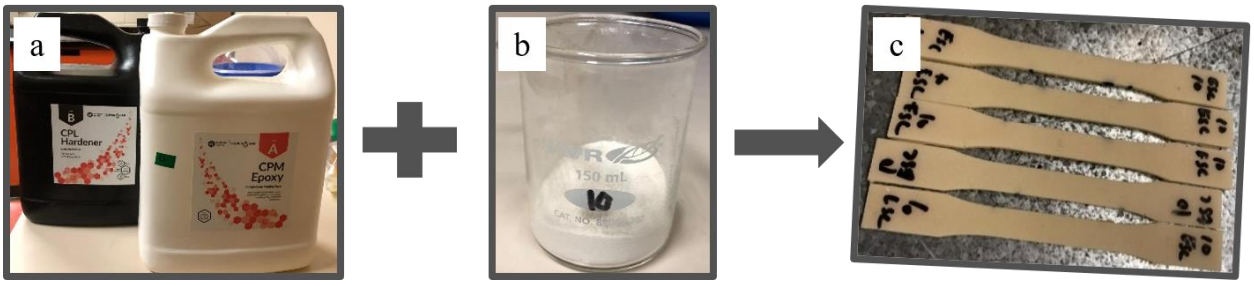

Figure 3.8. A photograph of (a) CPM epoxy and CPL hardener (b) ES or LS filler and (c) cured bio-epoxy/ES or LS composites.

Table 3.2. Formulation of filler in the bio-epoxy composites.

Filler type	Filler (wt. %)	Resin (wt. %)
-	0	100
ES	5	95
	10	90
	20	80
ES and SA	5	95
	10	90
	20	80
LS	5	95
	10	90
	20	80
LS and SA	5	95
	10	90
	20	80

3.4 Characterization of bio-epoxy/ES and bio-epoxy/LS composites

The mechanical, physical and thermal properties of the composites were determined by conducting several tests such as, tensile, flexural, Charpy impact toughness, composite density, water absorption and glass transition temperature (T_g).

3.4.1 Tensile tests of composites

Tensile test were performed on the as-prepared composites to obtain information on the tensile behavior of the composite under quasi-static loading. It was conducted on dog-bone samples of dimensions 165 mm × 13 mm × 3.2 mm (length × width × thickness) with a gauge length of 50 mm as shown in Figure 3.9 according to ASTM D638-14 standard [111]. The tension tests were

conducted using an Instron^{TM} universal testing machine (Model 3366) as shown in Figure 3.10 (b) using a load cell of 5 kN and a cross-head speed of 10 mm/min. Testing was conducted at room temperature and 40 % relative humidity (RH) until fracture occurred. The tensile strengths reported are an average value for five specimens for each composite formulation to minimize the error. The tensile strength was obtained using equation (3.3).

$$Tensile\ Strength\ (MPa) = \frac{Maximum\ load\ (N)}{Area\ (mm^2)} \quad (3.3)$$

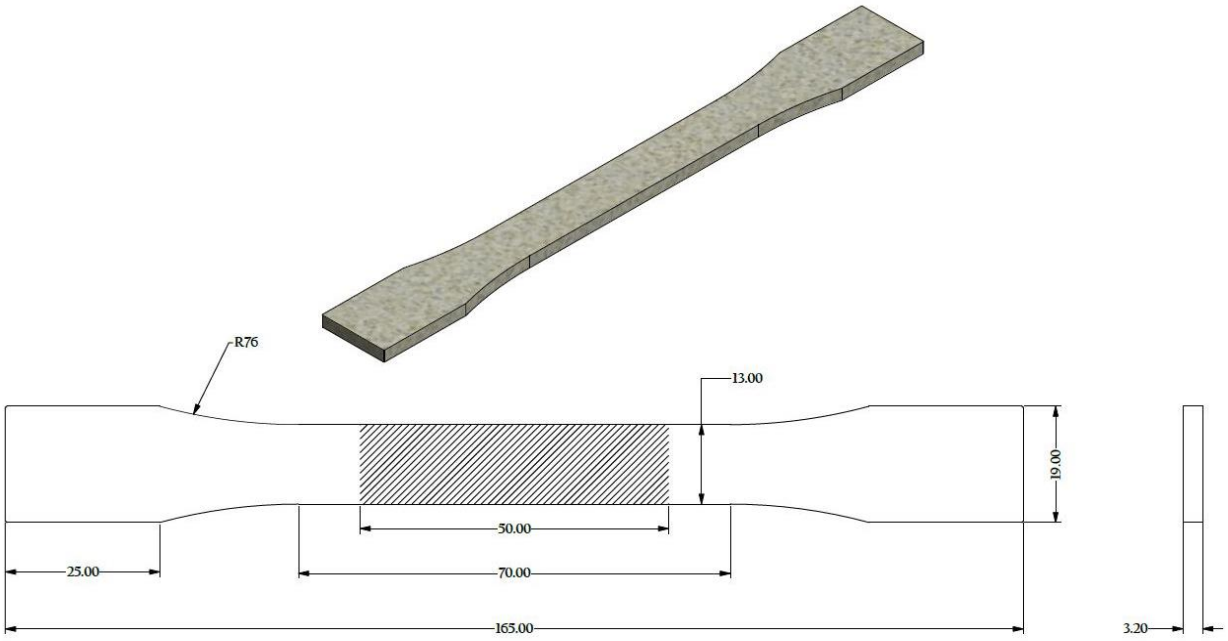

Figure 3.9. An AutoCAD image of dog-bone shaped specimens for tensile test (dimensions in mm).

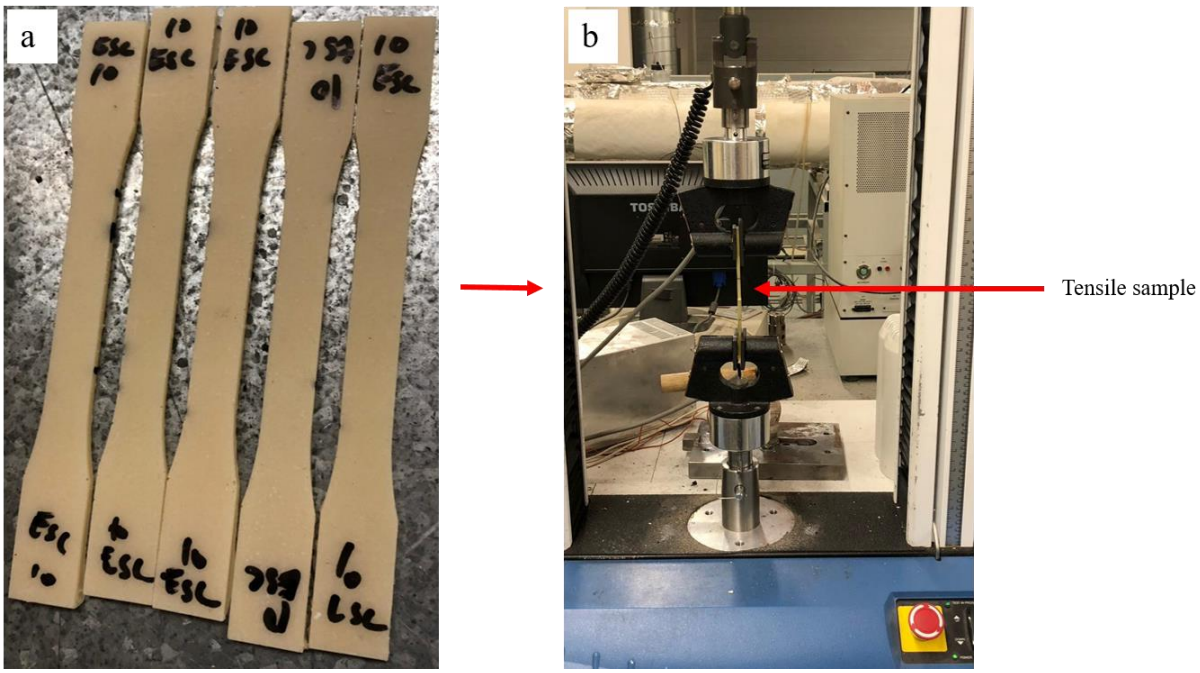

Figure 3.10. A digital image of (a) cured tensile composite sample (b) composite sample fractured by Instron tensile machine.

3.4.2 Flexural tests of composites

To further characterize the as-prepared composites, their response to three-point bending was evaluated in this study. It was performed using an Instron^{TM} universal testing machine (Model 3366) according to ASTM D790-17 standard [112] at room temperature and RH of 42 %. The sample dimensions used were 200 mm x 20 mm x 10 mm (l x w x t) with a span to depth ratio of 16:1 as recommended by the ASTM standard. The load cell and cross-head speed used were 5 kN and 4 mm/min, respectively. Hence, flexural stress (σf) and flexural modulus (Ef) values were calculated using equations (3.4) and (3.5), respectively [112]. The test results reported are an average for five samples of each composite formulation.

$$\sigma f = \frac{3PL}{2bd^2} \tag{3.4}$$

where, σf, P, L, b, and d, are maximum flexural strength (MPa), load at a given point (N), support span (mm), width (mm) and depth (mm) of tested specimens, respectively.

$$Ef = \frac{L^3 m}{4bd^3} \tag{3.5}$$

where Ef, L, m, b, and d, are modulus of elasticity in bending (MPa) and m is slope of tangent to the initial straight-line portion of load-deflection curve (N/mm), b and d are width (mm) and depth, respectively.

3.4.3 Charpy impact tests of composites

Charpy impact toughness values were obtained using an Instron Model 450 MPX series impact tester as shown in Figure 3.11. The tests were performed on non-standard un-notched specimens of dimensions 55 mm × 13 mm × 3.2 mm ($l \times w \times t$). Due to cracks initiating at agglomerates and flaws in the specimens, un-notched samples are better for determining the presence of agglomerates from powder fillers added to composite materials compared to notched that is insensitive to agglomerates [113].

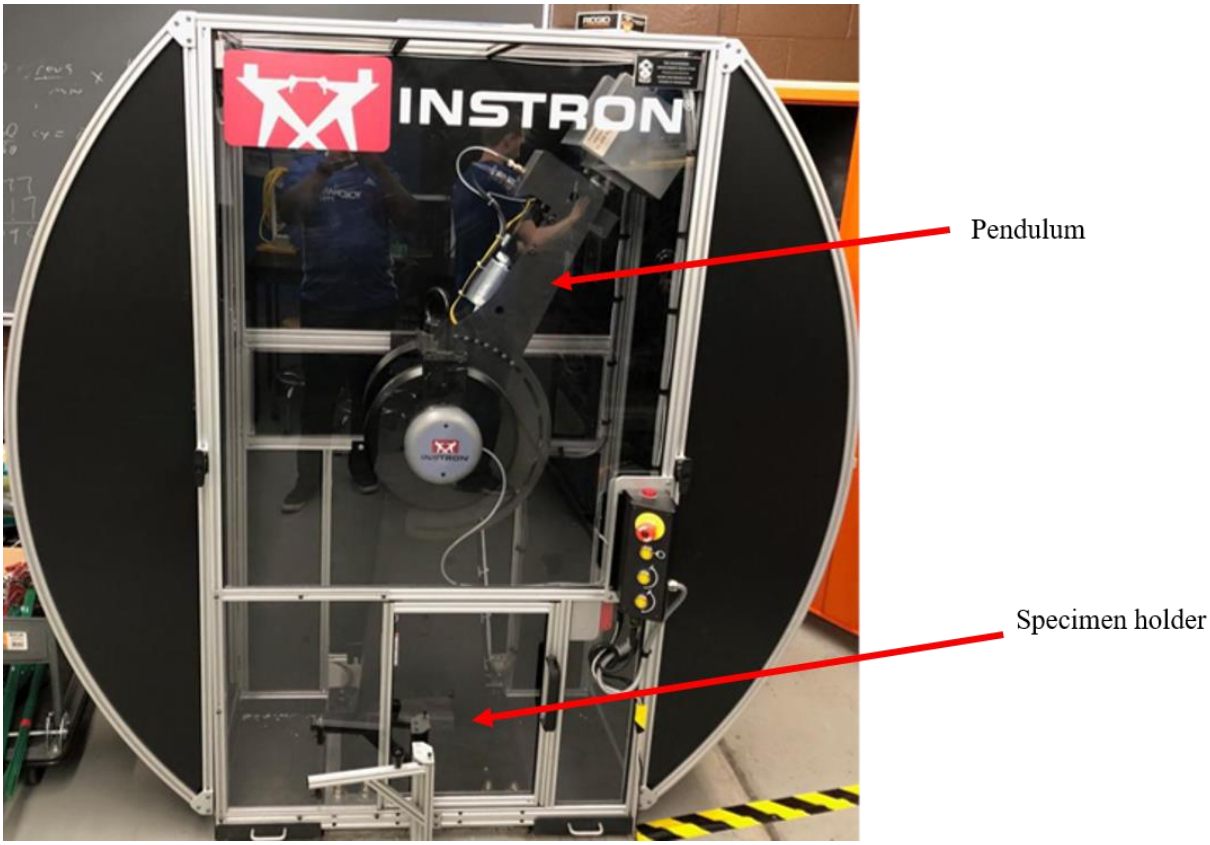

Figure 3.11. A photograph of the Charpy impact test machine.

The energy absorbed by the as-prepared composites at fracture was determined at temperatures of 23 °C and -40 °C. Prior to testing the composites, the specimens were conditioned using a Tenney

TJR temperature test chamber as shown in Figure 3.12 for 4 h at a temperature of 23 °C and -40 °C. In this test, ASTM standard D6110-18 [114] was used as a guide to compare the impact toughness of the composites at various filler loadings with respect to the unfilled bio-epoxy matrix. The values reported are an average of five samples of each composite formulation at different temperature levels. The energy absorbed per unit area $(Ea)\ in\ kJ/m^2$ was computed using equation 3.6.

$$Ea = \frac{E}{b \times d} \tag{3.6}$$

where, E, b, and d, are energy absorbed (kJ), width (mm), and thickness (mm), respectively.

Figure 3.12. A photograph of the Tenney TJR temperature chamber used to condition specimens prior to Charpy impact toughness test.

3.4.4 Density measurement

Figure 3.13 shows the experimental setup used in determining the bulk density of the as-produced composites. The density measurements were conducted on composite samples of dimensions, 20 mm x 20 mm x 3.2 mm (*l* x *w* x *t*). The samples were firstly weighed in air (M_a) (dry mass) and reweighed while immersed in liquid (distilled water) (M_w). The density of the samples was calculated using equation (3.7).

$$\rho_c = \frac{Ma}{Ma - Mw} \times \rho_d \quad (3.7)$$

where, ρ_c and ρ_d are the density of sample and liquid (1 g/cm^3) respectively.

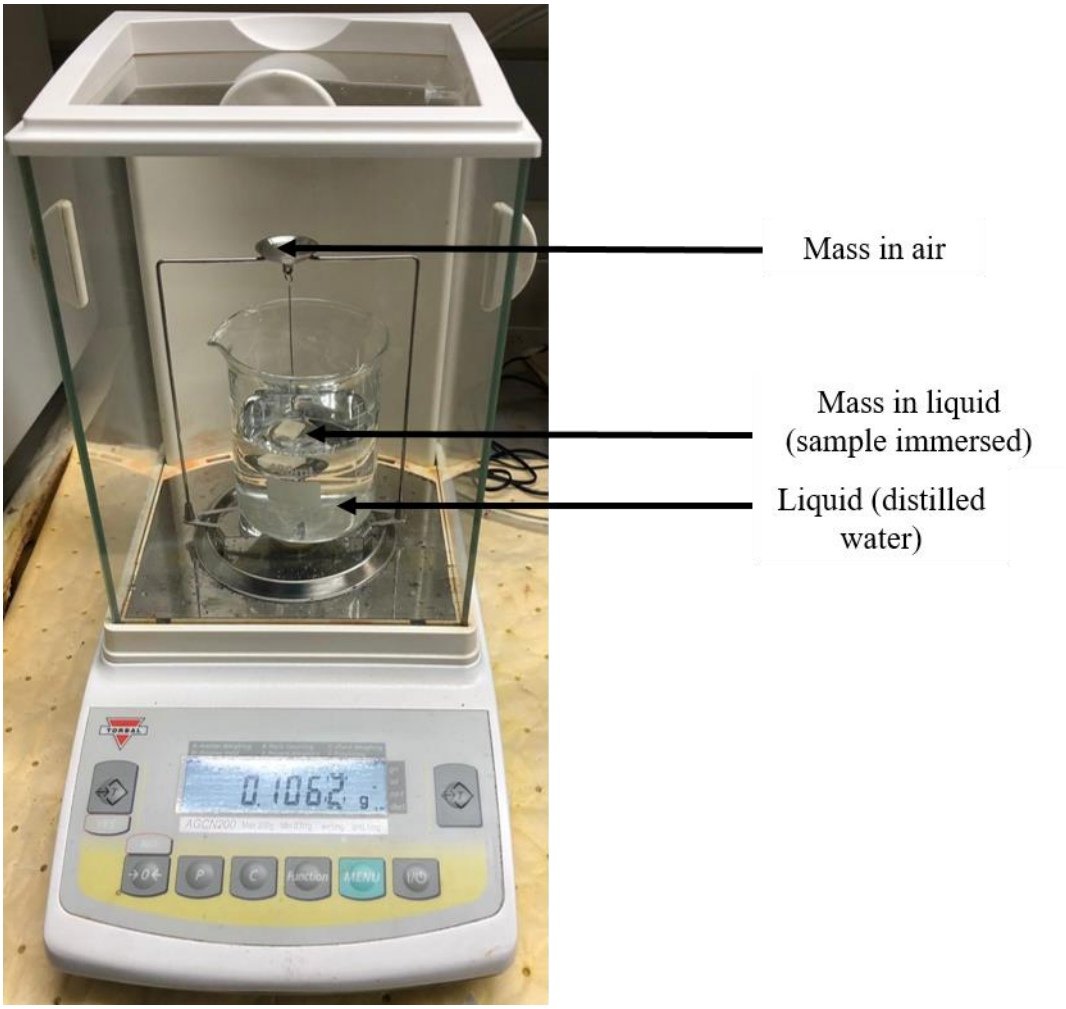

Figure 3.13. A photograph of the apparatus used for determining composite bulk density.

Furthermore, applying the Rule of Mixture (ROM), the composite theoretical density was obtained using equation (3.8) [27] and was subsequently compared with the experimentally obtained bulk density of the composites. The weight fraction of the filler particle was converted to volume fraction using equation (3.9) [115]. The volume fraction of the matrix was obtained using equation (3.10) [116].

$$\rho_c = \rho_m V_m + \rho_p V_p \quad (3.8)$$

$$V_p = \frac{W_p}{W_p + (1 - W_p)\ \rho_p/\rho_m} \quad (3.9)$$

$$V_m = 1 - V_p \quad (3.10)$$

where, W_p is the weight fraction of the filler particles, $\rho_c,\ \rho_m,\ \rho_p$ are the densities of the composite, matrix and particles, respectively. V_m and V_p are the volume fractions of the matrix and filler particles, respectively.

3.4.5 Void content of the composites

The void content of the composites as a percentage (%) were determined through the experimental and theoretical density according to ASTM D2734-16 standard using equation (3.11) [117].

$$Void\ content\ (\%) = \frac{\rho_{theoretical} - \rho_{experimental}}{\rho_{theoretical}} \quad (3.11)$$

where, $\rho_{theoretical}$ and $\rho_{experimental}$ are theoretical and experimental density, respectively.

3.4.6 Water absorption test

Water absorption tests were performed for a duration of 21 days on the as-prepared composites of dimensions 76.2 mm × 25.4 mm × 3.2 mm ($l \times w \times t$) in accordance with ASTM D570-98 [118] at room temperature. The samples were immersed in distilled water and were weighted as a function of time (at intervals of 24 h). This was done until a constant weight (saturation level) was reached for all composite samples. It was weighed using a balance with a precision of 0.0001g. Prior to immersion, the samples were dried in an oven for 12 h at a temperature of 50 °C. Afterwards, they were placed in a desiccator. Before each measurement, the sample surfaces were wiped with paper towel to remove surface water. The percentage of water absorbed was computed using equation (3.12).

$$W\% = \frac{W_1 - W_2}{W_2} \times 100 \quad (3.12)$$

where, $W\%$ is the weight gain in (%), W_1 is the weight of water absorbed (g) of the composite after a specific time t, and W_2 is the dry weight (g) of the sample before immersion in distilled water. The plotted values are average of three samples of each composite formulation.

3.4.7 Thermal analysis

A differential scanning calorimeter (DSC) (Model 2910 V4.4E, TA instruments, USA) shown in Figure 3.14 was used to obtain information on the glass transition temperature (T_g) of the composites according to ASTM E1356-08 standard [119]. Each composite composition was prepared in a powder form of approximately 7-10 mg and placed in an aluminum crucible (pan) and heated from room temperature to 180 °C at a heating rate of 10 °C/min. The T_g was calculated as the midpoint of the onset and end temperature on the thermal curve, which corresponds to half of the heat flow difference between these points (onset and end).

Figure 3.14. A digital image of DSC Model 2910 V4.4E used in determining the T_g of the composites.

3.4.8 Statistical analysis

Analysis of variance (ANOVA) was performed using Sigma plot 13 to validate the statistically significant differences in the obtained mechanical properties results (tensile strength, flexural strength, flexural modulus and Charpy impact toughness) of the composites. The analysis was done with a significance level of 0.05, which is a confidence level of 95 %. According to the

ANOVA results, the *p*-value determines if statistically significant difference exist between groups. If the *p*-value is < 0.05, the null hypothesis is rejected, and this means there is a statistically significant difference in their mean values. However, if the *p*-value is > 0.05, the null hypothesis is not rejected, thus there is no statistically significant difference in the mean values. Two-way ANOVA is used to confirm if there is an interaction between two independent variables on the dependent variable while three way is to determine if there is an interaction between three independent variables on a dependent variable.

CHAPTER 4

RESULTS AND DISCUSSION

The results obtained from the experiment conducted are presented in this Chapter.

4.1 Characterization of ES powder

The results of characterizations conducted on $CaCO_3$ fillers ((eggshells (ES) and limestone (LS)) which includes microstructural crystalline phase (XRD), analysis of chemical composition (ICP-MS), microstructural analysis (SEM), particle density measurements and particle size analysis are outlined in this section.

4.1.1 Chemical composition of ES

Chemical analysis was done to determine the potential of ES as a bio-$CaCO_3$ source. The analysis on the as-prepared ES confirmed a relatively high $CaCO_3$ content of 88 wt. % ± 0.7 and indicated minor traces of other elements such as magnesium (0.27 %) and phosphorus (0.13 %). Similarly, LS contain a $CaCO_3$ content of 99.9 wt. %, as reported in the supplier's data sheet [108]. In comparison to LS, the slight difference was expected due to the organic matter contained in ES which are not present in LS. Although an effort was made to remove the organic membranes after each grinding process, the results showed some membranes remained. From chemical analysis, ES powders are anticipated to serve as an alternative to LS as filler materials in composites due to the high $CaCO_3$ contents.

4.1.2 X-ray diffraction analysis

The X-ray diffraction patterns obtained for untreated ES, SA (stearic acid) treated ES, untreated LS and SA treated LS fillers, as well as SA particulates for comparison are presented in Figure 4.1. The diffraction peaks suggested a crystalline phase showing the main material of ES to be calcium carbonate phase in the form of calcite. As previously reported, the most thermodynamically stable polymorph of $CaCO_3$ is calcite [120]. The major XRD intensity peak is found at 2θ angle of 29.4°, while minor peaks occur at 23.2°, 31.5°, 36.1°, 39.6°, 43.3°, 47.7°, and 48.7° for both ES and LS as also reported in the literature [8,14,74].

For SA treated ES (Figure 4.1 (b)) and LS (Figure 4.1 (d)), the major and minor peak were diffracted at a similar 2Θ angle to the untreated ES (Figure 4.1 (a)) and LS (Figure 4.1 (c)) (29.4°). However, the SA particulates' major peak occurred at 2Θ angle of 21.5° and a minor peak at 24.1°. The diffracted peaks of SA particulates did not show on the SA treated ES and LS fillers. This suggests that the SA content (2 wt. %) used to treat the filler is too small to be identified by the XRD detector. The absence of SA peaks on $CaCO_3$ fillers was also observed by Shah et al. [70] for a 2.5 wt.% SA content.

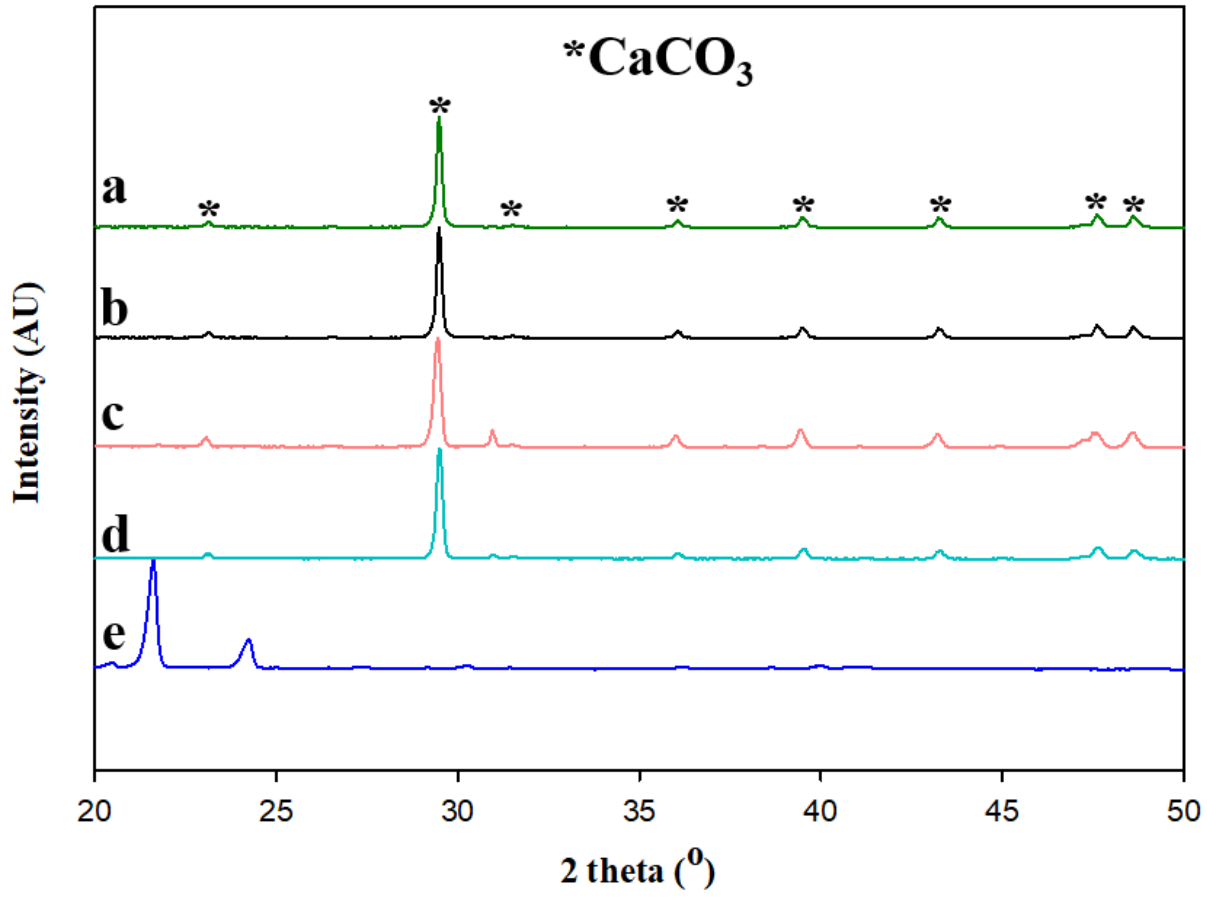

Figure 4.1. XRD diffraction pattern obtained for (a) ES (b) SA treated ES (c) LS (d) SA treated LS and (e) stearic acid (SA) particulates.

4.1.3 Microstructural examination

The micrographs of ES, LS, and SA treated ES and SA treated LS fillers are presented in Figure 4.2 (a-d). Both untreated and SA treated fillers showed similar structures. ES and SA treated fillers had coarse and irregular morphologies, which may be due to the grinding and ball milling process conducted. However, LS and SA treated particles had fewer rough surfaces thus, exhibiting a rhombohedral-like morphology (arrow marks). This rhombohedral morphology indicates the presence of calcite crystals [10]. From Figure 4.2 (a) and (c) ES and SA treated particles also have a rhombohedral morphology (calcite crystals).

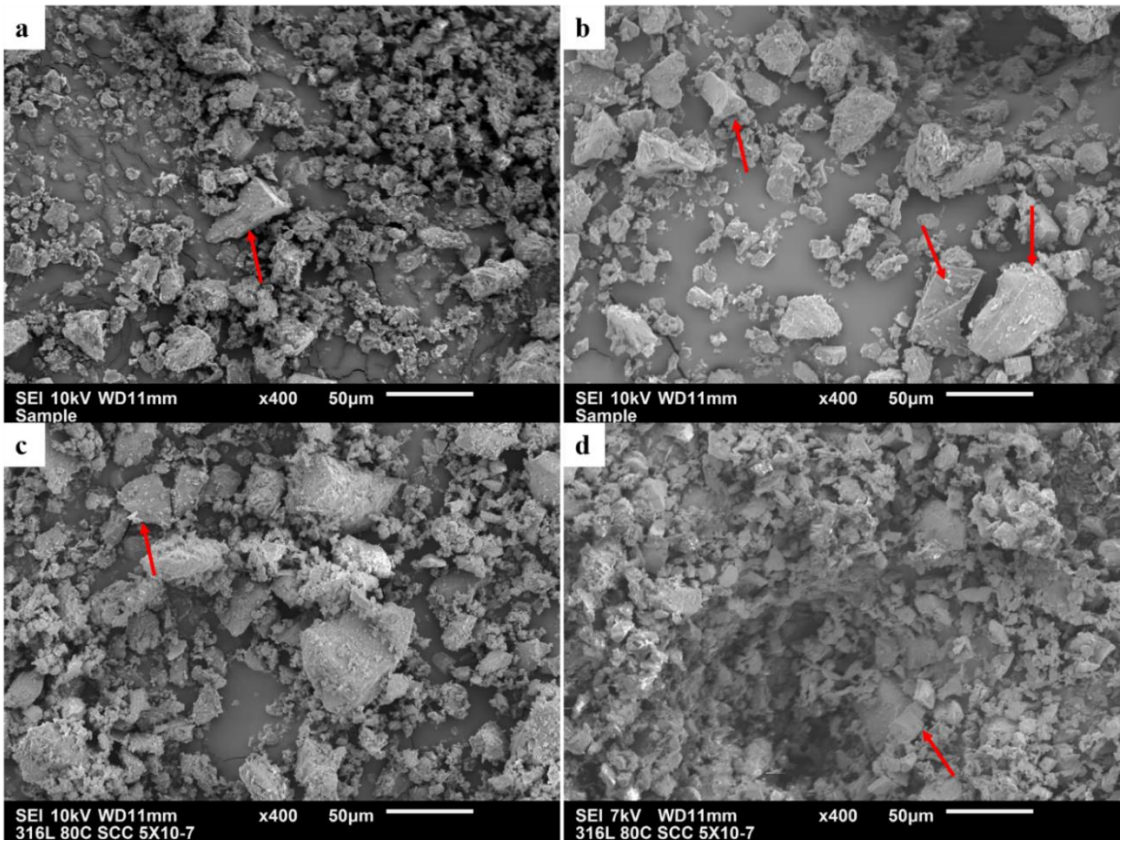

Figure 4.2. SEM micrographs showing morphologies of: (a) ES, (b) LS, (c) SA treated ES and (d) SA treated LS particles. (Arrows indicate rhombohedral-like morphology).

Furthermore, viewing the untreated ES, LS, SA treated ES and SA treated LS at a higher magnification (1000x), pores were observed with ES filler ((Figure 4.3 (a)) (arrow marks). As previously stated, a single chicken eggshell contains about 7,000-17,000 nano pores to permit the

exchange of gases and the transpiration of water throughout the shell [56,60]. The LS filler ((Figure 4.3 (b)) showed the absence of pores as well as SA treated ES ((Figure 4.3 (c)) and SA treated LS ((Figure 4.3 (d)). This suggested that there are no pores in LS and the SA treatment conducted on the filler material covered the pores in ES.

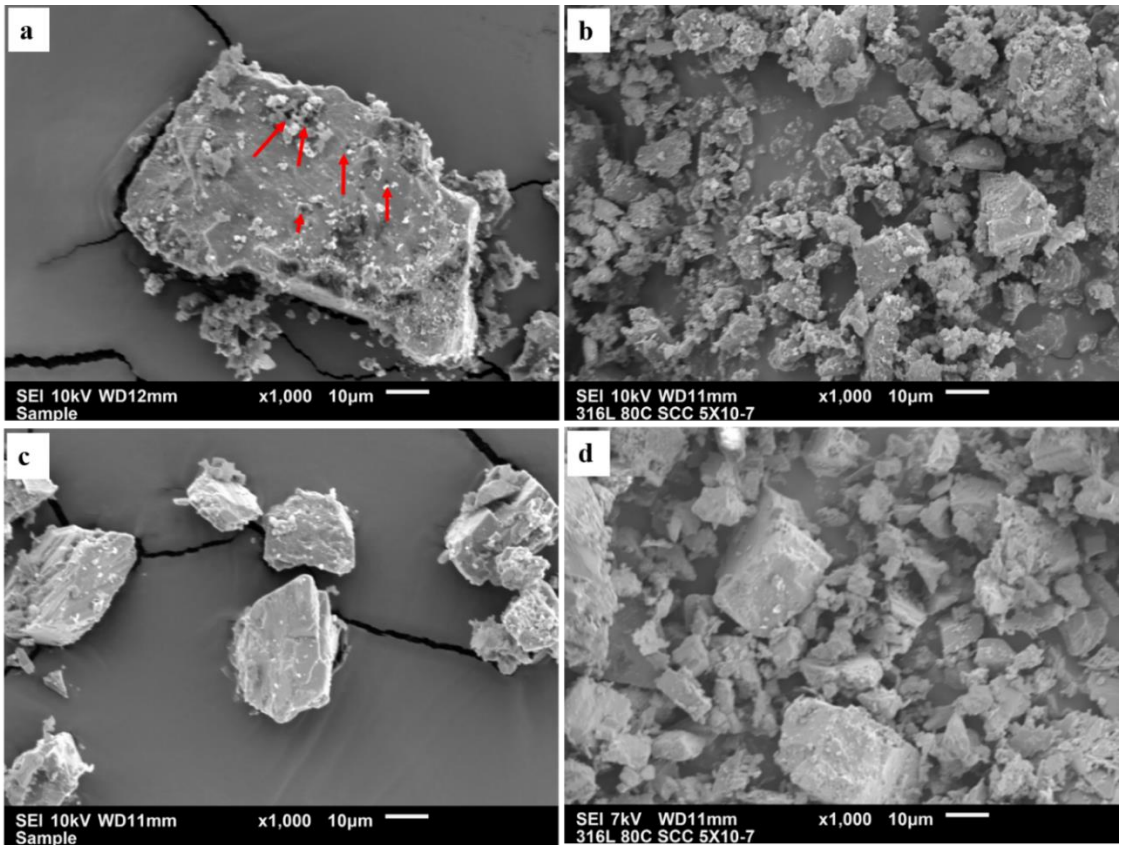

Figure 4.3. SEM micrographs of (a) ES showing the presence of pores (b) SA treated ES with the absence of pores and (c) LS with the absence of pores (d) SA treated LS with the absence of pores.

4.1.4 Particle density measurement

The particle density of the fillers (ES, LS and stearic acid treated ES and LS) are presented in Table 4.1 and Figure 4.4. The particle density of ES is slightly lower than that of LS possibly due to the more porous nature of the eggshells as shown in Figure 4.3. The particle density obtained is within the range of values reported in the literature. For example, previous studies reported ES to be between 2.53-2.62 g/cm^3 [10,15,37,38] and LS to be between 2.5-2.7 g/cm^3 [29,30]. A decrease

in the particle density was observed for the SA treatment for both fillers. For example, the particle density of ES and SA treated ES was 2.54 ± 0.00 and 2.48 ± 0.02 g/cm³, respectively. In a similar way, LS and SA treated LS particle density was 2.73 ± 0.00 and 2.57 ± 0.02 g/cm³, respectively. The result indicated a slight reduction in the particle density of the filler due to the treatment. This suggests the treatment done with the addition of SA of lower density 0.84 g/cm^3 (supplier's manufacturer datasheet) replaced more volume of the untreated higher density $CaCO_3$ particles.

Table 4.1. Particle density of ES, LS and stearic acid treated ES and LS fillers.

Fillers	Density (g/cm³)
ES	2.54 ± 0.00
SA treated ES	2.48 ± 0.02
LS	2.73 ± 0.00
SA treated LS	2.57 ± 0.02

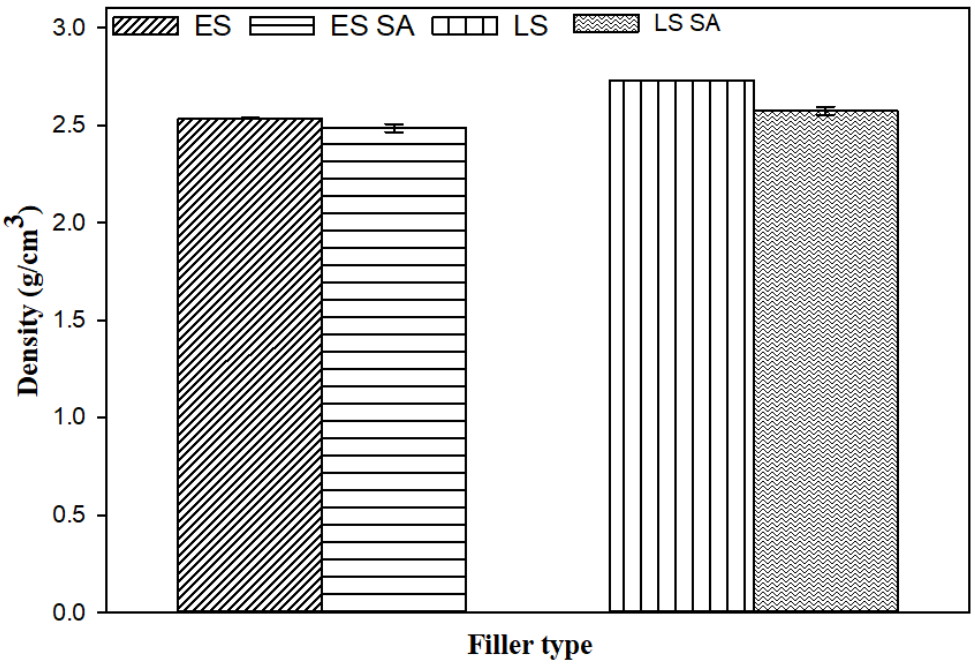

Figure 4.4. Particle density of ES, LS and stearic acid treated ES and LS.

4.1.5 Particle size analysis

The particle size distribution curve (PSDC) of the prepared ES and SA treated ES, as-received LS, and SA treated LS are shown in Figure 4.5 and 4.6 respectively. The average particle size based on volume distribution was determined to be 21.2 ± 2.0 µm, 11.5 ± 1.0 µm, 25.1 ± 2.2 µm and 12.8 ± 2.2 µm for ES, SA treated ES, LS, and SA treated LS, respectively.

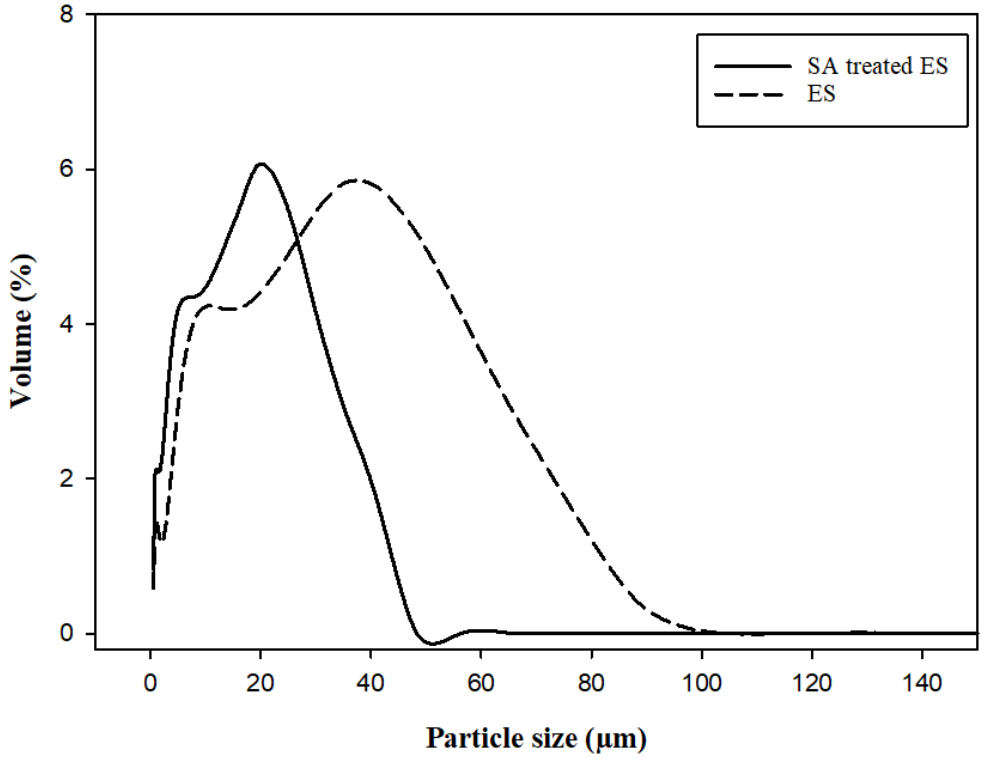

Figure 4.5. The particle size distribution curves for ES and SA treated ES.

The average particle size of the LS fillers was approximately 4 µm larger than that of ES filler, possibly due to the processing method of the waste eggshells. This reduction in particle size for untreated ES and LS is consistent with the reduction in particle density of SA treated fillers. As shown in Figure 4.5 and 4.6, the untreated ES and LS fillers had a broader particle size distribution range while SA treated ES and SA treated LS showed a significantly narrower particle size distribution range. Similar narrow particle size distribution range was reported with SA treated $CaCO_3$ particles [121]. This distribution range suggests the SA treatment reduced most agglomerated particles to smaller ones. As previously reported, the narrow distribution may suggest a removal of bio-organic impurities in the filler material due to the SA treatment [70].

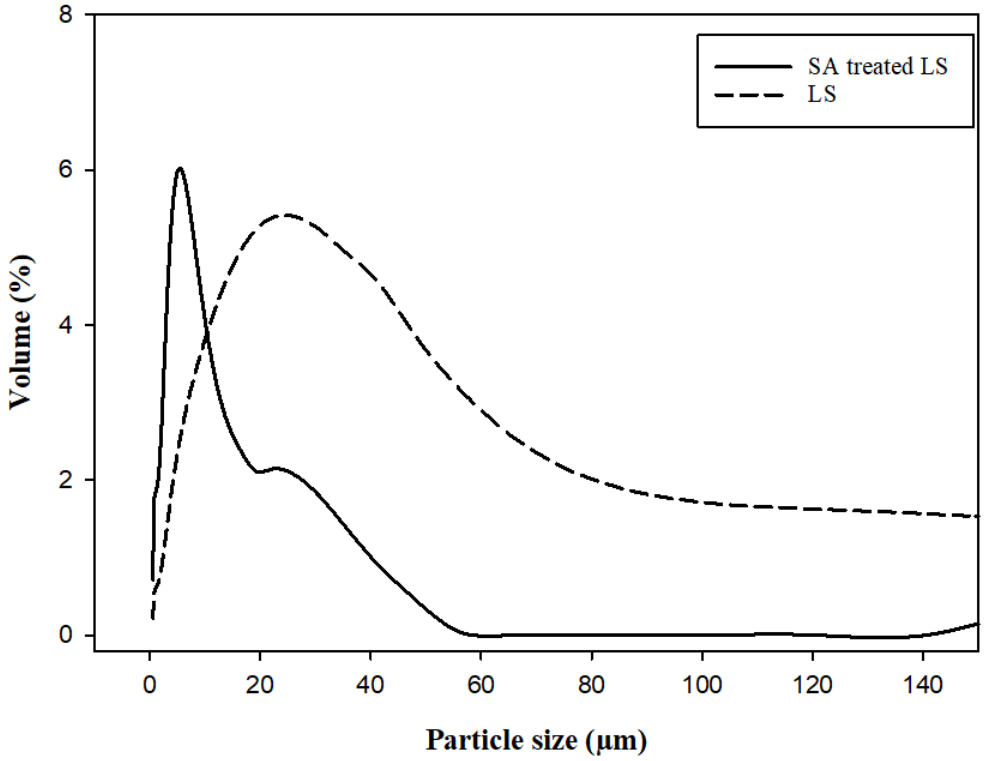

Figure 4.6. The particle size distribution curves for LS and SA treated LS.

4.2 Mechanical characterization of the composites

The effects of untreated and SA treated fillers (ES and LS) on the mechanical properties of bio-epoxy resin and the SEM micrographs of the composite fractured surfaces for the tensile, flexural and Charpy test are presented in this section.

4.2.1 Tensile properties of the composites

The effects of ES, LS and SA treated ES and SA treated LS filler loadings on the tensile strength of bio-epoxy polymer composites are shown in Figure 4.7. The inclusion of ES and LS to the bio-epoxy matrix decreased the tensile strength with an increase in filler loading up to 20 wt. %. The results showed the highest tensile strength was obtained for the unfilled bio-epoxy with a value of 60 MPa, which is close to the tensile strength provided in the manufacturers' data sheet (62 MPa). Although both untreated filler types exhibited similar tensile behaviors, ES composites had slightly better tensile strengths than that of LS composites, possibly due to the presence of inherent functionalization such as hydroxyl, amine and carboxylic groups in ES containing organic

membranes, which tends to promote hydrogen bonding with the epoxy matrix [122]. This suggests, removal of the organic membranes may not be required as they promote adhesion to the epoxy. For example, as the ES filler loading increased from 5, 10 and 20 wt. %, the composite tensile strength reduced by approximately 15 %, 25 % and 31 %, respectively, while the LS filler composites decreased by 16 %, 28 % and 32 %, respectively. The trend indicated higher strengths for low filler content composites. Depending on the end structural application of this composite, a reduction of 15-16 % tensile strength when 5 wt. % could be acceptable. Loading above 5 wt. % resulted in further reductions below the tensile strength of bio-epoxy matrix. Although the particles were thoroughly mixed into the resin during composite processing, particulate fillers added in greater amounts (e.g. 10 and 20 wt. %) may tend to agglomerate due to electrostatic forces existing between the small particles [123]. Agglomeration suggests poor dispersion of fillers in the matrix. These agglomerates are sites of stress concentration, which aid crack initiation and propagation to induce brittle failure [38,124]. These results are in agreement with Ghabeer et al. [72], who reported a decrease in tensile strengths with increase in untreated ES loadings in a polypropylene (PP) matrix. The authors believed the reductions may have been due to stress concentrations as a result of higher filler loadings (e.g. 20, 30, and 40 wt. %). In contrast, Murugan et al. [125] reported improved tensile strengths when low particle size ES fillers (0.2 µm) were added to polyvinyl chloride (PVC) at 10 wt. % filler content. The increase in the composite properties may have been attributed to the smaller particle size fillers and processing technique [31,126].

In an effort to improve the tensile strengths and reduce agglomeration of $CaCO_3$ particles, the effect of stearic acid coated fillers on the bio-epoxy matrix composites were determined. Similar to the untreated results, both SA treated filler types exhibited similar tensile behaviors. For example, as the SA treated ES filler loadings increased from 5, 10 and 20 wt. %, the tensile strengths reduced by approximately 5 %, 13 % and 26 %, respectively, while the SA treated LS filler decreased by 9 %, 20 % and 26 %, respectively compared to the unfilled bio-epoxy. Similar to the untreated fillers, depending on the final use of this composite, a 5-9 % tensile strength (compared to 15-16 % for untreated fillers) reduction when 5 wt. % could be tolerable. In comparison to untreated composites, the SA treated fillers had improved tensile strengths. For example, the tensile strengths increased by 12 %, 16 %, and 7 % for 5, 10, and 20 wt. % SA treated ES loadings, respectively, while for LS fillers, the values increased by 5 %, 11 %, and 7 % for 5,

10, and 20 wt. %, respectively. These results suggest improved dispersion of fillers and reduced agglomeration of particles, which promoted a more effective stress transfer from matrix to filler [31,72]. Despite the improvement in the tensile strengths of the SA treated fillers compared to untreated fillers, the strengths were not higher than the unfilled bio-epoxy matrix. These results are in agreement with Ghabeer et al. [127], who reported a decrease in tensile strength with low SA treated ES loadings in a polypropylene matrix, while at relatively higher loadings (20, 30 and 40 wt. %) the strength further reduced. Regardless of the treatment process done on natural limestone fillers, reductions in tensile strengths were observed when compared to the unfilled polymer matrix due to the agglomerates serving as stress concentration regions in the composite [10,128].

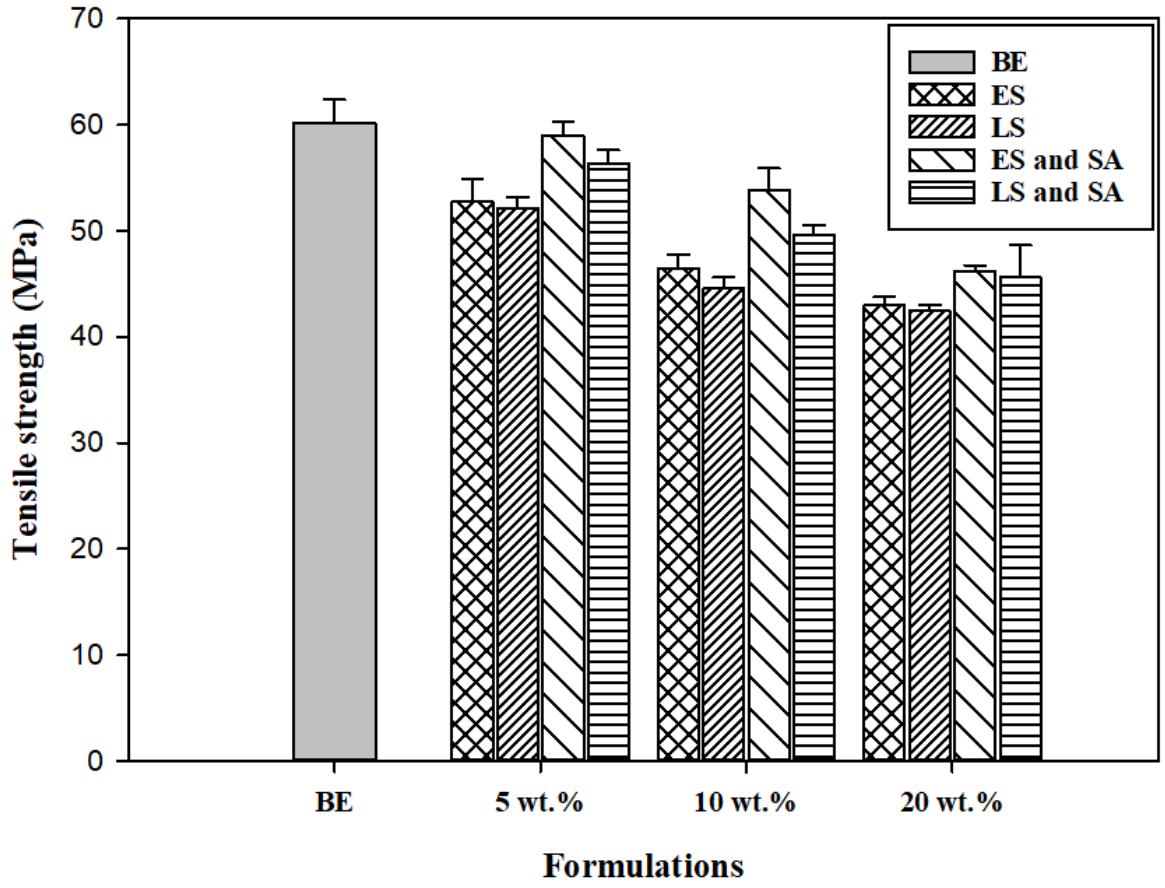

Figure 4.7. Effect of ES, LS and stearic acid treated ES and LS loadings on the tensile strength of bio-epoxy composite.

4.2.2 Fractography of fracture tensile specimens

The SEM micrographs of the tensile fractured surfaces of bio-epoxy untreated filler composites and bio-epoxy SA treated filler composites are shown in Figure 4.8 (a-e) and 4.9 (a-d), respectively. The fractured surface of the unfilled bio-epoxy resin had smooth and cleavage features indicative of a brittle fracture. It also showed fewer uninterrupted crack paths after initiation compared to the composites. Similar fractured surfaces were observed with untreated and SA treated composites. The micrographs of ES (Figure 4.8 (b)), LS (Figure 4.8 (d)), SA treated ES (Figure 4.9 (a)), and SA treated LS (Figure 4.9 (c)) (5 wt. %) composites fractured surfaces showed a greater degree of roughness (white ridges), which may be due to more crack initiation and propagation sites as a result of filler additions. The degree of roughness further increased at 20 wt. % loading (ES ((Figure 4.8 (c)), LS ((Figure 4.8 (e)), SA treated ES ((Figure 4.9 (b)), and SA treated LS ((Figure 4.9 (d))).

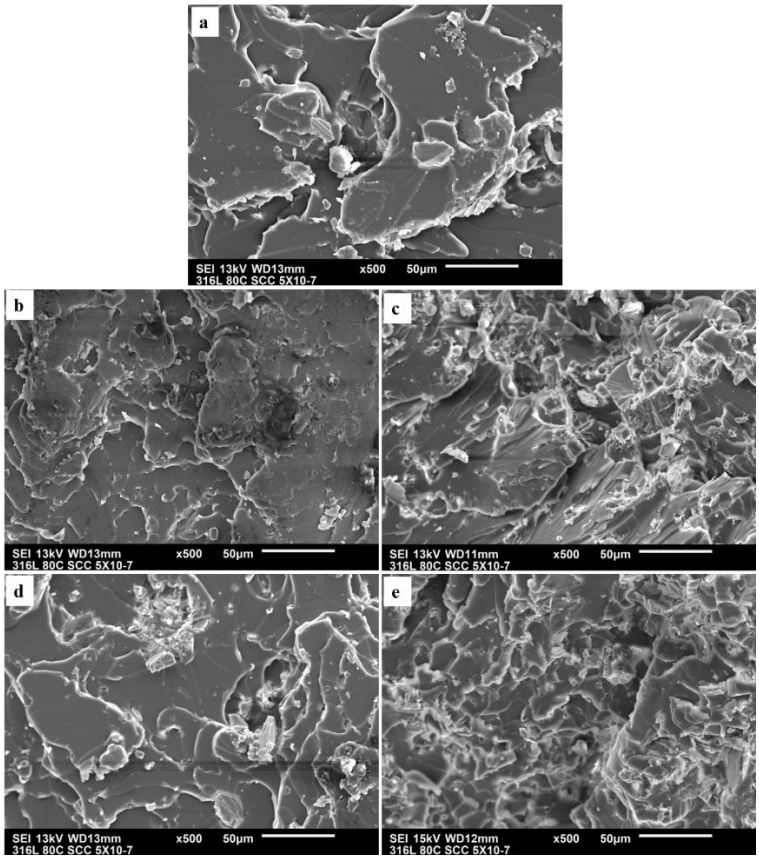

Figure 4.8. SEM micrographs of tensile fractured surfaces of (a) unfilled bio-epoxy resin (b) 5 wt. % ES loading, (c) 20 wt. % ES loading, (d) 5 wt. % LS loading and (e) 20 wt. % LS loading.

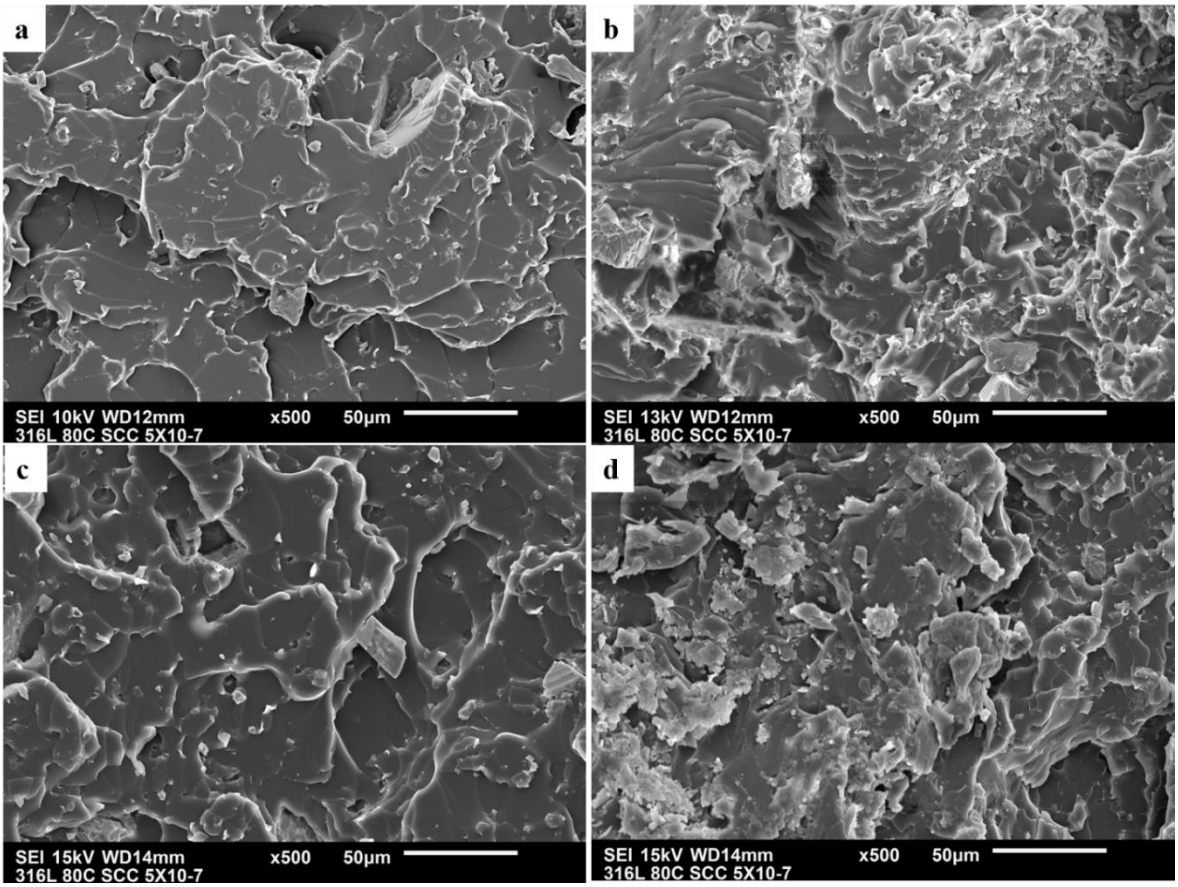

Figure 4.9. SEM micrographs of tensile fractured surfaces of (a) 5 wt. % SA treated ES loading, (b) 20 wt. % SA treated ES loading, (c) 5 wt. % SA treated LS loading and (d) 20 wt. % SA treated LS loading.

4.2.3 Flexural properties of the composites

The effect of ES, LS and SA treated ES and SA treated LS filler loadings on the flexural strength and flexural modulus of the bio-epoxy polymer composites are shown in Figure 4.10 and 4.11, respectively. The results indicated the highest flexural strength was obtained for the unfilled bio-epoxy with a value of 95.7 MPa, in-line with the manufacturers' data sheet (92.7 MPa). Both untreated filler types exhibited similar flexural behaviors. For example, as the ES filler loadings increased from 5, 10 and 20 wt. %, the composite flexural strengths reduced by 10 %, 25 % and 40 %, respectively, while the LS filler decreased the composite materials by 11 %, 24 % and 38 %, respectively. The trend indicates higher flexural strengths for low filler contents. Depending on the end application of this composite, a 10-11 % flexural strength reduction when 5 wt. % could

be adequate. Further inclusion above 5 wt. % resulted in a more pronounced decrease below the flexural strength of unfilled bio-epoxy matrix. Although the powders were carefully mixed into the resin during composite production, small filler particles in greater loadings (e.g. 10 and 20 wt. %) may gather in clusters due to electrostatic forces between the particles [123]. Similar to the tensile strength specimen results, clustering of particles creates stress concentration zones causing cracks to develop within the polymer matrix to induce early failure [38,124]. These results are in-line with Hassan et al. [127], who reported an increase in flexural strength with low ES loadings (1 and 2 wt. %) in a polyester matrix, while at higher loadings the strengths reduced (3 wt. %). In contrast, Tiimob et al. [8], reported a slight improvement (8-10 %) in flexural strengths when 5 wt. % and 10 wt. % nano-ES loadings were added to Super Sap epoxy. This increase in the composite flexural properties could be due to the smaller filler particle size and processing technique [31,126].

The addition of SA treated ES and LS presented similar flexural strength behaviors to the untreated fillers. For example, as the SA treated ES filler loading increased from 5, 10 and 20 wt. %, the composite flexural strengths reduced by approximately 5 %, 20 % and 35 %, respectively, while the SA treated LS filler decreased the composite strengths by 6 %, 20 % and 37 %, respectively. These results present a reduction of 5-6 % (compared to 10-11 % for untreated fillers) in flexural strength at 5 wt. % filler loading. When more filler particles are added, due to their high surface energy, particles have an affinity to agglomerate [129]. This improvement suggests the SA treatment reduced the surface energy of the filler particles, enhanced particle dispersion in the matrix and promoted good interfacial interaction between the filler and matrix.

The flexural modulus of both treated and untreated filler composites increased with increase in filler loadings. The flexural modulus of the unfilled bio-epoxy was 2.5 GPa similar to the manufacturers' data sheet (2.8 GPa). As the untreated ES filler loadings increased from 5, 10 and 20 wt. %, the composite flexural modulus increased by 8 %, 15 % and 15 %, respectively, while the LS filler increased the composite by 11 %, 17 % and 19 %, respectively. At 20 wt. %, filler loading for both ES and LS composites, the flexural modulus increased by 15 % and 19 %, respectively compared to the unfilled bio-epoxy. This improvement may be attributed to the higher stiffness of the filler material ($CaCO_3$, 88 GPa [130]) compared to the bio-epoxy [131]. The

increase in flexural modulus is in agreement with results obtained by other studies which reinforced green polyethylene [10] and Super Sap epoxy [8] with ES fillers. Similarly, Fombuena et al. [11] reported an increase in flexural modulus of a GreenPoxy composite with inclusions of ground seashell fillers up to 30 wt.% loadings.

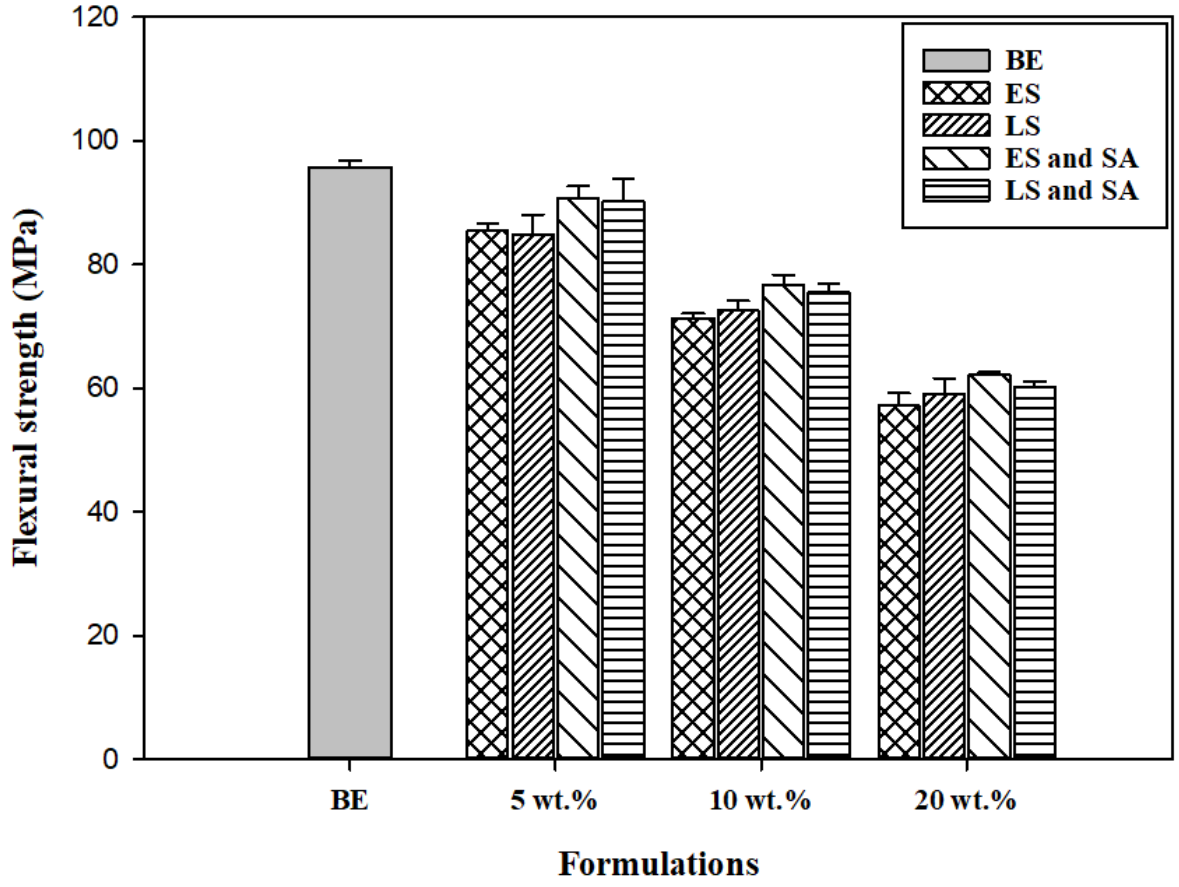

Figure 4.10. Effect of ES, LS and stearic acid treated ES and LS loadings on the flexural strength of bio-epoxy composites.

In a similar way, the composite flexural modulus of the SA treated fillers increased with increase in filler loadings. As the ES filler loading increased from 5, 10 and 20 wt. %, the flexural modulus improved by 17 %, 19 % and 21 %, respectively, while the LS filler increased by 16 %, 18 % and 20 %, respectively. At 20 wt. %, filler loading for both SA treated ES and SA treated LS, the composite flexural modulus increased by 20 % and 21 % (15 % and 19 % for untreated fillers), respectively compared to the unfilled bio-epoxy.

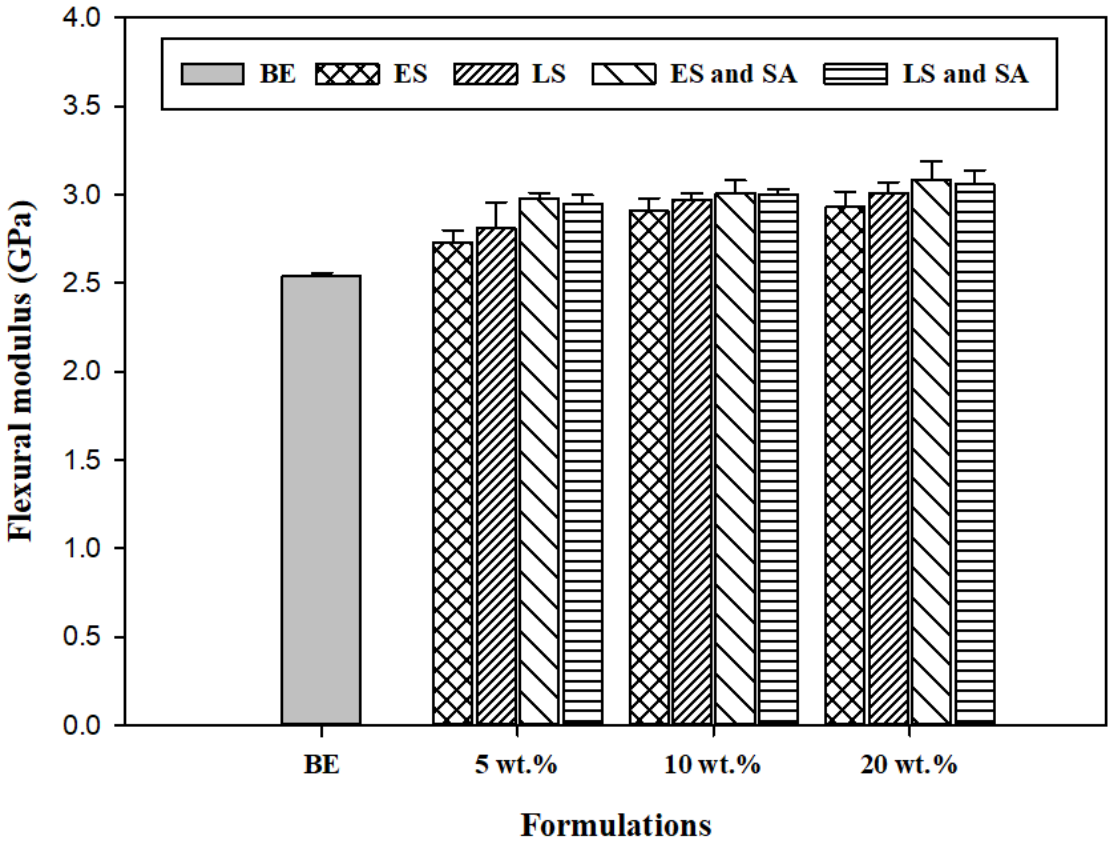

Figure 4.11. Effect of ES, LS and stearic acid treated ES and LS loadings on the flexural modulus of bio-epoxy composites.

4.2.4 Fractography of fractured flexural specimens

The SEM micrographs of the flexural fractured surfaces are shown in Figure 4.12 and 4.13. The fractured surface of the unfilled bio-epoxy resin presented a smooth, plate-like and cleavage surface suggesting brittle failure. In a similar way as the tensile fractured surfaces, the unfilled bio-epoxy presented fewer uninterrupted crack paths after initiation in comparison to the composites. The micrographs of ES (Figure 4.12 (b)), LS (Figure 4.12 (d)), SA treated ES (Figure 4.13 (a)), and SA treated LS (Figure 4.13 (c)) (5 wt. %) composites fractured surfaces showed rough surfaces due to filler addition. For 20 wt. % ES (Figure 4.12 (c)), LS (Figure 4.12 (e)), SA treated ES (Figure 4.13 (b)), and SA treated LS (Figure 4.13 (d)) loadings, the degree of roughness further increased.

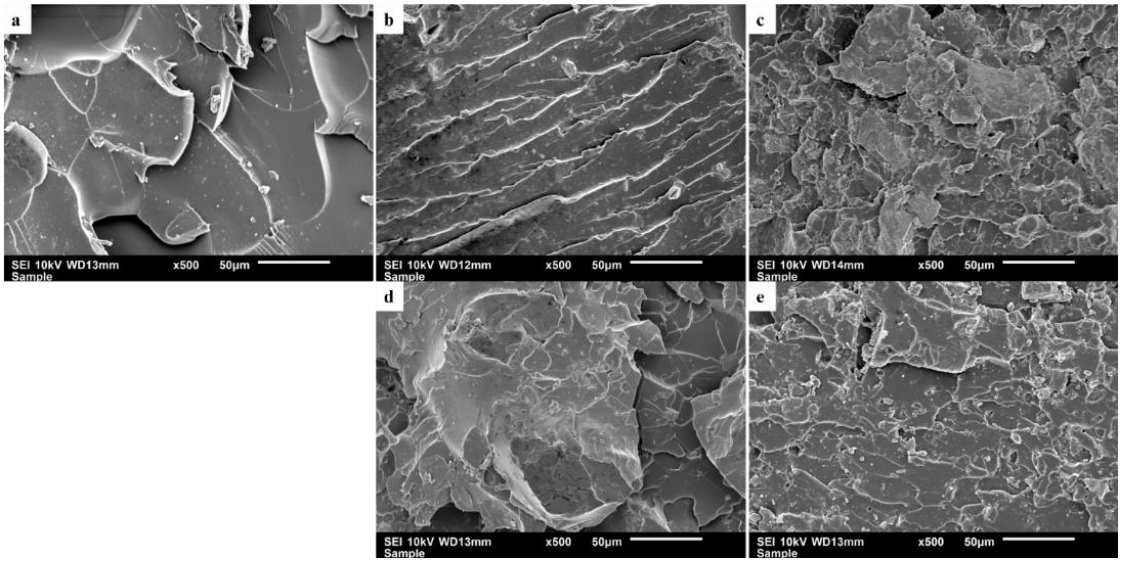

Figure 4.12. SEM micrographs of flexural fractured surfaces of (a) unfilled bio-epoxy resin (b) 5 wt. % ES loading, (c) 20 wt. % ES loading, (d) 5 wt. % LS loading and (e) 20 wt. % LS loading.

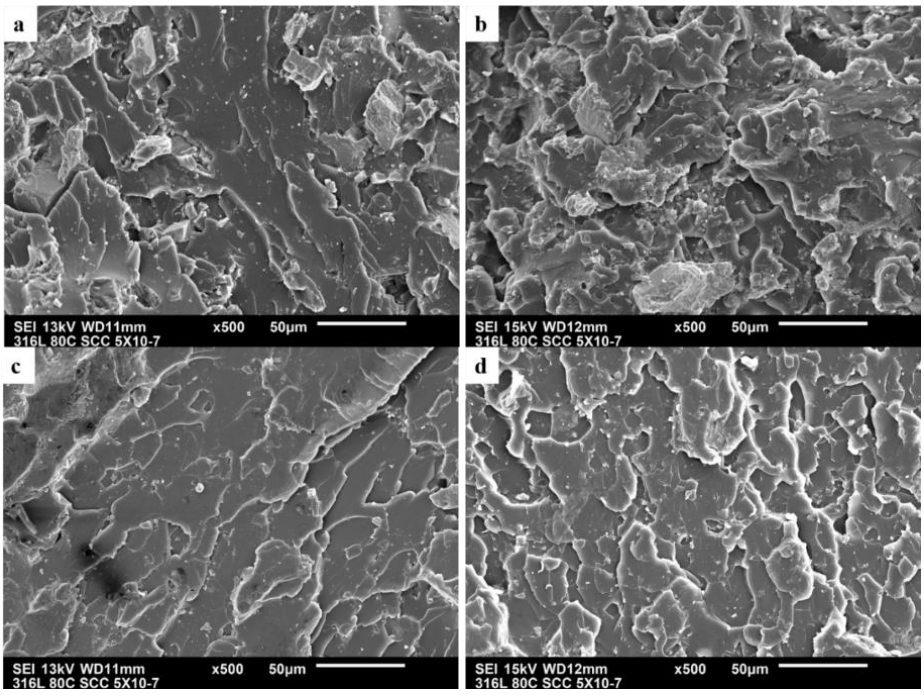

Figure 4.13. SEM micrographs of flexural fractured surfaces of (a) 5 wt. % SA treated ES loading, (b) 20 wt. % SA treated ES loading, (c) 5 wt. % SA treated LS loading and (d) 20 wt. % SA treated LS loading.

4.2.5 Charpy impact toughness of the composites

In this study, the effect of ES, LS and SA treated ES and SA treated LS fillers on the Charpy impact energy of bio-epoxy composites was determined at different temperatures (23 °C and -40 °C). The Charpy impact toughness results for the bio-epoxy composites with various filler types and contents tested at 23 °C are shown in Figure 4.14 and tested at -40 °C in Figure 4.15. The unfilled bio-epoxy had an impact energy of 8.21 kJ/m^2. The energy absorbed decreased with an increase in filler content for both untreated filler types at 23 °C and -40 °C. As the ES filler loadings increased from 5, 10 and 20 wt. %, the composite Charpy impact energy decreased by 14 %, 34 % and 44 %, respectively, while the LS fillers reduced the composites by 9 %, 31 % and 41 %, respectively. In a similar way, the SA treated composites exhibited a decrease in Charpy impact toughness with increase in filler loadings. As the ES filler loadings increased from 5, 10 and 20 wt. %, the Charpy impact toughness decreased by 24 %, 37 % and 47 %, respectively, while the LS filler decreased the composites by 20 %, 36 % and 43 %, respectively. This reduction may be due to the presence of accumulated particles in the composites, which reduced the energy absorbing capacity [132], similar to the tensile strength and flexural strength results.

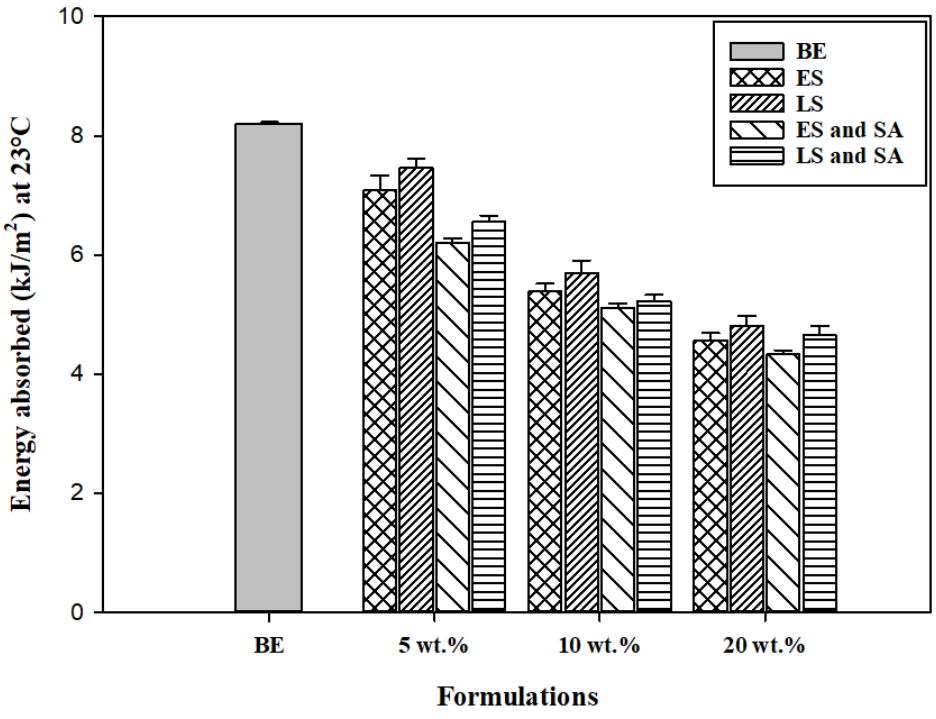

Figure 4.14. Effect of filler loadings on the impact energy absorbed by bio-epoxy composites at 23 °C.

Comparable impact toughness behavior were reported for polystyrene containing nano-clays as the filler material where the toughness decreased as a result of the presence of agglomerates in the nano-composites [132]. Similarly, Fombuena et al. [11] reported a remarkable decrease (86-92 %) in toughness at all untreated filler (5, 10, 20, 30, and 40 wt. %) loading levels of ground seashells added to a GreenPoxy composite.

In addition, for the composites (0, 5, 10, and 20 wt. %) tested at -40 °C, the toughness values decreased remarkably compared to the tests conducted at 23 °C for both filler types as shown in Figure 4.15. At -40 °C, the unfilled bio-epoxy had an impact energy of 3.38 kJ/m^2 (58 % decrease from its room temperature value)), thus, presenting a decrease in impact energy with a decrease in temperature. This suggests a more brittle behavior for the composites fractured at this lower temperature due to the composites absorbing low energy before fracture. The Charpy impact toughness at this reduced temperature was almost negligible due similar values (3.13–3.38 kJ/m^2) obtained for all composites. For example, as the ES filler loadings increased from 5, 10 and 20 wt. %, the Charpy impact energy of the composites decreased by 5 %, 7 % and 9 %, respectively, while the LS fillers reduced the composite impact energy by 4 %, 7 % and 9 %, respectively.
In a similar way, the Charpy impact toughness presented a reduction with increase in filler loading of SA treated fillers up to 20 wt. %. For instance, the Charpy impact toughness decreased by 3 %, 7 %, and 9 % with increases in SA treated ES loadings of 5, 10, and 20 wt. %, respectively while with SA treated LS loadings, reduced the composites by 4 %, 5 %, and 7 % for 5, 10, and 20 wt. %, respectively.

In summary, irrespective of the filler type or SA treatment conducted, the Charpy impact toughness presented reductions with decrease in temperature. These drops in impact energy are in agreement with Khan et al. [133], who reported a decrease in impact fracture toughness with carbon fiber loadings in epoxy matrix at low temperature (-20 °C). In addition, Charpy impact toughness of bio-epoxy composites tested at -40 °C below the T_g of 56 °C (Figure 4.21) reduced its energy absorbing capacity due to the bio-epoxy being less pliable, hard and brittle at cryogenic temperature. The results suggest these composites should not be used in cold weather applications if it will be exposed to impact load. The composites application could be utilized effectively at

room temperature as a result of 5 wt. % filler loading only decreased the impact energy by 9-14 % at room temperature compared to 61 % decrease at extreme cold condition (-40 °C).

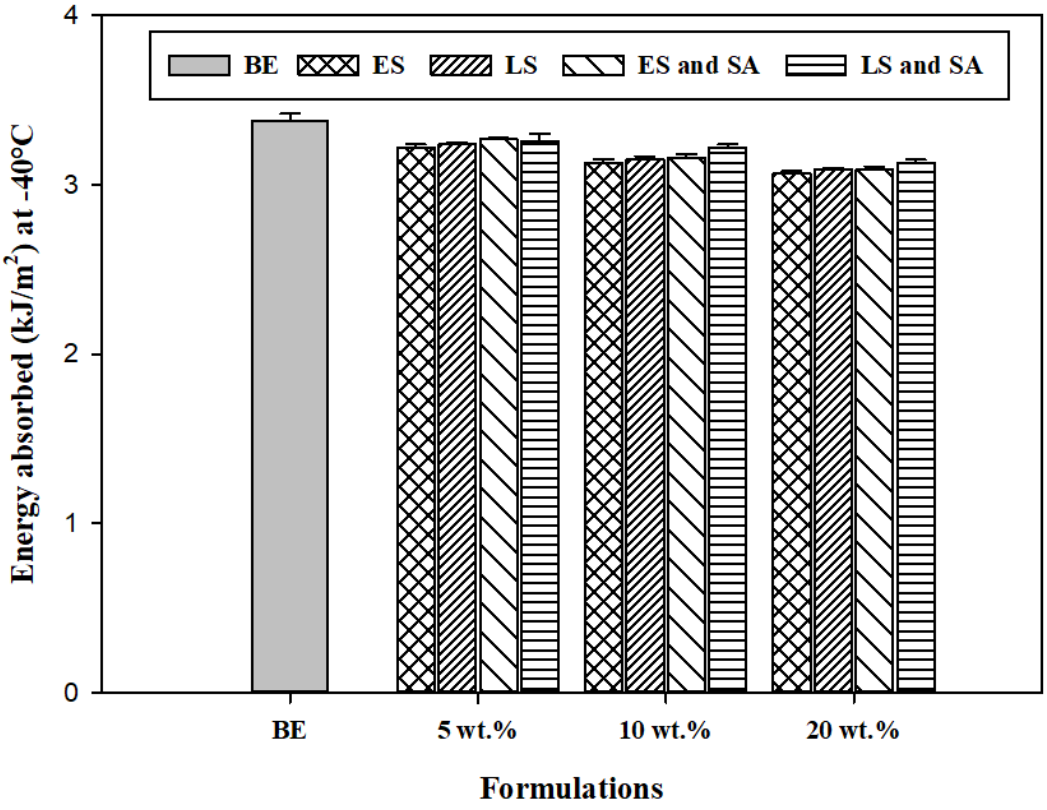

Figure 4.15. Effect of filler loadings on the impact energy absorbed by bio-epoxy composites at -40 °C.

4.2.6 Fractography of fractured Charpy impact specimens

The SEM micrographs of the Charpy impact fractured surfaces of the composites are shown in Figure 4.16-4.19 for composites fractured at 23 °C and -40 °C. The unfilled bio-epoxy resin fractured surface at temperature 23 °C (Figure 4.16 (a)) had a flat, smooth, plate-like and cleavage surface suggesting brittle failure. However, the unfilled bio-epoxy resin fractured at -40 °C showed smooth, flatter and cleavage features (Figure 4.18 (a)). This suggested the unfilled resins are harder and more brittle at low temperatures. Although, fewer uninterrupted crack paths after initiation are visible in the unfilled bio-epoxy compared to the composites, the untreated and SA treated composites still showed a flat and cleavage surface, which was different from the tensile and flexural fracture surface. This might be due to the high strain rate testing conducted on unnotched

specimens. In addition, the inclusion of 5 wt. % ES (Figure 4.16 (b)), LS (Figure 4.16 (d)), SA treated ES (Figure 4.17 (a)) and SA treated LS (Figure 4.17 (c)) fillers presented a rougher surface compared to unfilled bio-epoxy resin. For 20 wt. % ES (Figure 4.16 (c)), LS (Figure 4.16 (e)), SA treated ES (Figure 4.17 (b)) and SA treated LS (Figure 4.17 (d)) loadings, the composite roughness further increased. Similar features with composites (untreated and treated fillers) tested at 23 °C showed an increase in the degree of roughness of their fractured surfaces (Figure 4.18 and 4.19) with increase in filler contents which was also observed with composites fractured at -40 °C.

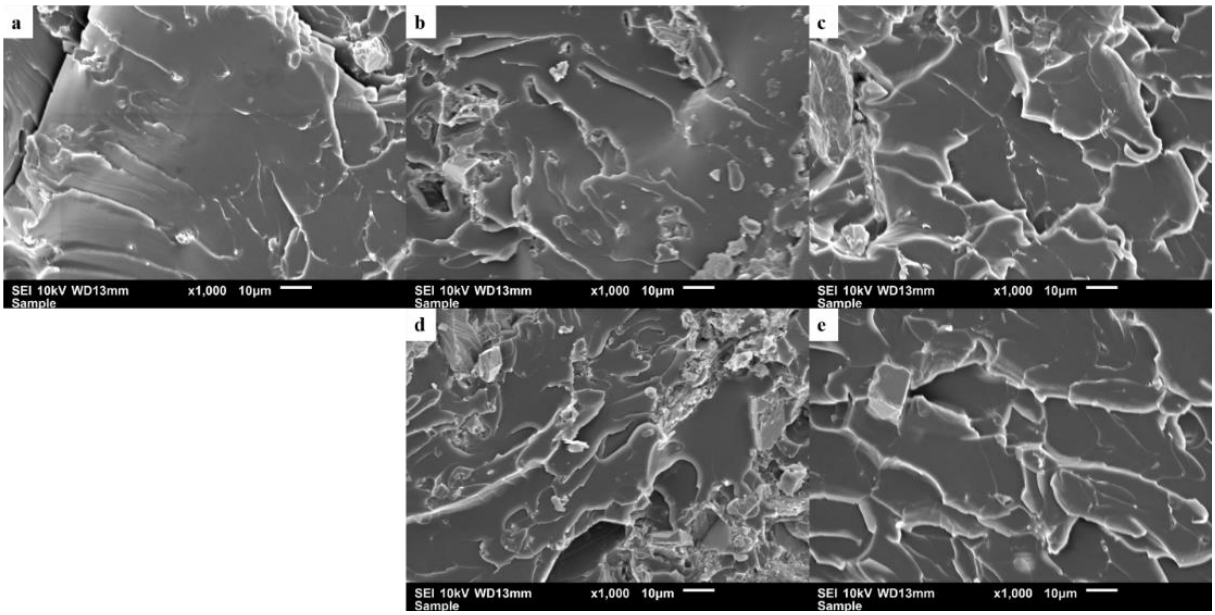

Figure 4.16. SEM micrographs of Charpy impact fractured surfaces at room temperature for (a) unfilled bio-epoxy resin, (b) 5 wt. % ES loading, (c) 20 wt. % ES loading, (d) 5 wt. % LS loading and (e) 20 wt. % LS loading.

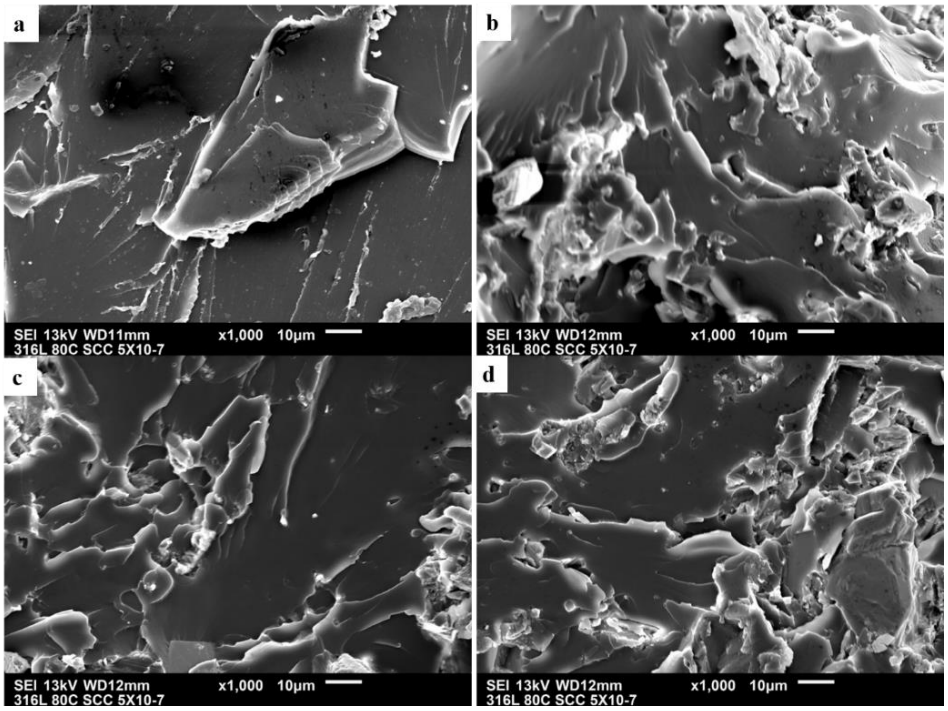

Figure 4.17. SEM micrographs of Charpy impact fractured surfaces at room temperature for (a) 5 wt. % SA treated ES loading, (b) 20 wt. % SA treated ES loading, (c) 5 wt. % SA treated LS loading and (d) 20 wt. % SA treated LS loading.

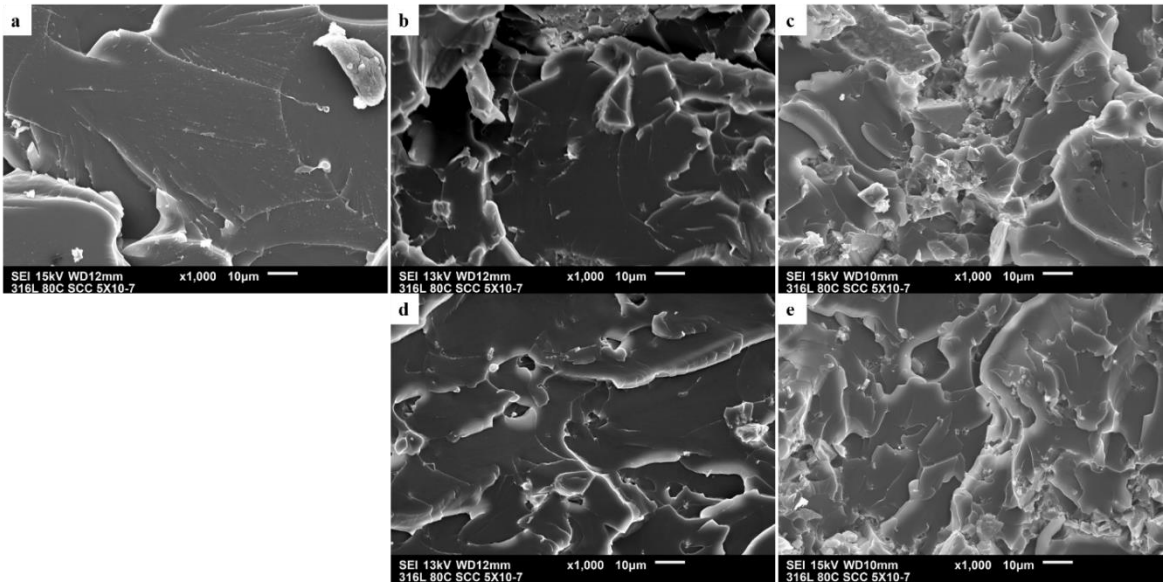

Figure 4.18. SEM micrographs of Charpy impact fractured surfaces at – 40 °C for (a) unfilled bio-epoxy resin, (b) 5 wt. % ES loading, (c) 20 wt. % ES loading, (d) 5 wt. % LS loading, and (e) 20 wt. % LS loading

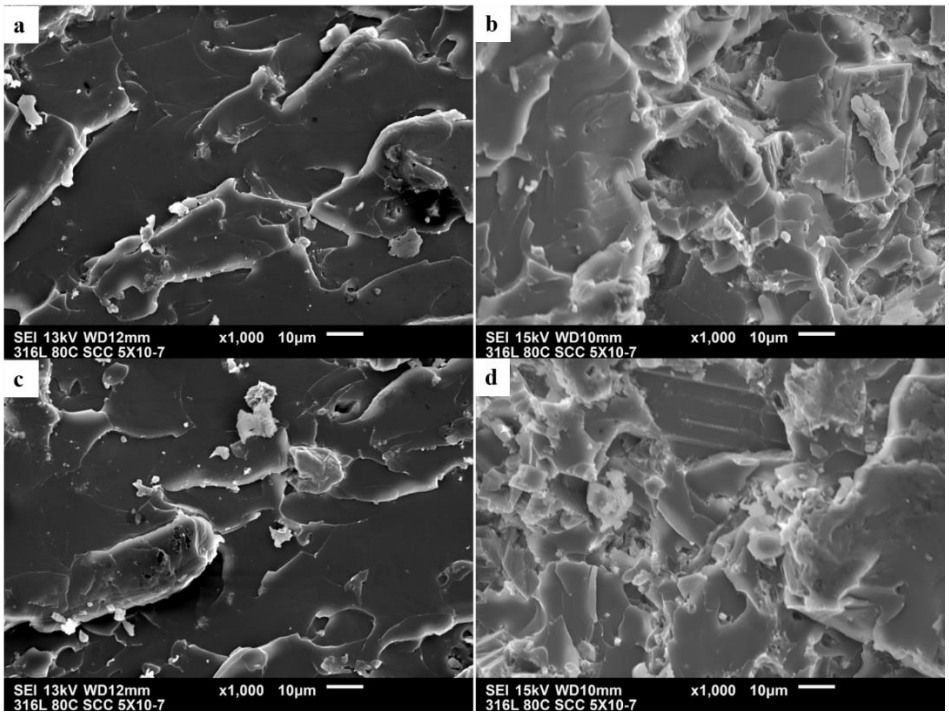

Figure 4.19. SEM micrographs of Charpy impact fractured surfaces at – 40 °C for (a) 5 wt. % SA treated ES loading, (b) 20 wt. % SA treated ES loading, (c) 5 wt. % SA treated LS loading and (d) 20 wt. % SA treated LS loading.

4.3 Effect of filler addition on the bulk density of bio-epoxy resin

The effect of filler particles (ES, LS and SA treated ES and SA treated LS) on the bulk density of the bio-epoxy composites are shown in Table 4.2. The bulk density of the unfilled bio-epoxy resin is (1.109 ± 0.006 g/cm³) comparable to the manufacturers' data sheet (1.08 g/cm³). The addition of these filler particles (both untreated and treated) slightly increased the density of the bio-epoxy composites with increase in filler loadings of 5, 10 and 20 wt. %. The increase is attributed to the addition of the filler materials having higher densities than the unfilled bio-epoxy resin. For example, filler densities were ES (2.54 ± 0.00 g/cm³), LS (2.73 ± 0.00 g/cm³), SA treated ES (2.48 ± 0.02 g/cm³) and SA treated LS (2.57 ± 0.02 g/cm³). In addition, the stearic acid treated composite formulations indicated a slight density decrease over the untreated composites.

Applying the ROM (equation (3.8)), the theoretical obtained densities were compared with experimentally obtained densities as shown in Table 4.2. The theoretical densities of all composite formulations, irrespective of the SA treatment, increased slightly over the experimentally obtained

values. For example, 5 wt. % ES had an experimental and theoretical density of 1.133 g/cm^3 and 1.142 g/cm^3, respectively which suggests the presence of voids in the composites. These results are in agreement with Khalil et al. [107] who reported an increase in theoretical density over experimental density with the addition of oil palm ash in an epoxy matrix. In a similar way, Periasamy et al. [30] reported an increase of theoretical density over experimental density with cuttlebone (seashell) particle loadings into an epoxy matrix.

Table 4.2. Density and void content of bio-epoxy composites with different filler loadings.

Composite formulations	Experimental density (g/cm^3)	Theoretical density (g/cm^3)	Void content (%)
BE	1.109 ± 0.006	-	-
5 wt. % ES	1.133 ± 0.004	1.142	0.810
5 wt. % ES and SA	1.131 ± 0.006	1.142	0.930
10 wt. % ES	1.163 ± 0.002	1.176	1.102
10 wt. % ES and SA	1.158 ± 0.002	1.175	1.426
20 wt. % ES	1.191 ± 0.002	1.251	4.771
20 wt. % ES and SA	1.192 ± 0.008	1.248	4.474
5 wt. % LS	1.131 ± 0.002	1.144	1.161
5 wt. % LS and SA	1.131 ± 0.002	1.142	1.031
10 wt. % LS	1.166 ± 0.006	1.180	1.227
10 wt. % LS and SA	1.172 ± 0.005	1.188	1.311
20 wt. % LS	1.237 ± 0.003	1.259	1.818
20 wt. % LS and SA	1.227 ± 0.004	1.253	2.005

4.4 Void content of the composites

The void content of the composites are in the range of 0.810-4.771 % as shown in Table 4.2. The void content increased with an increase in filler loading from 5-20 wt. %. The results indicated an

increase in the percentage of void content with the addition of fillers. The void contents significantly have effects on the mechanical properties and the performance of the composites. In polymer composites, voids are formed due to processing effects arising from sources such as entrapped air bubbles [134]. Higher void contents in composites suggest greater susceptibility to water penetration [107]. In this study, the composite with the highest void content was 20 wt. % ES, with a void content of ~ 4.77 %. The void content may have an effect on the water absorption level of these composites.

4.5 Water absorption tests

The water absorption behavior of the as-produced composites are shown in Figure 4.20 – 4.24. Bio-epoxy is a hydrophobic bio-based polymer and as shown in Figure 4.20 and Figure 4.21, the water uptake was low compared to the as-prepared composites. The inclusion of hydrophilic fillers (ES and LS) into the bio-epoxy polymer increased the water absorption as shown in Figure 4.20. The water absorbed increased with immersion time for all filler loading until reaching a saturation point at 504 h (or 21 days). Interestingly, ES composites at all filler loadings (5, 10, and 20 wt. %) absorbed more water than the 20 wt. % LS composites where 20 wt. % ES had the highest absorption. This indicated a lower water absorption for LS composites. Increased water absorption of ES composites may be due to the presence of pores in the eggshell particles as observed in the SEM micrograph of Figure 4.3 (a) (arrow marks). The water absorption results are consistent with the void content results and shows the composites with 20 wt. % ES had both the highest void contents as well as the highest water uptake.

In an effort to reduce the water absorption of the as-prepared composites, stearic acid was used to treat the fillers to make them hydrophobic. The results obtained are shown in Figure 4.21 and suggests a reduction in the hydrophilicity of treated fillers. The water absorption level of the different filler loadings (untreated and treated) composites are shown in Figure 4.22 - 4.24. Despite the SA treatments, the composites absorbed more water than unfilled bio-epoxy matrix. This may be due to the inclusion of particles in the polymers in contrast to unfilled resin without particles. However, the behavior presented a reduced absorption for SA treated composites (5-20 wt. %) in comparison to the untreated composites for both filler types.

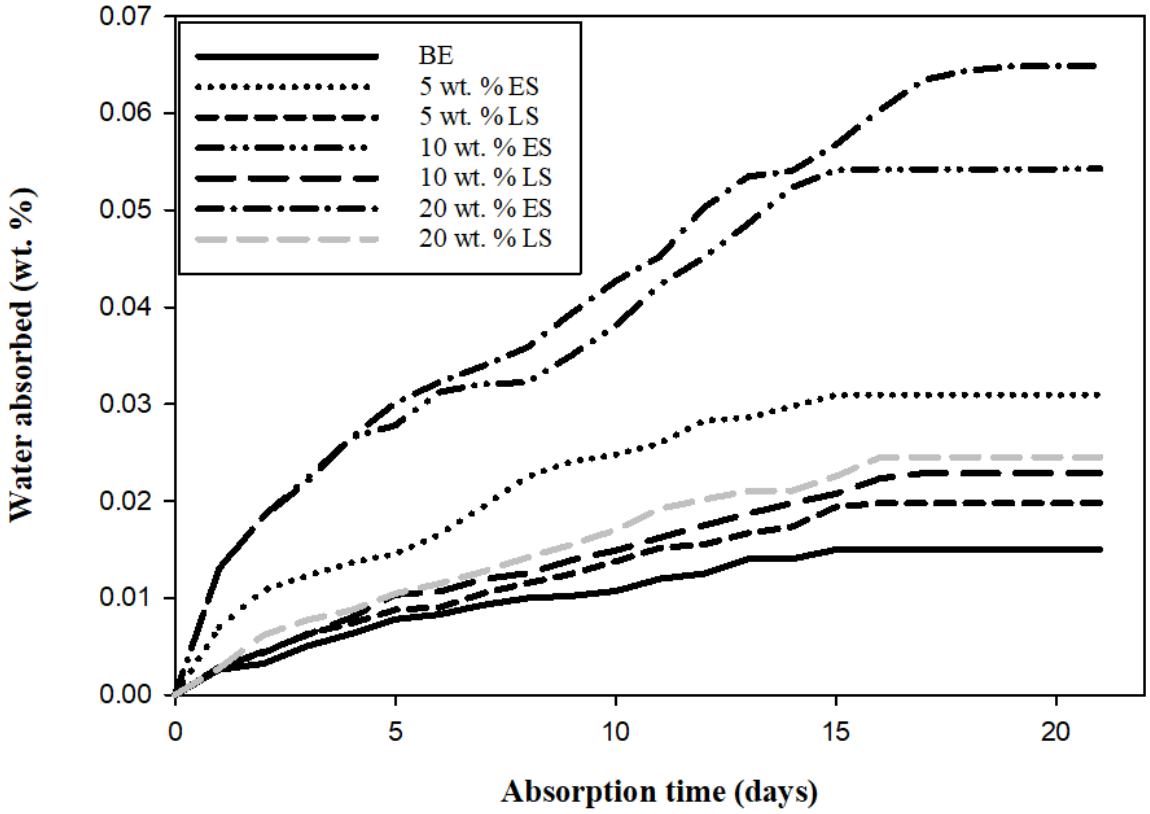

Figure 4.20. Effect of untreated ES and LS filler content on the water absorption of bio-epoxy composites.

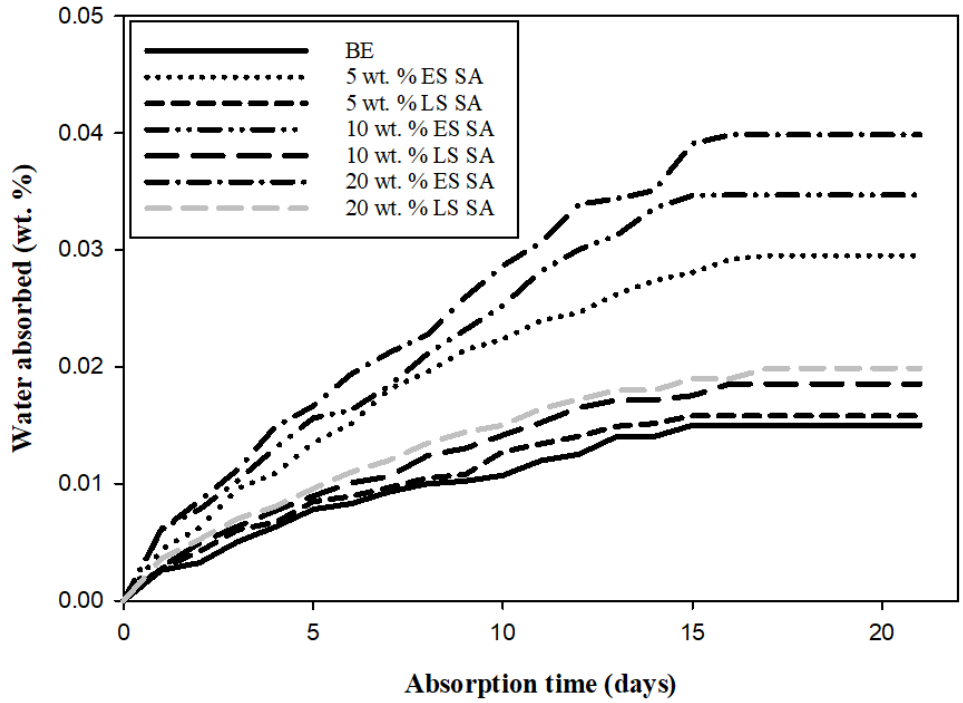

Figure 4.21: Effect of SA treated ES and LS filler content on the water absorption of bio-epoxy composites.

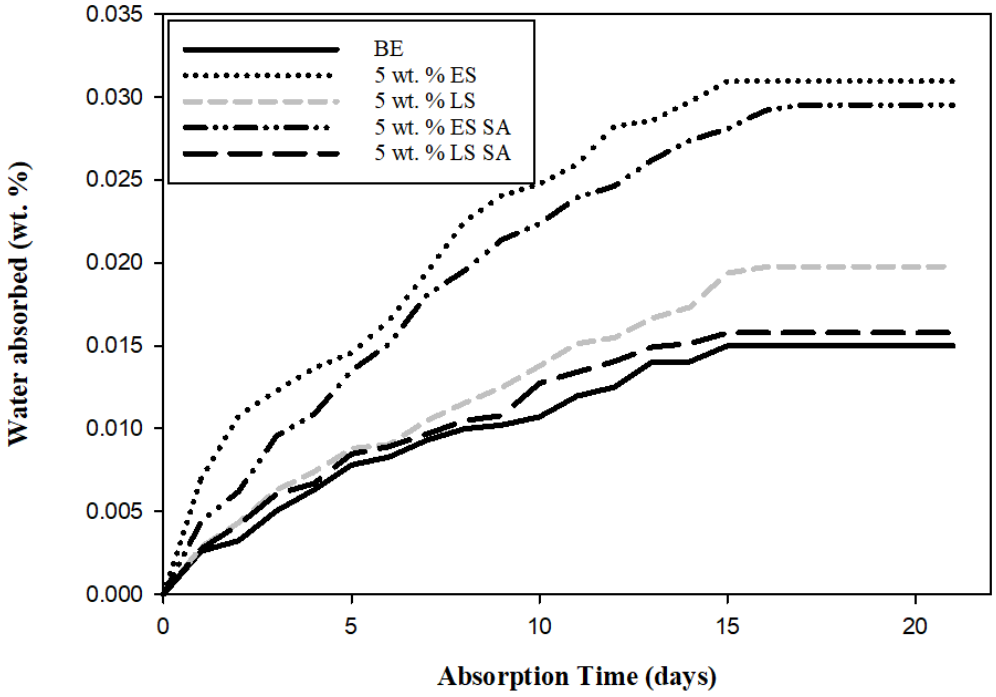

Figure 4.22. Effect of 5 wt. % ES and LS filler content (untreated and SA treated) on the water absorption of bio-epoxy composites.

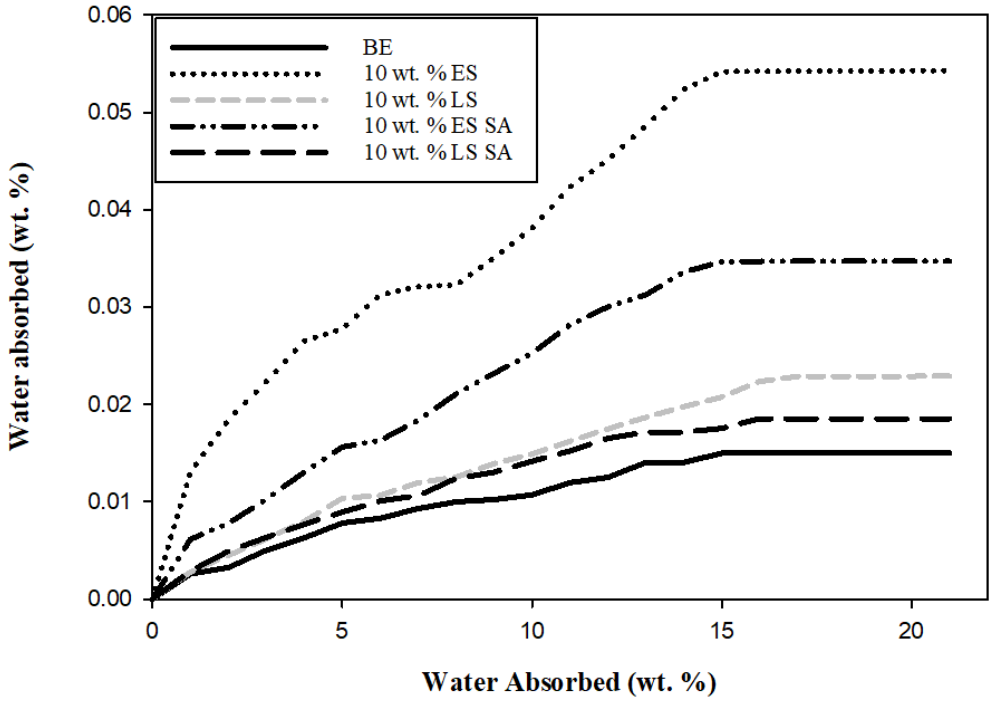

Figure 4.23. Effect of 10 wt. % ES and LS filler content (untreated and SA treated) on the water absorption of bio-epoxy composites.

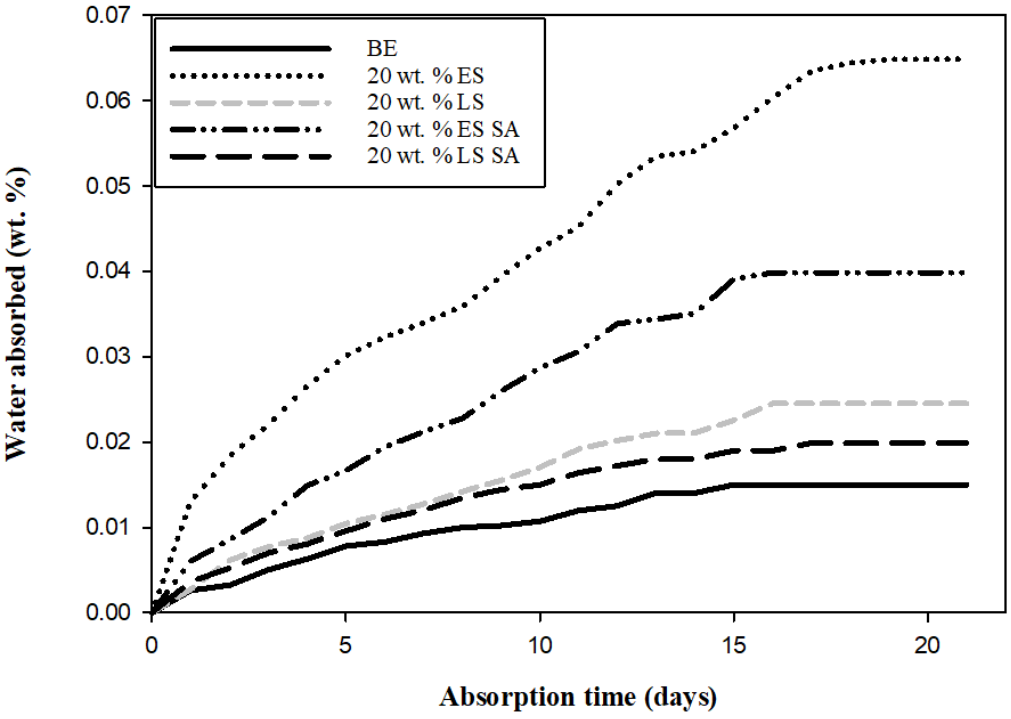

Figure 4.24. Effect of 20 wt. % ES and LS filler content (untreated and SA treated) on the water absorption of bio-epoxy composites.

4.6 Thermal analysis

The DSC thermographs of the unfilled bio-epoxy resin and 5 wt. % (ES, LS, SA treated ES and SA treated LS fillers) composites are shown in Figure 4.25. Only 5 wt. % filled composites were evaluated since they presented better mechanical properties (most promising material) than with increased filler loadings. The results showed the T_g-midpoint obtained for the unfilled bio-epoxy was 56.3 °C, which is close to the T_g-midpoint in the manufacturers' data sheet (54.0 °C). The inclusion of untreated fillers (ES and LS) into the bio-epoxy matrix had an effect on the polymer network formation, which slightly increased the T_g-midpoint compared to unfilled bio-epoxy. The T_g onset and end temperature obtained for all composite formulations are outlined in Table 4.3. The inclusion of 5 wt. % untreated ES filler increased the T_g-midpoint by 2 °C. This may be due to the reduction in the movement of bio-epoxy polymer chains around the filler particles [135].

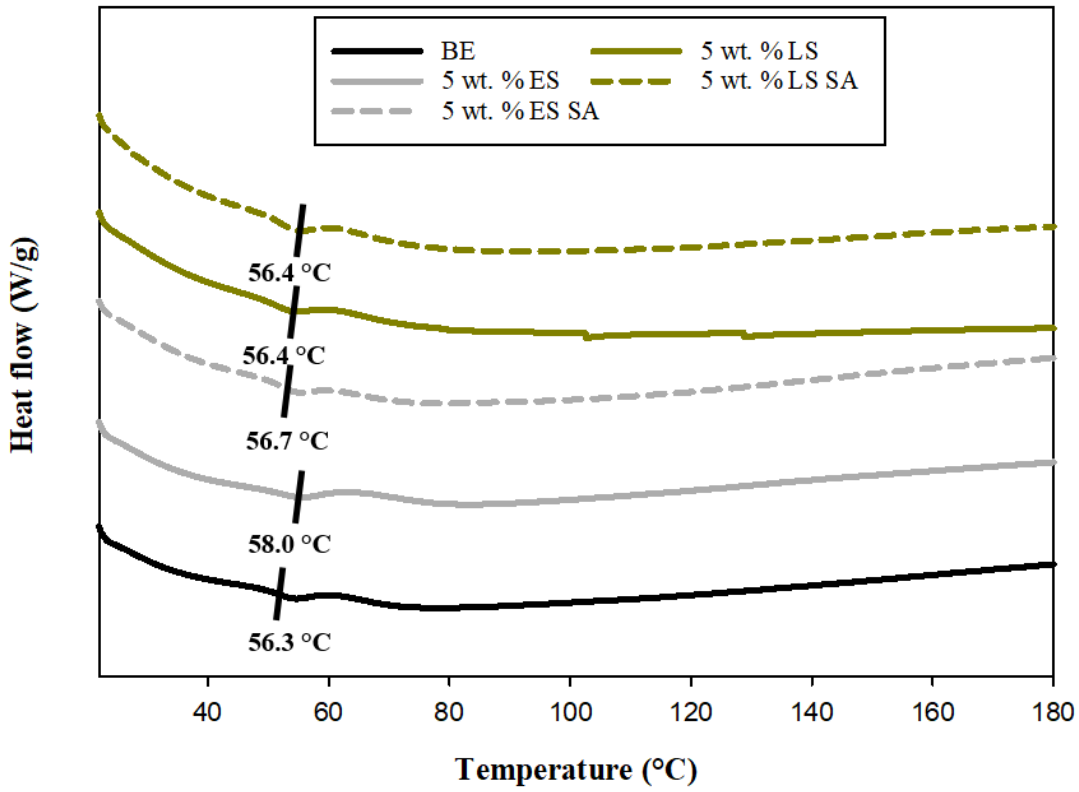

Figure 4.25. A DSC thermograph showing the effect of 5 wt. % ES, LS and SA treated ES and LS fillers on the T_g of bio-epoxy composites.

A similar increase in T_g-midpoint was observed with the addition of nano-$CaCO_3$ to synthetic epoxy in which the authors suggested the fillers may restrict polymer chain mobility [96]. The mobility of chains increases with temperature [136] and in a rubbery state, higher mobility of polymer chains occurs. Interestingly, for 5 wt. % LS composites, there was no significant change in the T_g-midpoint in comparison to the unfilled bio-epoxy resin as both had the same value. Similar observations have been reported by Jin et al. [103] in which there was no significant change in the T_g-midpoint of synthetic epoxy resin with the addition of 6 wt. % $CaCO_3$ filler contents. There may be not enough filler material distributed within the bio-epoxy to make a significant change in the T_g-midpoint. Similarly, the treated SA composites did not have a significant change in T_g-midpoint compared to unfilled bio-epoxy resin. This suggests the low content of SA treatment process may have eased the mobility of the chains in the polymer.

Table 4.3. Onset, midpoint and end temperature of bio-epoxy composites.

Composite formulation	Onset temperature (°C)	T_g midpoint temperature (°C)	End temperature (°C)
BE	54.1	56.3	58.4
5 wt. % ES	55.6	58.0	60.2
5 wt. % ES SA	54.9	56.7	58.5
5 wt. % LS	55.1	56.4	57.7
5 wt. % LS SA	54.8	56.4	58.0

4.7 Economic analysis

The amount of $CaCO_3$ that could be recovered from the top thirty-one egg producing countries in the world was calculated and shown in the analysis in Table 2.2. In Canada, the amount of $CaCO_3$ that can be recovered annually for various applications based on an empty shell weight of 6.6 g is ~ 18,117,000 kg (603,900 bags of 30 kg) as illustrated in Table 2.2.

In the city of Saskatoon, Saskatchewan, it costs ~ $ 120 to dispose waste weighing about 150 kg to the landfills [137]. Based on the analysis shown in Table 2.2, using the weight of an empty shell of ~ 6.6 g and the approximate number of eggshells sent to egg breaker plants, it would cost

companies in Canada approximately $ 14,493,600 (~ $ 14 million) annually to dispose their waste eggshells to landfills. This value is based on the assumption that 30 % of all eggs produced in Canada are sent to breaker plants. Or on the extreme end, if the analysis considers the total number of eggs produced annually in Canada with the same empty shell weight, it would cost approximately $ 48,312,000 (~ $ 48 million) to dispose this waste to landfills.

Furthermore, the annual production of mineral LS in Canada is approximately 1,805,000,000 kg (1805 kilotonnes) [138]. Based on the annual recovery of $CaCO_3$ from waste eggshells (18,117,000 kg), it indicated a potential replacement of mineral LS of only 1.00 % for use in various applications in Canada. It is important to note, the aim of this analysis was not to eliminate the current uses of mineral LS derived from rocks, but simply make use of a waste material while saving disposal costs.

4.8 Statistical analysis

Tables 4.4–4.6 and Table 4.7 showed the results of two-way ANOVA and three-way ANOVA analysis on the mechanical properties of the composites, respectively. The two-way ANOVA analysis confirmed that there was a statistically significant interaction between the treatment done on fillers and different filler loadings on the tensile strength, flexural strength and flexural modulus of the composite. In a similar way, the three-way ANOVA analysis revealed that there was a statistically significant interaction between the treatment, different filler loadings and test temperatures performed on the Charpy impact toughness of the composites. Furthermore, the analysis indicated the effect of treatment and the filler loading on Charpy impact toughness depended on temperature.

Table 4.4. Results of two-way analysis of variance of the effect of SA treatment and filler loading (ES and LS) on the tensile strength of bio-epoxy resin.

Property	Source of Variation	DF	SS	MS	F	P
ES loading	Filler load	2	428.584	214.292	70.122	<0.001
	Treatment	2	1225.227	612.614	200.464	<0.001
	Filler load x Treatment	4	237.418	59.354	19.422	<0.001
	Residual	36	110.015	3.056		
	Total	44	2001.244	45.483		
LS loading	Filler load	2	362.957	181.479	56.687	<0.001
	Treatment	2	1503.502	751.751	234.818	<0.001
	Filler load x Treatment	4	185.940	46.485	14.520	<0.001
	Residual	36	115.251	3.201		
	Total	44	2167.651	49.265		

DF = degree of freedom, SS = sum of squares, MS = mean square, F = F-test statistic and *p*-value = calculated probability

Table 4.5. Results of two-way analysis of variance of the effect of SA treatment and ES loading on the flexural strength and flexural modulus of bio-epoxy resin.

Property	Source of Variation	DF	SS	MS	F	P
Flexural strength	Filler load	2	2684.763	1342.382	772.022	<0.001
	Treatment	2	4954.464	2477.232	1424.689	<0.001
	Filler load x Treatment	4	1342.692	335.673	193.050	<0.001
	Residual	36	62.596	1.739		
	Total	44	9044.516	205.557		
Flexural modulus	Filler load	2	0.0825	0.0412	9.932	<0.001
	Treatment	2	1.785	0.892	214.973	<0.001
	Filler load x Treatment	4	0.0725	0.0181	4.365	0.006
	Residual	36	0.149	0.00415		
	Total	44	2.089	0.0475		

Table 4.6. Results of two-way analysis of variance of the effect of SA treatment and LS loading on the flexural strength and flexural modulus of bio-epoxy resin.

Property	Source of Variation	DF	SS	MS	F	P
Flexural strength	Filler load	2	2598.165	1299.083	297.346	<0.001
	Treatment	2	4912.538	2456.269	562.213	<0.001
	Filler load x Treatment	4	1323.442	330.861	75.730	<0.001
	Residual	36	157.281	4.369		
	Total	44	8991.426	204.351		
Flexural modulus	Filler load	2	0.0769	0.0384	8.701	<0.001
	Treatment	2	1.847	0.924	209.025	<0.001
	Filler load x Treatment	4	0.0556	0.0139	3.147	0.026
	Residual	36	0.159	0.00442		
	Total	44	2.139	0.0486		

Table 4.7. Results of three-way analysis of variance of the effect of SA treatment, filler loading (ES and LS) and temperature on the Charpy impact toughness of bio-epoxy resin.

Property	Source of Variation	DF	SS	MS	F	P
ES loading	Filler Load	2	9.525	4.762	734.289	<0.001
	Treatment	2	45.340	22.670	3495.442	<0.001
	Temperature	1	221.402	221.402	34137.649	<0.001
	Filler Load x Treatment	4	5.041	1.260	194.307	<0.001
	Filler Load x Temperature	2	7.017	3.508	540.940	<0.001
	Treatment x Temperature	2	33.027	16.514	2546.224	<0.001
	Filler Load x Treatment x Temp	4	3.847	0.962	148.304	<0.001
	Residual	72	0.467	0.00649		
	Total	89	325.665	3.659		
LS loading	Filler load	2	9.569	4.784	81.902	<0.001
	Treatment	2	35.794	17.897	306.367	<0.001
	Temperature	1	248.868	248.868	4260.181	<0.001
	Filler load x Treatment	4	5.330	1.333	22.811	<0.001
	Filler load x Temperature	2	7.590	3.795	64.960	<0.001
	Treatment x Temperature	2	26.265	13.133	224.805	<0.001
	Filler load x Treatment x Temp	4	4.288	1.072	18.351	<0.001
	Residual	72	4.206	0.0584		
	Total	89	341.910	3.842		

CHAPTER 5

CONCLUSIONS AND RECOMMENDATIONS

In this research, two types of calcium carbonate fillers were added to a bio-epoxy resin using a solution mixing technique. The physical properties ((eggshell (ES) and limestone (LS) particle morphology, composite fractured surfaces, particle size analysis, density (particle and bulk), void content, water absorption)), chemical (ICP-MS and XRD), mechanical (tensile, flexure, Charpy), thermal (glass transition temperature), economic and statistical analysis were determined. Furthermore, the fillers were also treated with SA, which indicated a change in properties.

5.1 Conclusions

The following conclusions are made based on the analysis and results obtained:

1. Mass spectrometry analysis indicated a lower $CaCO_3$ content for ES filler compared to LS filler due to the organic membrane remaining on the ES, while XRD analysis indicated the presence of $CaCO_3$ in the form of calcite for both untreated and SA treated fillers.
2. The SEM micrographs showed similar features for all fillers with LS and SA treated LS having less coarse surfaces to ES and SA treated ES. Both filler particles have a rhombohedral-like morphology indicating the presence of calcite. The fractured tensile and flexural surfaces of unfilled bio-epoxy resin had smooth features indicative of a brittle material, while the composites exhibited a greater degree of roughness with increase in filler loadings. The Charpy impact toughness fractured surface showed flat surface for unfilled bio-epoxy as well as for filled composites due to the higher strain rate testing.
3. The particle density of LS was higher than that of ES due to the pores present in ES. The particle density of SA treated fillers decreased in comparison to the untreated fillers, possibly due to the lower density of SA which replaced the volume of the higher density untreated fillers. The average particle size of LS was measured to be slightly larger than the ES filler. In addition, the SA treated fillers showed a narrower particle distribution curve to the untreated fillers suggesting, the SA treatment reduced most agglomerated particles.
4. The mechanical tests conducted showed ES and LS fillers exhibited similar behaviours. Both the tensile and flexural strengths decreased with increase in filler loadings possibly

due to agglomeration of particles caused by electrostatic forces while flexural modulus improved with increase in filler loadings due to the stiffer filler calcium carbonate particles. In addition, the Charpy impact toughness results at cryogenic temperature had a lower value compared to room temperature due to the composites becoming less pliable, harder and more brittle, leading to low absorbed energies. In general, for all mechanical properties evaluated, it is suggested filler loadings up to 5 wt. % would not have a significant effect on these properties.

5. Both experimental (bulk) and theoretical densities (ROM) showed an improvement with increase in filler loadings which was due to the inclusion of filler particles of higher densities. The theoretical density showed a slight increase over their experimental results due to the presence of voids in the molded composites. The highest void content was observed for composites with 20 wt. % ES. Unfilled bio-epoxy resin had the least water uptake level, while all ES filled composites absorbed more water than the highest LS filled composites containing 20 wt. % which is attributed to the more porous nature of eggshells compared to LS particles. The SA treated filler composites absorbed less water compared to the untreated filler composites indicating SA had a hydrophobic effect on the particles.
6. DSC results showed an increase in the glass transition temperature with the inclusion of 5 wt. % ES content but there was no significant change with 5 wt. % LS, 5 wt. % SA treated ES and 5 wt. % SA treated LS filler contents.
7. From the production of eggs in Canada, the economic analysis conducted in this study showed that approximately 18,117,000 kg of $CaCO_3$ could be recovered from egg breaking plants annually. Furthermore, based on the city of Saskatoon waste disposal charges, it would cost an egg breaking plant $ 14,493,600 (~ $ 14 million) annually to dispose this waste to landfills. In addition, from the annual production of mineral limestone in Canada, ES could potentially replace about 1.00 % for use in various applications.
8. The ANOVA analysis confirmed that there was a statistically significant interaction between the treatment and filler loadings on the tensile strength, flexural strength and flexural modulus, while test temperature also had a statistically significant effect on the Charpy impact toughness of the composites.

From the results obtained, waste ES presented a promising approach to serve as a possible alternative to mineral LS used as fillers in bio-epoxy composites. Although ES waste represents only a small fraction of the mineral LS usage in Canada, the aim of this work is to promote the use of waste materials and divert them from landfills. Developing new purposes for waste eggshells may reduce the disposal to landfills.

5.2 Recommendations for future work

The following are suggested for future work:

1. Investigation into the removal of the organic membrane by heat at temperatures below the calcium oxide (CaO) formation, or using chemicals (e.g. sodium hypochlorite (NaOCl) (e.g. bleach), sodium hydroxide (NaOH)), or by heating above 750 °C to form CaO and further reacting to carbon dioxide (CO_2) to form $CaCO_3$ without any organic membrane.
2. Determine the effect of ES without organic membrane (purified form) on the physical, mechanical and thermal properties of bio-epoxy resin composites.
3. Design a model for egg breaker plant companies in Canada that will take into account the conversion of waste ES to $CaCO_3$ after separating the liquid egg from their shell. Perform an economic analysis for processing the waste eggshells.

References

[1] F. Campbell, Manufacturing processes for advanced composites, 4th Edition, Elsevier, Oxford, UK 2004.

[2] M. Groover, Fundamentals of mordern manufacturing, 4th Edition, John Wiley & Sons, Inc., Danvers, Massachusetts, USA 2010.

[3] M. Rosso, Ceramic and metal matrix composites: Routes and properties, J. Mater. Process. Technol. 175 (2006) 364–375.

[4] O. Faruk, A.K. Bledzki, H. Fink, M. Sain, Progress in polymer science biocomposites reinforced with natural fibers : 2000 – 2010, Prog. Polym. Sci. 37 (2012) 1552–1596.

[5] B. Elyse, K. Santosh, P. Giuseppe, S. Joseph, Recent advances in bio-based epoxy resins and bio-based epoxy curing agents, J. Appl. Polym. Sci. 133 (2016) 1-19.

[6] Entropy resins, Super Sap Cpf-Cpl technical data sheet - Available online: https://wjayc3fs2tlk6mip9ccjq208-wpengine.netdna-ssl.com/wp-content/uploads/CPM-TDS-v2.pdf (accessed on June 16, 2019).

[7] E. Omrani, B. Barari, A. Dorri Moghadam, P.K. Rohatgi, K.M. Pillai, Mechanical and tribological properties of self-lubricating bio-based carbon-fabric epoxy composites made using liquid composite molding, Tribol. Int. 92 (2015) 222–232.

[8] B. Tiimob, S. Jeelani, V. Rangari, Eggshell reinforced biocomposite - An advanced "green" alternative structural material, J. Appl. Polym. Sci. 133 (2016) 1–10.

[9] Sicomin, SR Greenpoxy 55 technical datasheet - Available online: http://www.matrix-composites.co.uk/prod-data-sheet/old/greenpoxy-55-ft-uk.pdf (acessed online on July 28, 2019).

[10] T. Boronat, V. Fombuena, D. Garcia-Sanoguera, L. Sanchez-Nacher, R. Balart, Development of a biocomposite based on green polyethylene biopolymer and eggshell, Mater. Des. 68 (2015) 177–185.

[11] V. Fombuena, L. Bernardi, O. Fenollar, T. Boronat, R. Balart, Characterization of green Composites from biobased epoxy matrices and bio-fillers derived from seashell wastes,

Mater. Des. 57 (2014) 168–174.

[12] A.K. Kaw, Mechanics of composite materials, 2nd Edition, United States of America: CRC Press, 2006.

[13] J. Wu, Eggs and egg products processing, in: Food Process. Princ. Appl., 2nd Edition, 2014: pp. 437–455.

[14] P. Pliya, D. Cree, Limestone derived eggshell powder as a replacement in Portland cement mortar, Constr. Build. Mater. 95 (2015) 1–9.

[15] P. Intharapat, A. Kongnoo, K. Kateungngan, The potential of chicken eggshell waste as a bio-filler filled epoxidized natural rubber (ENR) composite and its properties, J. Polym. Environ. 21 (2013) 245-258.

[16] H.Y. Li, Y.Q. Tan, L. Zhang, Y.X. Zhang, Y.H. Song, Y. Ye, M.S. Xia, Bio-filler from waste shellfish shell: Preparation, characterization, and its effect on the mechanical properties on polypropylene composites, J. Hazard. Mater. (2012) 256–262.

[17] M. Felipe-Sese, D. Eliche-Quesada, A.F. Corpas-Iglesias, The use of solid residues derived from different industrial activities to obtain calcium silicate for use as insulating construction materials, Ceram. Int. 37 (2011) 3019–3028.

[18] C. Sonenklar, Famous for egg waste, Res. State News, Penn State Univ. (1999) 1–2.

[19] M.C. Barros, P.M. Bello, M. Bao, J.J. Torrado, From waste to commodity: transforming shells into high purity calcium carbonate, J. Clean. Prod. 17 (2009) 400–407.

[20] M. Mustakimah, S. Yusup, S. Maitra, Decomposition study of calcium carbonate in cockle shell., J. Eng. Sci. Technol. 7 (2012) 1–10.

[21] G.L. Yoon, B.T. Kim, B.O. Kim, S.H. Han, Chemical-mechanical characteristics of crushed oyster-shell, Waste Manag. 23 (2003) 825–834.

[22] M. Hamester, P. Balzer, D. Becker, Characterization of calcium carbonate obtained from oyster and mussel shells and incorporation in polypropylene, Mater. Res. 15 (2012) 204–208.

[23] Z.T. Yao, T. Chen, H.Y. Li, M.S. Xia, Y. Ye, H. Zheng, Mechanical and thermal properties

of polypropylene (PP) composites filled with modified shell waste, J. Hazard. Mater. 262 (2013) 212–217.

[24] P. Lertwattanaruk, N. Makul, C. Siripattarapravat, Utilization of ground waste seashells in cement mortars for masonry and plastering, J. Environ. Manage. 111 (2012) 133–141.

[25] H.E.A. Tudor, C.C. Gryte, C.C. Harris, Seashells: Detoxifying agents for metal-contaminated waters, Water, Air, Soil Pollut. 173 (2006) 209–242.

[26] H. Moustafa, A.M. Youssef, S. Duquesne, N.A. Darwish, Characterization of bio-filler derived from seashell wastes and its effect on the mechanical, thermal, and flame retardant properties of ABS composites, Polym. Compos. 38 (2017) 2788-2797.

[27] W. Callister, D. Rethwisch, Materials science and engineering: An introduction, 9th Edition, John Wiley & Sons, Inc., Danvers, Massachusetts, USA 2014.

[28] C. Dearmitt, R. Rothon, Particulate fillers, selection, and use in polymer composites, Polymers and Polymeric Composite, Springer, Verlag Berlin Heidelberg, Germany 2016.

[29] P. Patnaik, Handbook of inorganic chemicals, McGraw-Hill Companies, Inc., New York, USA 2003.

[30] K. Periasamy, G.C. Mohankumar, Sea coral-derived cuttlebone reinforced epoxy composites: Characterization and tensile properties evaluation with mathematical models, J. Compos. Mater. 50 (2016) 807–823.

[31] Z. Cao, M. Daly, L. Clémence, L.M. Geever, I. Major, C.L. Higginbotham, D.M. Devine, Chemical surface modification of calcium carbonate particles with stearic acid using different treating methods, Appl. Surf. Sci. 378 (2016) 320–329.

[32] C. Tyler, K. Simkiss, A study of the eggshells of Ratite birds, Proc. Zool. Soc. 133 (1959).

[33] DSM, A practical guide to the efficient evaluation of egg quality at farm level, in: DSM Egg Qual. Man., DSM Nutritional Products Ltd, Basel, Switzerland, 2018

[34] S. John-Jaja, U. Udoh, S. Nwokolo, Repeatability estimates of egg weight and egg-shell weight under various production periods for Bovan Nera black laying chicken, Beni-Suef Univ. J. Basic Appl. Sci. 5 (2016) 389–394.

[35] J.. Stadelman, Eggs and egg products, Encycl. Food Sci. Technol. (2000) 593–599.

[36] D. Siva Rama Krishna, A. Siddharthan, S.K. Seshadri, T.S. Sampath Kumar, A novel route for synthesis of nanocrystalline hydroxyapatite from eggshell waste, J. Mater. Sci. Mater. Med. 18 (2007) 1735–1743.

[37] A. Mittal, M. Teotia, R.K. Soni, J. Mittal, Applications of egg shell and egg shell membrane as adsorbents: A review, J. Mol. Liq. 223 (2016) 376-387.

[38] T. Mohan, K. Kanny, Thermal, mechanical and physical properties of nanoegg shell particle-filled epoxy nanocomposites, J. Compos. Mater. (2018) 1–12.

[39] K. Beck, X. Brunetaud, J.-D. Mertz, M. Al-Mukhtar, On the use of eggshell lime and tuffeau powder to formulate an appropriate mortar for restoration purposes, Geol. Soc. London, Spec. Publ. 331 (2010) 137-145.

[40] U.N. Okonkwo, I.C. Odiong, E.E. Akpabio, The effects of eggshell ash on strength properties of cement-stabilized lateritic, Int. J. Sustain. Constr. Eng. Technol. 3 (2012) 18-25.

[41] J. Koudele, E. Heinsohn, The egg products industry of the United States: Part I. Historical highlights, 1900-59, Kan. Agr. Expt. Stn. Bull. No. 423. (1960) 1–46.

[42] D. Cree, A. Rutter, Sustainable Bio-inspired limestone eggshell powder for potential industrialized applications, ACS Sustain. Chem. Eng. 3 (2015) 941–949.

[43] Food and Agriculture Organization of the United Nations (FAO), Corporate Statistical Database - Available online: http://www.fao.org/faostat/en/#data/CL (accessed online on January 09, 2019).

[44] D. Liao Dexiang, W. Zheng, X. Li, Q. Yang, X. Yue, L. Guo, G. Zeng, Removal of lead(II) from aqueous solutions using carbonate hydroxyapatite extracted from eggshell waste, J. Hazard. Mater. 177 (2010) 126–130.

[45] H.A. De Paula, J.G. Becker, A.P. Davis, Characterization of the uptake of divalent metal ions by a hatchery residual, Environ. Eng. Sci. 25 (2008) 737–746.

[46] Y.S. Ok, S.S. Lee, W.T. Jeon, S.E. Oh, A.R.A. Usman, D.H. Moon, Application of eggshell

waste for the immobilization of cadmium and lead in a contaminated soil, Environ. Geochem. Health. 33 (2011) 31–39.

[47] E.M. Rivera, M. Araiza, W. Brostow, V.M. Castaño, J.R. Díaz-Estrada, R. Hernández, J.R. Rodríguez, Synthesis of hydroxyapatite from eggshells, Mater. Lett. 41 (1999) 128–134.

[48] F.S. Murakami, P.O. Rodrigues, C.M.T. de Campos, M.A.S. Silva, Physicochemical study of $CaCO_3$ from egg shells, Ciência e Tecnol. Aliment. 27 (2007) 658–662.

[49] D.A. Oliveira, P. Benelli, E.R. Amante, A literature review on adding value to solid residues: Egg shells, J. Clean. Prod. 46 (2013) 42–47.

[50] P.K. Mallick, Particulate and short fiber reinforced polymer composites, Pergamon Press, Oxford, UK 2000.

[51] S. Yoo, J.S. Hsieh, P. Zou, J. Kokoszka, Utilization of calcium carbonate particles from eggshell waste as coating pigments for ink-jet printing paper, Bioresour. Technol. 100 (2009) 6416–6421.

[52] Z. Wei, C. Xu, B. Li, Application of waste eggshell as low-cost solid catalyst for biodiesel production, Bioresour. Technol. 100 (2009) 2883–2885.

[53] S.C. Wu, H.C. Hsu, S.K. Hsu, Y.C. Chang, W.F. Ho, Synthesis of hydroxyapatite from eggshell powders through ball milling and heat treatment, J. Asian Ceram. Soc. 4 (2016) 85–90.

[54] S.W. Lee, S.G. Kim, C. Balázsi, W.S. Chae, H.O. Lee, Comparative study of hydroxyapatite from eggshells and synthetic hydroxyapatite for bone regeneration, Oral Surg. Oral Med. Oral Pathol. Oral Radiol. 113 (2012) 348–355.

[55] H. Zhou, J. Lee, Nanoscale hydroxyapatite particles for bone tissue engineering, Acta Biomater. 7 (2011) 2769–2781.

[56] E.C.Y. Li-Chan, W.D. Powrie, S. Nakai, The chemistry of eggs and egg products, in: Egg Sci. Technol., 4th Edition, Haworth Press, New York, USA 1995.

[57] G. Whittow, Sturkie's avian physiology, 5th Edition, Academic Press, San Diego, CA, 2000.

[58] W.T. Tsai, J.M. Yang, C.W. Lai, Y.H. Cheng, C.C. Lin, C.W. Yeh, Characterization and adsorption properties of eggshells and eggshell membrane, Bioresour. Technol. 97 (2006) 488–493.

[59] A.H. Parsons, Structure of the eggshell, Poult. Sci. 61 (1982) 2013–2021.

[60] W.J. Stadelman, O. Cotterill, Egg science and technology, 4th Edition, CRC Press, Boca Raton, Florida, 1995.

[61] N. Betancourt, D. Cree, Mechanical properties of poly (lactic acid) composites reinforced with $CaCO_3$ eggshell based fillers, Mater. Res. Soc. 3 (2017) 6–11.

[62] Z. Yao, M. Xia, H. Li, T. Chen, Y. Ye, H. Zheng, Bivalve shell: Not an abundant useless waste but a functional and versatile biomaterial, Crit. Rev. Environ. Sci. Technol. 44 (2014) 2502–2530.

[63] M. Olivia, A.A. Mifshella, L. Darmayanti, Mechanical properties of seashell concrete, in: Procedia Eng., (2015) 760–764.

[64] M. Olivia, R. Oktaviani, Ismeddiyanto, Properties of concrete containing ground waste cockle and clam seashells, in: Procedia Eng., (2017) 658–663.

[65] J.H. Jung, B.H. Shon, K.S. Yoo, K.J. Oh, Physicochemical characteristics of waste seashells for acid gas cleaning absorbent, Korean J. Chem. Eng. 17 (2000) 585–592.

[66] B. Safi, M. Saidi, A. Daoui, A. Bellal, A. Mechekak, K. Toumi, The use of seashells as a fine aggregate (by sand substitution) in self-compacting mortar (SCM), Constr. Build. Mater. 78 (2015) 430–438.

[67] E.I. Yang, S.T. Yi, Y.M. Leem, Effect of oyster shell substituted for fine aggregate on concrete characteristics: Part I. Fundamental properties, Cem. Concr. Res. 35 (2005) 2175–2182.

[68] H. Yoon, S. Park, K. Lee, J. Park, Oyster shell as substitute for aggregate in mortar, Waste Manag. Res. 22 (2004) 158–170.

[69] B.Y. Zhong, Q. Zhou, C.F. Chan, Y. Yu, Structure and property characterization of oyster shell cementing material, Jiegou Huaxue. 31 (2012) 85–92.

[70] A.H. Shah, Y. Zhang, X. Xu, A.Q. Dayo, X. Li, S. Wang, W. Liu, Reinforcement of stearic acid treated egg shell particles in epoxy thermosets: Structural, thermal, and mechanical characterization, Materials (Basel). 11 (2018) 1–18.

[71] Y. Lin, H. Chen, C. Chan, J. Wu, The toughening mechanism of polypropylene / calcium carbonate nanocomposites, Polymer (Guildf). 51 (2010) 3277–3284.

[72] T. Ghabeer, R. Dweiri, S. Al-Khateeb, Thermal and mechanical characterization of polypropylene/eggshell biocomposites, J. Reinf. Plast. Compos. 32 (2013) 402–409.

[73] B. Bittmann, F. Haupert, A.K. Schlarb, Ultrasonic dispersion of inorganic nanoparticles in epoxy resin, Ultrason. Sonochem. 16 (2009) 622–628.

[74] M.M. Rahman, A.N. Netravali, B.J. Tiimob, V.K. Rangari, Bioderived “green” composite from soy protein and eggshell nanopowder, ACS Sustain. Chem. Eng. 2 (2014) 2329–2337.

[75] D.W. Kim, J.Y. Lee, S.M. Lee, J.C. Lim, Surface modification of calcium carbonate nanoparticles by fluorosurfactant, Colloids Surfaces A Physicochem. Eng. Asp. 536 (2018) 213–223.

[76] H. He, K. Li, J. Wang, G. Sun, Y. Li, J. Wang, Study on thermal and mechanical properties of nano-calcium carbonate/epoxy composites, Mater. Des. 32 (2011) 4521–4527.

[77] K. Premphet, P. Horanont, Phase structure of ternary polypropylene/elastomer/filler composites : effect of elastomer polarity, Polym. 41. (2000) 9283–9290.

[78] D. Ciprari, K. Jacob, R. Tannenbaum, Characterization of polymer nanocomposite interphase and its impact on mechanical properties, Macromolecules. 39 (2006) 6565–6573.

[79] Y. Lin, H. Chen, C.-M. Chan, J. Wu, High impact toughness polypropylene/$CaCO_3$ nanocomposites and the toughening mechanism, Macromolecules. 41 (2008) 9204–9213.

[80] M. Rahmani, F. Ashenai, G. Payganeh, Effect of surface modification of calcium carbonate nanoparticles on their dispersion in the polypropylene matrix using stearic acid, Mech. Ind. 67 (2014) 63–67.

[81] S.R. Mihajlović, D.R. Vučinić, Ž.T. Sekulić, S.Z. Milićević, B.M. Kolonja, Mechanism of stearic acid adsorption to calcite, Powder Technol. 245 (2013) 208-216.

[82] E. Yoğurtcuoğlu, M. Uçurum, Surface modification of calcite by wet-stirred ball milling and its properties, Powder Technol. 214 (2011) 47-53.

[83] R.N. Rothon, R.N. Ronthon, R.N. Rothon, Particulate-filled polymer composites, 2nd Edition, 2003.

[84] M. Xanthos, Modification of polymer properties with functional fillers, in: Funct. Fill. Plast., 2nd Edition, John Wiley & Sons, Inc., New Jersey, USA 2010.

[85] S. Mihajlović, Ž. Sekulić, A. Daković, D. Vučinić, V. Jovanović, J. Stojanović, Surface properties of natural calcite filler treated with stearic acid, Ceram. - Silikaty. 53 (2009) 268–275.

[86] Y. Sheng, B. Zhou, J. Zhao, N. Tao, K. Yu, Y. Tian, Z.C. Wang, Influence of octadecyl dihydrogen phosphate on the formation of active super-fine calcium carbonate, J. Colloid Interface Sci. 272 (2004) 326–329.

[87] M. Osman, A. Atallah, U. Suter, Influence of excessive filler coating on the tensile properties of LDPE–calcium carbonate composites, Polym. 45. (2004) 1177–1183.

[88] F.-L. Jin, X. Li, S.-J. Park, Synthesis and application of epoxy resins: A review, J. Ind. Eng. Chem. 29 (2015) 1–11.

[89] C.A. May, Epoxy resins: Chemistry and technology, 2nd Edition, Marcel Dekker, New York, USA, 1988.

[90] B.J. Tiimob, V.K. Rangari, S. Jeelani, Effect of reinforcement of sustainable β-$CaSiO_3$ nanoparticles in bio-based epoxy resin system, J. Appl. Polym. Sci. 131 (2014) 1-10.

[91] J.M. Raquez, M. Deléglise, M.F. Lacrampe, P. Krawczak, Thermosetting (bio) materials derived from renewable resources: A critical review, Prog. Polym. Sci. 35 (2010) 487–509.

[92] S. Ma, X. Liu, Y. Jiang, Z. Tang, C. Zhang, J. Zhu, Bio-based epoxy resin from itaconic acid and its thermosets cured with anhydride and comonomers, Green Chem. 15 (2013) 245–254.

[93] D.P. Nick, The world of epoxy adhesives, Philadelphia, 2003.

[94] R. Masoodi, K.M. Pillai, Modeling the processing of natural fiber composites made using

liquid composite molding, in: Handb. Bioplastics biocomposites Eng. Appl., 2011: pp. 43–73.

[95] Change climate bio-epoxy resin technical datasheet - Available online:https://docs.wixstatic.com/ugd/0f5b2f_ae89d5de7b574a878fbaa2dd31433efb.pdf (accessed on July 28, 2019).

[96] R. Jain, K.A. Narula, V. Choudhary, Studies on epoxy/calcium carbonate nanocomposites, J. Appl. Polym. Sci. 114 (2009) 2161–2168.

[97] S. Mishra, S. Sonawane, V. Chitodkar, Comparative study on improvement in mechanical and flame retarding properties of epoxy-$CaCO_3$ nano and commercial composites, Polym. Plast. Technol. Eng. 44 (2005) 463–473.

[98] L. Li, H. Zou, L. Shao, G. Wang, J. Chen, Study on mechanical property of epoxy composite filled with nano-sized calcium carbonate particles, J. Mater. Sci. 40 (2005) 1297–1299.

[99] G. Yang, Y. J. Heo, S. J. Park, Effect of morphology of calcium carbonate on toughness behavior and thermal stability of epoxy-based composites, processes 7 (2019) 1–10.

[100] N.G. Shimpi, S. Mishra, Sonochemical synthesis of mineral nanoparticles and its applications in epoxy nanocomposites, Polym. Plast. Technol. Eng. 51 (2012) 111–115.

[101] G. Ji, H. Zhu, C. Qi, M. Zeng, Mechanism of interactions of eggshell microparticles with epoxy resins, Polym. Eng. Sci. (2009) 1383–1388.

[102] Q. Shi, L. Wang, S. Jiang, Z. Zhao, X. Dong, A novel epoxy resin/$CaCO_3$ nanocomposite and its mechanism of toughness improvement, Macromol. Mater. Eng. 291 (2006) 53–58.

[103] F.L. Jin, S.J. Park, Thermal stability of trifunctional epoxy resins modified with nanosized calcium carbonate, Bull. Korean Chem. Soc. 30 (2009) 334–338.

[104] F. Mustata, N. Tudorachi, D. Rosu, Thermal behavior of some organic/inorganic composites based on epoxy resin and calcium carbonate obtained from conch shell of Rapana thomasiana, Compos. Part B. 43 (2012) 702–710.

[105] M. Bootklad, K. Kaewtatip, Biodegradation of thermoplastic starch/eggshell powder composites, Carbohydr. Polym. 97 (2013) 315–320.

[106] M. Azadi, M.J. Olya, S. Vahedi, N.F. Sangani, The effect of the chemical composition and the volume of coated carbonate calcium on epoxy paint properties, Russ. J. Appl. Chem. 90 (2017) 1181–1187.

[107] H.P.S. Abdul Khalil, A.H. Bhat, M. Jawaid, C.K. Abdullah, H.M. Fizree, Development and characterization of epoxy nanocomposites based on nano-structured oil palm ash, Compos. Part B Eng. 53 (2013) 324–333.

[108] Imasco Minerals Inc., technical data sheet - Available online: https://www.imascominerals.com/download.php?file=SDS-Imasco-Sands-and-Agg-Ju1-13-2015.pdf (acessed July 28, 2019).

[109] R.M. Jones, Particle size analysis by laser diffraction: ISO 13320, standard operating procedures and Mie theory, Am. Lab. (2003) 44–47.

[110] A. Chatterjee, M.S. Islam, Fabrication and characterization of TiO_2-epoxy nanocomposite, Mater. Sci. Eng. A. 487 (2008) 574–585.

[111] ASTM D638-14, Standard test method for tensile properties of plastics, ASTM Int. U.S.A 2003.

[112] ASTM D790-17, Standard test methods for flexural properties of unreinforced and reinforced plastics and electrical insulating materials, ASTM Int. U.S.A 2017.

[113] R. Rothon, Particulate-filled polymer composites, 2nd Edition, Rapra Technology Limited, Shropshire, UK 2003.

[114] ASTM D6110-18, Standard test method for determining the Charpy impact resistance of notched specimens of plastics, ASTM Int. U.S.A 2018.

[115] M. El Messiry, Theoretical analysis of natural fiber volume fraction of reinforced composites, Alexandria Eng. J. 52 (2013) 301–306.

[116] G.R. Liu, A step-by-step method of rule of mixture of fiber and particle-reinforced composite materials, Compos. Struct. 40 (1998) 313–322.

[117] ASTM D2734-16, Standard test methods for void content of reinforced plastics, ASTM Int. U.S.A 2016.

[118] ASTM D570-98, Standard test method for water absorption of plastics, ASTM Int. U.S.A 2018.

[119] ASTM E1356-08, Standard test method for assignment of the glass transition temperatures by differential scanning calorimetry, ASTM Int. U.S.A 2014.

[120] L.N. Schultz, M.P. Andersson, K.N. Dalby, D. Müter, D. V. Okhrimenko, H. Fordsmand, S.L.S. Stipp, High surface area calcite, J. Cryst. Growth, 371 (2013) 34-38.

[121] Y. He, Y. Fan, P. Luo, Q. Yang, Synthesis of stearic acid modified ground calcium carbonate (SA-GCC) hybrid material and properties of SA-GCC/epoxy composites coating, Russ. J. Appl. Chem. 88, (2015) 962–969.

[122] V. Apalangya, V. Rangari, B. Tiimob, S. Jeelani, T. Samuel, Development of antimicrobial water filtration hybrid material from bio source calcium carbonate and silver nanoparticles, Appl. Surf. Sci. 295 (2014) 108–114.

[123] E. DesRosiers Lachiver, N. Abatzoglou, L. Cartilier, J.S. Simard, Insights into the role of electrostatic forces on the behavior of dry pharmaceutical particulate systems, Pharm. Res. 23 (2006) 997–1007.

[124] M. Rahman, S. Zainuddin, M. Hosur, J. Malone, M. Salam, A. Kumar, S. Jeelani, Improvement in mechanical and thermo-mechanical properties properties of e-glass/epoxy composites using amino functionalized MWCNTs, Compos Struct. 94 (2012) 2397–2406.

[125] S. Murugan, Y. Munusamy, H. Ismail, Effects of chicken eggshell filler size on the processing, mechanical and thermal properties of PVC matrix composite, Plast. Rubber Compos. 46 (2017) 42–51.

[126] D. Wu, X. Wang, Y. Song, R. Jin, Nanocomposites of poly(vinyl chloride) and nanometric calcium carbonate particles: Effects of chlorinated polyethylene on mechanical properties, morphology, and rheology, J. Appl. Polym. Sci. 92 (2004) 2714–2723.

[127] T.A. Hassan, V.K. Rangari, S. Jeelani, Mechanical and thermal properties of bio-based $CaCO_3$/soybean-based hybrid unsaturated polyester nanocomposites, J. Appl. Polym. Sci. 130 (2013) 1442–1452.

[128] V. Fombuena, S.N. L, S. Md, J. D, B. R, Study of the properties of thermoset materials derived from epoxidized soybean oil and protein fillers, JAOCS, J. Am. Oil Chem. Soc. 90 (2013) 449-457.

[129] M.Z. Rong, M.Q. Zhang, W.H. Ruan, Surface modification of nanoscale fillers for improving properties of polymer nanocomposites: a review, Mater. Sci. Technol. 22 (2006) 787–796.

[130] F. Bassam, P. York, R.C. Rowe, R.J. Roberts, Young's modulus of powders used as pharmaceutical excipients, Int. J. Pharm. 64 (1990) 55–90.

[131] L.W. McKeen, Introduction to plastics and elastomers, The effect of creep and other time related factors on plastics and elastomers, 2nd Edition, 2009, 1–31.

[132] B. Chen, J.R.G. Evans, impact and tensile energies of fracture in polymer-clay nanocomposites, Polymer (Guildf). 49 (2008) 5113–5118.

[133] S.U. Khan, K. Iqbal, A. Munir, J.K. Kim, Quasi-static and impact fracture behaviors of CFRPs with nanoclay-filled epoxy matrix, Compos. Part A Appl. Sci. Manuf. 42 (2011) 253–264.

[134] Ö. Bülent, Hybrid Effect in the mechanical properties of jute/rockwool hybrid fibres reinforced phenol formaldehyde composites, Fibers Polym. 11 (2010) 464–473.

[135] A. Omrani, L.C. Simon, A.A. Rostami, The effects of alumina nanoparticle on the properties of an epoxy resin system, Mater. Chem. Phys. 114 (2009) 145–150.

[136] R.E. Abhari, P.A. Mouthuy, N. Zargar, C. Brown, A. Carr, Effect of annealing on the mechanical properties and the degradation of electrospun polydioxanone filaments, J. Mech. Behav. Biomed. Mater. 67 (2017) 127–134.

[137] City of Saskatoon, Landfill - Available online: https://www.saskatoon.ca/services-residents/waste-recycling/garbage/landfill (accessed online on July 29, 2019).

[138] Government of Canada, Annual statistics of mineral production - Available online: http://sead.nrcan.gc.ca/prod-prod/ann-ann-eng.aspx (accessed online on July 29, 2019).